2021-03-02

Induction Machine with Integrated Magnetic Gear

Abdelhamid, Dalia Zaky Bassuny

UNIVERSITY OF CALGARY

Induction Machine with Integrated Magnetic Gear

by

Dalia Zaky Bassuny Abdelhamid

A THESIS

SUBMITTED TO THE FACULTY OF GRADUATE STUDIES

IN PARTIAL FULFILMENT OF THE REQUIREMENTS FOR THE

DEGREE OF DOCTOR OF PHILOSOPHY

GRADUATE PROGRAM IN ELECTRICAL AND COMPUTER ENGINEERING

CALGARY, ALBERTA

MARCH, 2021

ABSTRACT

There have been many recent advancements in magnetic gears and pseudo-direct drive permanent magnet machines with integrated magnetic gears. Despite these advances, there several applications where induction machine drives are preferable. This proposed work investigates the feasibility of a pseudo direct drive induction machine, with an integrated magnetic gear. It presents some of the difficulties in the design process as compared to the design process for permanent magnet machines. The performance of a pseudo direct drive induction machine, with an integrated magnetic gear, is investigated. A prototype design at a small scale is developed, and simulation results demonstrate the potential for high torque density with good loading characteristics.

This research work presents a design process to integrate a magnetic gear with an induction machine. The resulting integrated machine has the potential to offer a high torque density with asynchronous speed characteristics. Such characteristics may be desirable for applications that require a sensorless operation or may be subject to severe backlash or jamming.

An investigation into magnetic gear modulating ring design geometry and the performance of a magnetic gear integrated into an induction machine are presented. Modulating ring construction is one of the difficult aspects of magnetic gear design, and a compromise between magnetic performance, losses in conductive supporting parts, and manufacturability is often required. Six possible designs for modulating rings are presented, and their magnetic performances are compared with an ideal but unrealistic case of independent modulating parts. Results are presented for the case with a magnetic gear integrated with an induction machine but may be generally applicable to all radial flux magnetic gear configurations.

.

The assembly of the prototype machine and its experimental performance are presented. Complications during the experimental work and modulating ring failure are discussed. Finally, recommendations for design improvement and future work are suggested.

ACKNOWLEDGEMENTS

In the Name of Allah, the Most Gracious, the Most Merciful, who says in his glorious book "Praise to Allah, who has guided us to this; and we would never have been guided if Allah had not guided us". (The Qur'an Al-A'raf 7:43)

It is hard to state in a few words my sincere appreciation to all who helped me to accomplish the journey towards earning my PhD degree. First and foremost, I would like to thank my supervisor, Dr. Andrew Knight for giving me the opportunity to work under his supervision, for guiding me all the way in my research, and for his kindness and support. Furthermore, I would also like to acknowledge my supervisory committee members, Dr. Ed Nowicki, and Dr. Hamid Zareipour for their useful suggestions and comments throughout my research. I would like to acknowledge my internal examiner Dr. David Wood for his valuable feedback. I would I like to acknowledge my external examiner Dr. Jonathan Bird for his supportive comments. I would like to extend my sincere thanks and appreciation to Dr. Om P. Malik for his role in my candidacy committee. I would like to thank the ECE Department administration personnel and the University of Calgary.

My special gratitude goes to my parents (May Allah bless their souls and grant them the supreme paradise) who were the prime source of my inspiration and who made me the person I am today. Similarly, I acknowledge the inspiration and teaching from all my teachers from my early years who had faith in my abilities.

I would like to acknowledge the moral support from my husband and children, my siblings, and their families.

Dedication

To Allah the almighty sake

To the memory of my beloved parents

To my children

To my beloved country Egypt

Table of Contents

List of Tables

List of Figures and Illustrations

List of Symbols, Abbreviations and Nomenclature

Symbol	Definition
μ_o	Permeability of free space
B	Flux density
E	Electromotive force
G	Gear ratio
g	Air gap length
h	Modulating rig height
I	Current
L	Machine effective length
M_H	Magnetomotive force (mmf) for inner rotor
M_L	Magnetomotive force (mmf) for outer rotor
Θ	Angular displacement
N_s	Modulating ring ferromagnetic steel poles
P	Permeance of the modulating ring
P_{F+W}	Friction and windage losses
p_H	Inner rotor permanent magnet pole pairs
p_L	Outer rotor permanent magnet pole pairs
P_{LR}	Locked rotor active power
P_{nl}	No load active power
Q_{LR}	Locked rotor reactive power
Q_{nl}	No load reactive power
r	Machine radius
R	Resistance
R_c	Core resistance
t	Time
V	Voltage
W	Airgap stored energy
X	Reactance
X_m	Magnetizing reactance
Z	Impedance
τ	Torque
ω_H	Inner rotor rotation speed (rad/s)
ω_L	Outer rotor rotation speed (rad/s)
ω_s	Modulating ring rotation speed (rad/s)

CHAPTER 1: INTRODUCTION

Today's industry demands innovative solutions and the use of developing technologies. To improve efficiency, decreasing operating cost, and increasing productivity, high maintenance gearboxes, hydraulic systems, and conventional machines are becoming unattractive to future industry. High torque low-speed machines offer a low-cost, high-efficiency alternative. With the absence of mechanical transmission and direct motor coupling to the load, direct drive increases torsional stiffness, improves positioning accuracy, provides backlash-free operation, introduces high and safe dynamic load reversals, has quiet, low maintenance rate, and no lubrication operation. Direct drive motors are widely used in pharmaceutical machinery, gearless Elevators, extruders, painting and packing machines, and any application that needs low speed and high torque wherever gearbox can be eliminated. Direct drive generators are used with renewable power generation where the speed is low as in wind.

Permanent magnet (PM) machines have been proven to offer high performance direct drive, with high pole numbers and high torque density. With the wide variety of applications that are candidates for direct drive utilization, there are however some applications that are not the best fit for the PM machines. This study introduces an alternative for the loads that are not suitable for the PM machines. For example, systems with a long cable that require an isolation transformer between drive and motor; or systems that may exhibit significant backlash, windup, or potential for jamming. In these cases, an induction motor with integrated magnetic gear may be a good solution. Induction motors are easy to operate, durable, and have high starting torque. Furthermore, induction machines offer simplified open-loop control or simple 'sensorless' closed-loop control,

lower cost, can be used with systems with long cables requiring isolation or filtering, and are also suitable for systems with significant backlash, windup or potential to jam.

When machines fail to meet load requirements or are incapable of matching load torque, gears are commonly used. Mechanical gearboxes are used widely to match the prime-movers operating speeds to the requirements of their loads. It is usually more cost and weight effective to employ a high-speed electrical machine together with a gearbox to transform speed and torque. Although, high system torque densities can be achieved, due to mechanical contact, mechanical gears often need lubrication, cooling, and maintenance. Also, noise, vibration, wear, and reliability can be significant issues [1-5].

Magnetic gears were offered to replace mechanical gears. Magnetic gears have been proposed as a means of increasing torque density within electromechanical systems while avoiding problems associated with traditional mechanical gears. Magnetic gear engages magnetic poles instead of mechanical teeth. Magnetic gear transmits torque -without any contact- by different magnetic poles through flux modulating pieces. Since the torque transmission occurs without any contact, magnetic gears have high efficiency, low acoustic noise, fewer vibrations, low maintenance, low cooling requirements, long estimated life, and improved reliability. Furthermore, magnetic gears are smaller and lighter than mechanical gears. Magnetic gears inherently protect against overloads by harmlessly slipping if an overload torque is applied, and automatically and safely re-engaging when the fault torque is removed. Furthermore, magnetic gears significantly reduce harmful drivetrain pulsations, allow for misalignment/vibration of shafts [6-8]. Magnetic gear loadability depends on the level of magnetic loading, there are no electrical loading limits as there are no electrical coils. Magnetic gears are used in many applications such as hybrid vehicle drives, marine propulsion, wind turbine, aerospace, renewable energies, and industrial automation [1-18].

A gear using permanent magnets dates back as early as the 1901's with a US patent by Armstrong [19]. Followed by another US patent by Neuland in 1916 [20] and in the 1940's by Faus [21]. A few more patents over the years have followed. Early magnetic gears using ferrite magnets and spur gear configurations yielded poor torque densities. With the introduction of rare-earth permanent magnets, more work has been done at achieving greater torque density out of magnetic gears.

Based on their operations, magnetic gears can be classified into three types: linear magnetic gears, coaxial magnetic gears, and axial magnetic gears. The work presented in this thesis considers a coaxial radial flux magnetic gear to be able to integrate it within an induction machine.

1.1 Coaxial Radial Flux Magnetic Gear

A magnetic gear consists of three mechanically centered rotors. The middle rotor is an array of steel pieces and the other two rotors have permanent magnets on them, shown in Figure 1-1. The magnetic gear concept is based on the modulation of permanent magnets magnetic fields by steel modulating pieces. A magnetic gear transmit torques between an input and output shaft without mechanical contact.

The outer rotor contains an array of a low number of permanent magnets and rotates at a higher speed. The modulating ring- middle rotor - contains an array of steel pieces that modulates the pole numbers of the inner and outer rotor magnetic fields such that the relative speed of rotation of the inner and outer rotor is constant.

Considering Fig 1-1, the inner rotor, consists of p_H pole pair permanent magnets (PM) rotating at ω_H, a middle rotor with N_s individual ferromagnetic steel poles that can rotate at ω_s and p_L pole-pair PM outer rotor rotating at ω_L. The inner and outer rotors that contain PMs interact with the

middle steel poles to create space harmonics. If the relationship between the steel poles is chosen to be

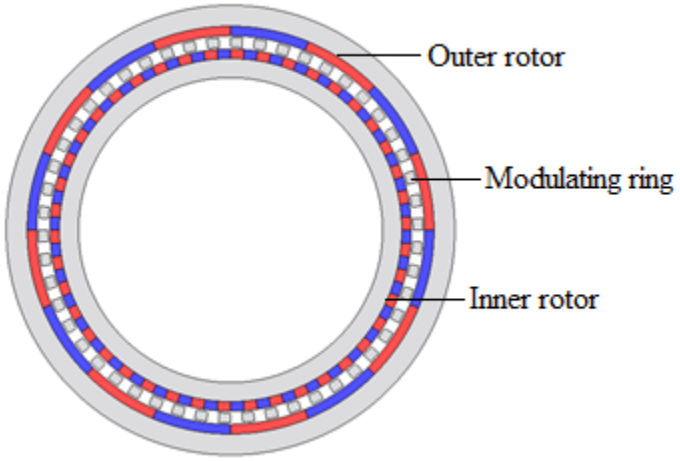

Figure 1-1 Magnetic gear

$$p_H = |p_L - N_s| \qquad (1-1)$$

then the rotors will interact via a common space harmonic and the rotational angular velocities for each rotor is then

$$\omega_H = \frac{N_s\omega_s - p_L\omega_L}{N_s - p_L} \qquad (1-2)$$

Where subscripts "H" "L" and "S" denote high-speed rotor, low-speed rotor, and modulating ring respectively.

The operation of this gear differs depending on which of these "rotors" is kept stationary. Most often, the middle rotor of steel pieces is kept stationary while the inner and outer rotors are used as the input and outputs of the gear. There are three possibilities for operation, each with its own gearing ratio. If the outer permanent magnet rotor is fixed $\omega_L=0$, while the steel modulating ring and inner permanent magnet rotor rotate and the gear ratio is $G = \frac{N_S}{p_H}$. If the modulating ring is

fixed while the two permanent magnet rotors are counter-rotated, the gear ratio is $G = -\frac{p_L}{p_H}$. If the inner rotor is fixed while the outer rotor and modulating ring rotate concurrently, the gear ratio is $G = \frac{N_S}{p_L}$. A negative sign in the gear ratio indicates that the rotors are counter-rotating.

1.2 Electric Machines Integrated with a Magnetic Gear

Mechanical gearboxes have been used for a long time to fulfill the load requirements when the output of the electric machine doesn't match the load. Even though high torque densities are obtained, the gearbox then becomes a point of concern due to noise, maintenance, and failure consequences [9–13].

Low-speed, high-torque electric machines have many industrial applications. To obtain a high-torque at low-speed from an electrical machine, a machine is designed to operate at the desired speed or the output of the machine is geared to the desired speed. Usually, the objective of the final design is not only to satisfy the load requirements, but to do so with efficiency, low cost, minimal size, and simplicity. Since the size of electric machinery is proportional to the torque required, high required torque leads to large machines. Low-speed, high-torque machines are a significant problem in an application where size and mass are big concerns. For example, electric machines for marine propulsion applications can range in the tens of megawatts and can weigh hundreds of tones. An induction machine rated for 19MW and 150 rpm weighed 117 tones and occupied over 85 m^3 [22]. In other cases, gears are combined in-line with the generator to take the high-torque, low-speed output of the turbine and transfer it to the high-speed, low-torque input of the generator [11, 12]. These make direct-drive solutions more functionally and/or economically attractive. The advantage of magnetic gear over mechanical gears is not only in improvements in noise, maintenance, and failure consequences but most interestingly, it affords the ability to

combine the gear and machine into one package. As the next stage in this evolution, pseudo-direct-drive motors, with a magnetic gear integrated with a permanent magnet motor have been developed for many applications, including electric vehicle traction, wind turbines, ship propulsion systems, aerospace actuation, and industrial applications that require a high torque, low-speed drive.

To have a smaller and a higher torque density machine, an electric machine can be integrated with a magnetic gear. Due to its high torque density, permanent magnet (PM) machines were integrated with magnetic gears and resulted in a high-torque low-speed drive PM machine integrated with magnetic gears have been used in many applications such as electric vehicle traction, wind turbines, ship propulsion systems, aerospace actuation, and industrial applications that require a high-torque, low-speed drive [1-18].

Documented machine topologies that incorporate the concepts of this gear are presented in the following section.

1.2.1 Permanent Magnet Machines

The combination of the magnetic gear and permanent magnet machine was introduced in different topologies: Outer-rotor permanent magnet machine, this machine configuration consists of direct addition of an outer-rotor permanent magnet synchronous machine to the center of the magnetic gear resulting in a complex structure with three arrays of permanent magnets and three air gaps. This machine structure is complex due to the multiple air gaps, and the inability to mechanically support the rotors on both ends so that the center of the machine can be accessed. Additionally, the stator at the center of the machine leads to difficulties in heat removal [23].

This configuration was proposed for an in-wheel motor for electric vehicles to achieve compact construction. Some motors are designed, simulated results, built and the experimental

results obtained. [24] – [34]. Evaluation for the motors and loss measurement have been performed [35] - [37]. Some papers discuss the simulation of the design and the different optimization techniques [38] – [42]. A two air gap simplified design was proposed and simulated [43].

Outer-rotor, flux modulated, permanent magnet machine in this configuration the inner two arrays of magnets to gear the magnetic poles created by the stator to those of the outer rotor directly. Neither the stator nor flux modulator move. This arrangement results in a less complicated structure, but still has the often undesirable feature that the outer parts of the machine rotate and the excitation has to be delivered to the center stator which can make heat removal more problematic. Topology and principle of operation were introduced [44].

Inner-rotor, flux-modulated, permanent-magnet synchronous machine combined a conventional inner-rotor PM machine with inside out gear was introduced. Inside-out gear is when the inner rotor now contains the large number of permanent magnets and is slow-moving while the outer rotor has the low number of magnets and is the high-speed rotor. This machine structure is simpler incorporating a magnetic gear inside the machine as there is a single moving part, the inner rotor, and the stator is on the outside of the machine. [23]

Magnetic gear integrated brushless PM machine combines the magnetic gear with an inner rotor permanent magnet machine. The operation of this machine consists of the interaction of the inner magnet array with the magnetic poles created by the stator whose rotation is then geared through the steel modulator rotor and the outer array of permanent magnets that are fixed to the stator. Design and simulation of the performance were introduced in [45].

“Pseudo” direct-drive machine is obtained by combining a magnetic gear and electrical machine both mechanically and magnetically. This method of coupling a magnetic gear and a permanent magnet brushless machine was proposed and the machine was built and the

performance has been evaluated [46]-[48]. A group of papers discussed the different control techniques that have been tested with pseudo direct drive machines [49] – [56]. Analytical and simulation for a large pseudo direct drive for wind turbine application was discussed [57] and also scaling it was introduced in [58].

1.2.2 Induction machine

There remain several applications where low speed, high torque characteristics are required, but the industrial system to be driven is well suited to an induction machine drive. Examples may include systems with a long cable, an isolation transformer between drive and motor, or systems that may exhibit significant backlash, windup, or potential for jamming. In these cases, an induction motor with integrated magnetic gear may be a good solution. To develop a high-power-density high-efficiency motor at a lower cost integrating a three-phase induction machine with magnetic gear is being investigated.

Induction motors are simple and rugged in construction, robust and can operate in any environmental condition, low cost, maintenance-free, can be operated in polluted and explosive environments, 3 phase induction motors will have self-starting torque, easy operation, durability, and high starting torque. [59]

However, although PM machines can be made with very high torque densities and high pole numbers (for low-speed operation), induction machines offer simplified open-loop control or simple ‘sensorless’ closed-loop control, lower cost, can be used with systems with long cables requiring isolation or filtering, and are also suitable for systems with significant backlash, windup or potential to jam.

One potential solution to this issue investigated a machine with an additional wound rotor circuit [60]. After the introduction of the machine under study, there were a few research studying integrating an outer rotor induction machine inside the magnetic gear [61]-[63].

1.3 Significance of the Work

Integrating a magnetic gear and permanent magnet machines has introduced high-torque low-speed drive which eliminates mechanical gearbox with all its related concerns and has high reliability, low maintenance, low cooling requirements, Inherent torque overload protection, and low NVH (Noise, Vibration, and Harshness) [1-18].

Besides induction machines offer simplified open-loop control, lower cost, can be used with systems with long cables requiring isolation or filtering, and also suitable for systems with significant backlash, windup, or the potential to jam.

However, PM machines can be made with very high torque densities and high pole numbers (for low-speed operation). Induction machines are not well suited to those applications. A system that integrates magnetic gearing with induction machines can provide high-torque low-speed with simple open-loop control or simple 'sensorless' closed-loop control. Presently, there is no solution for low-speed drives that use induction machines without using mechanical gearboxes, which can a major point of failure (e.g., in Type 3 wind turbines [64]).

Potential applications would be drilling, crushers, wind generation, and other applications where high torque low speed is required.

Compared to other solutions to meet similar drive requirements, the induction machine with integrated magnetic gear combines the benefits of magnetic gears and induction motors and

offers lower cost, standard inverter operation & control, low cogging torque, and higher torque density / lower weight.

To the best of my knowledge, there is no induction motor with integrated magnetic gear was built. There is one proposed design that to my knowledge has not been constructed [60]. It required additional DC boost windings, and an additional three-phase rotating diode rectifier i.e. it was not an induction machine with integrated gear, but a hybrid induction / synchronous machine with magnetic gear. That proposed design was not suitable for systems that require a central drive mechanism (e.g. top drive for drilling).

To benefit from the induction motor and magnetic gear specifications and to find a suitable drive for applications where a PM motor may not be the best fit, this research work investigates the potential of integration of an induction motor with a magnetic gear. Potential applications for an induction motor with integrated magnetic gear are those where high torque density is desirable and the operating environment may make conventional gearing undesirable. Relative to PM machines, a clear advantage is the case where the machine is remote from the control. Such cases may require transformers or filtering between the drive and the machine, making sensorless control difficult. The combination of an induction machine with magnetic gearing also has the potential to be lower cost than a PM machine with integrated gear. Potential applications for this machine could include as an alternative to hydraulic motors, such as in oilfield applications, including would be drilling motors or other applications such as mechanical crushers or wind generation, where high-torque and low-speed mechanical characteristics are required.

In this thesis an investigation into the potential of a cage induction motor with integrated internal magnetic gear is presented. While the target application may typically be a large machine, the potential of such a system is investigated at a reduced scale, with a target of 1.5kW, and speed

in the 220 rpm range. This proposed work presents the design process, initial design, and the performance of the induction motor with integrated magnetic gear at different loading conditions. This thesis will present the step-by-step process of design methodology, detailed simulated analysis, and building an induction machine integrated with a magnetic gear.

1.3 Thesis Organization

This thesis has six chapters. The first chapter introduces the low speed- high torque drives to the reader, summarizes the work done in the research point by previous researchers, and explains the motivation behind this research work. This chapter also outlines the contribution of this thesis. The second chapter is introducing the magnetic gear design process; mathematical model and detailed finite element analysis (FEA) simulated performance. The design of the induction machine and integration of the induction machine with the magnetic gear are elaborated on in Chapter 3. This chapter introduces the FEA simulation of the integrated machine and the loading performance of the machine. Chapter 4 describes the details of the proposed machine building and the test facility set up. Chapter 5 presents the experimental results of the proposed machine, problems that have been faced during machine operation, and suggested solutions. Finally, Chapter 6 also concludes the research work by discussing the summary and possible future work on this topic.

CHAPTER 2: MAGNETIC GEARS

This chapter discusses magnetic gear construction and design, and introduces the different proposed designs for the modulating ring. The design steps, simulations, and data analysis will be discussed in detail.

Gears are used when machines fail to fulfill load torque or speed requirements. Mechanical gears are been used for a long time with machines. Mechanical gearboxes are been used widely to match the prime movers operating speeds to the requirements of their loads. They are been used to change speed, torque, or direction of power. They may increase speed and decrease torque as in wind turbines or decrease speed and increase torque as in electric vehicles. Due to mechanical contact mechanical gears has many problems such as wear, noise, vibration, low reliability and need for lubrication, maintenance, and cooling [1-9].

Magnetic gears have been proposed as a means of increasing torque density within electromechanical systems while avoiding problems associated with traditional mechanical gears. Magnetic gears are magnetic devices that transmit torque between two rotating parts with different magnetic pole pairs through flux modulation poles. Magnetic gears use permanent magnet (PM) excitation and a spatial flux modulator to transmit torque between an input and output shaft without mechanical contact. Due to their contactless operation, magnetic gears have high efficiency, low noise, fewer vibrations, and improved reliability. Furthermore, magnetic gears are smaller and lighter than mechanical gears and have inherent overload protection. In case of overload, it slips and when the fault is cleared it reengaged safely [1]-[18]. Torque densities in the range of 100 k Nm/m^3 can be achieved with higher efficiency than a mechanical gear at both full load and part load [2],[3]. Furthermore, magnetic gears significantly reduce harmful drive train pulsations, allow for misalignment/vibration of shafts, have improved reliability, and long estimated life [6]-

[8]. The magnetic gear mechanical loadability depends on the level of magnetic loading and there are no electrical loading limits as there are no electrical coils. For higher power ratings, a magnetic gear will be smaller, lighter, and lower cost than a mechanical gear. Magnetic gears may be used in many applications such as hybrid vehicle drives, marine propulsion, wind turbine, aerospace, renewable energies, and industrial automation [1-10].

2.1 Proposed Magnetic Gear

The gear in this research consists of three rotors. The outer rotor contains an array of a low number of permanent magnets and rotates at a high speed. The inner rotor contains an array of a large number of permanent magnets and rotates slowly. The middle rotor contains an array of steel pieces that meshes the outer rotor to the inner rotor. Fig. 2-1 shows a cross-sectional view of the magnetic gear.

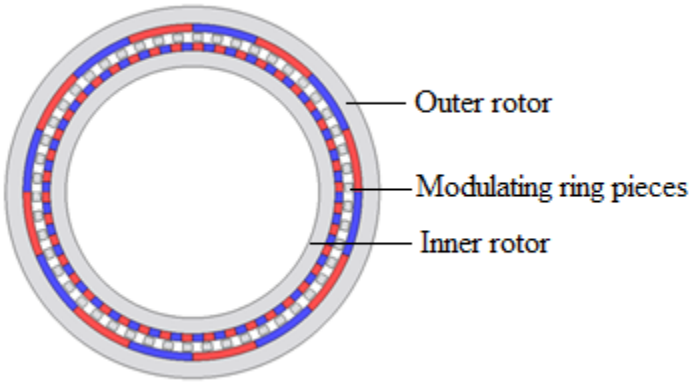

Figure 2-1 Magnetic gear

Magnetic gear topology has been shown to compete with mechanical gears in torque density. The advantage of this gear over mechanical gears is not only in improvements in noise, maintenance, and failure consequences but most interestingly, it affords the ability to combine the gear and machine into one package.

2.2 Magnetic Gear Design

Magnetic gears consist of three mechanically centered rotors of which at least two must be free to rotate with respect to each other. These components typically include a high-speed rotor with a low number of permanent magnetic poles, a low-speed rotor with a high number of permanent magnetic poles, and a modulating ring with magnetic steel pole pieces. As the name suggests, the modulating ring modulates the magnetic fields between the two sets of permanent magnets, creating a magnetic coupling between them. Two of the rotors are mounted with PM's and the third is an array of ferromagnetic pole pieces to create space harmonics and modulate the magnetic flux generated by the two rotors to create a stable gear ratio [10]. This magnetic gear used is similar to planetary gear where the high-speed rotor is the sun gear, modulation ring as the planet carrier, and the low-speed rotor as the ring gear. Although all three components of a magnetic gear may be rotating, typically one of the components is held stationary. The operation of the magnetic gear and the gear ratio depending on which rotor is kept stationary [6]-[12], [65]-[79]

To have torque production between two magnetic field harmonics which have different pole pairs and mechanical rotational speeds and there are flux modulation poles between them, the two magnetic fields should have the same frequency and their pole-pair numbers, satisfying; $N_s = p_L \pm p_H$

To design a magnetic gear, the gear ratio, and the torque will be given. To attain the highest torque density, the relationship between the number of poles is given by:

$$N_s = |p_L + p_H| \tag{2-1}$$

The relation between the pole pairs and the angular speed for all three rotors for maximum

torque transmission is given by:

$$\omega_s N_s = \omega_L p_L + \omega_H p_H \tag{2-2}$$

where subscripts “H” “L” and “S” denote high-speed rotor, low-speed rotor magnet pieces, and modulating ring respectively. In the system under consideration, the modulating ring is stationary, giving a gear ratio, *G*, which is the ratio of the speeds of:

$$\mathrm{G} = \frac{p_L}{p_H} \tag{2-3}$$

In this system, the inner and outer rotors are counter-rotating.

To explain the torque production, the magnetic gear has two sets of permanent magnets and a modulating ring. The magnetomotive force (mmf) due to the magnets and permeance harmonics due to the modulating ring are given by

The mmf equation for high-speed rotor:

$$M_H = \sum_{i=1}^{\infty} M_i \cos(p_H \theta_i - \omega_{Hi}\, t) \tag{2-4}$$

The mmf equation for low-speed rotor:

$$M_L = \sum_{j=1}^{\infty} M_j \cos(p_L \theta_j - \omega_{Lj}\, t) \tag{2-5}$$

The permeance equation:

$$P = P_0 + \sum_{k=1}^{\infty} P_k \cos(N_s \theta_k - \omega_{sk} t) \tag{2-6}$$

By superposition, the flux density

$$B = M_H P + M_L P \tag{2-7}$$

Coupling between two magnetic fields occurs if they have the same space and time harmonics. In this condition:

$$N_s = |p_L + p_H| \tag{2-8}$$

$$\omega_H = \frac{\omega_s N_s - p_L \omega_L}{N_s - p_L} \tag{2-9}$$

The field components, which contribute to torque production, are determined and harmonics up to the 11th harmonic are taken into consideration. A Matlab program is developed to find the torque producing B terms. According to the energy equation, energy can be calculated, and then the torque equation can be obtained. Energy,

$$W = \frac{rlg}{2\mu_o} \int_0^{2\pi} B^2 \, d\theta \tag{2-10}$$

Assuming that the components are rotating synchronously, and defining α to be the relative position of one of the rotors to asynchronously rotating reference frame, the torque harmonics may be found using;

$$\tau = \frac{rlg}{2\mu_o} \frac{d}{d\alpha} \int_0^{2\pi} B^2 \, d\theta \tag{2-11}$$

To investigate pole combinations that minimize unwanted torque components, the field components which contribute to torque production are identified and harmonics up to the 11th harmonic are taken into consideration. The analysis is implemented in Matlab to identify the components that produce a steady torque while limiting unwanted torque ripple. The resulting low-speed torque may be written as

$$\tau = \frac{\pi p_L rlg M_H P_o M_L P}{4\mu_o} \sin p_L \alpha \tag{2-12}$$

Where r is the machine radius, l is the core length and g is the air gap length.

This equation is used to design the magnetic gear and determine the number of poles in each rotor and the machine dimensions.

As the target machine speed is 220 rpm and the synchronous speed of a 6 pole 60 Hz induction motor is 1200 rpm, a gear ratio of 5.25 is selected to enable integrating the induction motor with the magnetic gear. Also, as the target machine power is 1.5 kW and by using the torque equation, two combinations of poles can be used: 21 and 4 pole pairs for inner and outer rotor respectively or 42 and 8 pole pairs for inner and outer rotor respectively can be used. Both gears are simulated and integrated with the induction motor.

2.2.1 21/4 gear

A gear ratio of 5.25, corresponding to 21 inner poles and 4 outer poles is found to be a suitable fit for the desired speed ratio and is simulated to see if it can fulfill the torque requirements. Significant dimensions and parameters are given in Table 2-I. and a schematic of the proposed magnetic gear is shown in Fig. 2-2.

Table 2-I 21/4 Magnetic Gear Parameters

Inner rotor pole pairs, p_H	21
Outer rotor pole pairs, p_L	4
Modulating ring pieces, N_S	25
Gear ratio, G	5.25
Air gap (inner and outer rotor sides)	0.5 mm
Magnet thickness	2.5 mm
Modulating ring piece thickness	2.5 mm
Outer airgap radius	59 mm
Inner airgap radius	47.5 mm
Shaft radius	40 mm
Stack length	54 mm

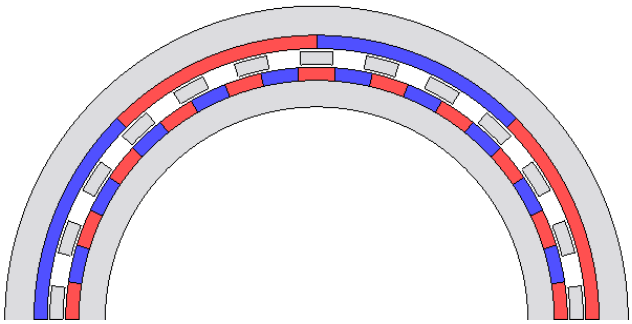

Figure 2-2 Section of 21/4 magnetic gear

At the desired rating of 1.5 kW 220 rpm, the high torque side requirement is 65.1 Nm, corresponding to 12.4 Nm at the low torque side. An investigation of the torque-angle properties is carried out using 2-D FEA. With one of the rotors stationary, the other rotor is rotated through 90 electrical degrees. The resulting data is plotted in Fig. 2-3. It can be seen that the peak torque is less than the required value, which makes this gear not suitable to be integrated with the induction machine for the desired torque value.

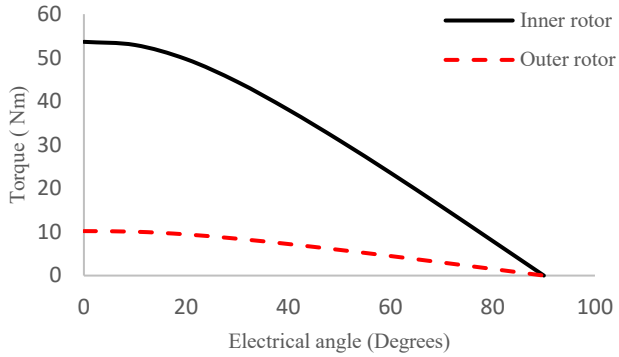

Figure 2-3 Torque – Load angle plot for 21/4 magnetic gear

The predicted torque for constant speed operation at an angle of 0 electrical degrees is plotted in Fig. 2-4, demonstrating a low torque ripple on the high torque output rotor. As expected, the

electromagnetic torques are in the same direction, supporting the motion for one rotor and opposing the rotation for the other rotor.

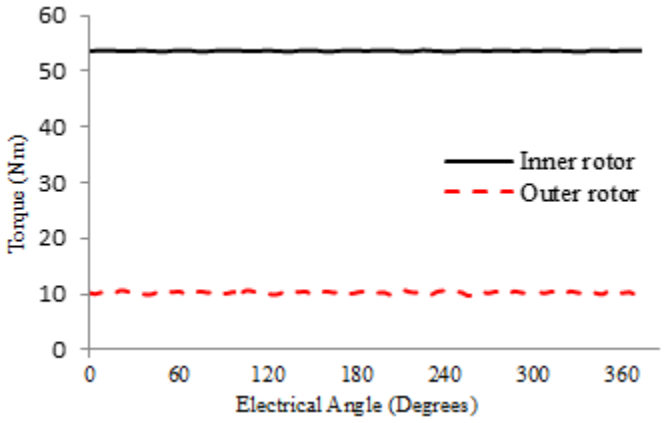

Figure 2-4 Gear torques at constant speed gear

Zooming in the torque curve to see the ripple content. Fig. 2-5 is showing the ripple content in the inner rotor and Fig. 2-4 is the outer rotor ripples.

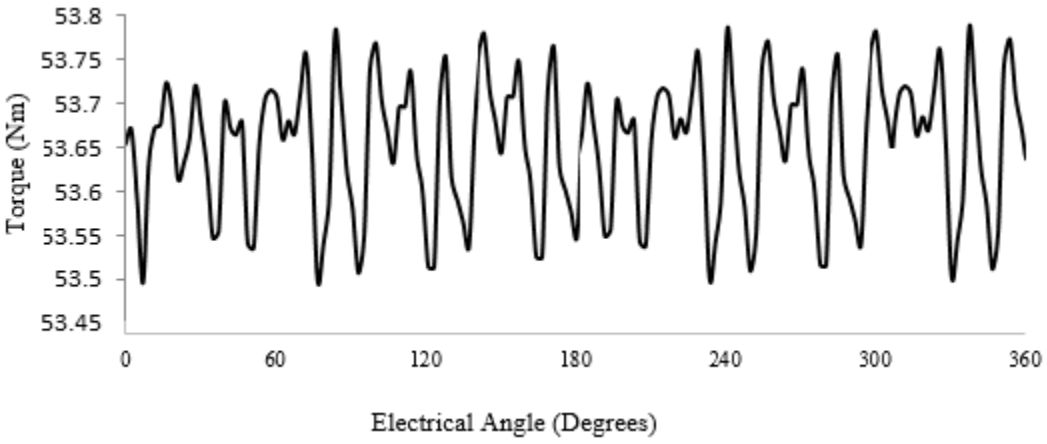

Figure 2-5 Inner rotor torque ripples

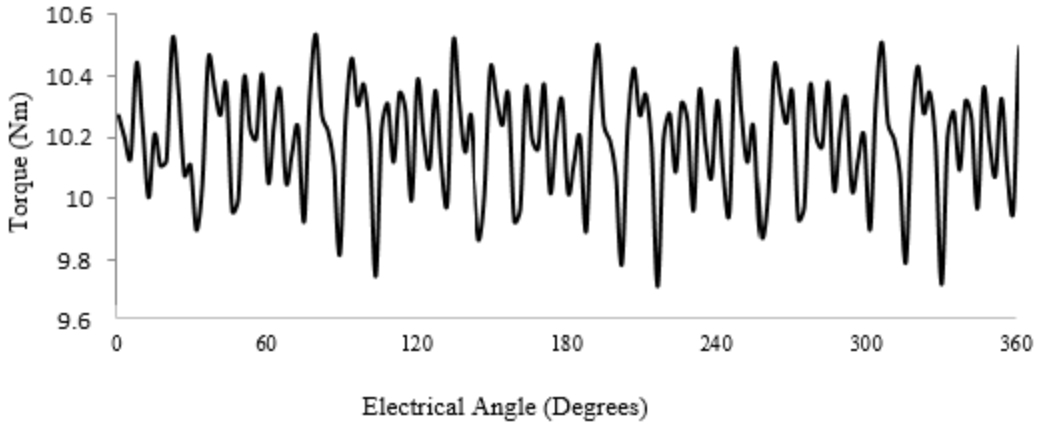

Figure 2-6 Outer rotor torque ripples

2.2.2 42/8 gear

As the 21/4 cannot fulfill the torque requirements and according to the torque equation Eq 19, the number of poles is directly proportional to the torque.

A gear ratio of 5.25, corresponding to 42 inner poles and 8 outer poles is found to be a suitable fit. At this gear ratio, the outer gear rotor speed is 1155 rpm at the desired inner rotor speed of 220 rpm, corresponding to a slip of 0.0375 for a 6 pole 60Hz induction machine. The choice of gear ratio and pole numbers is constrained by minimum magnet dimensions, chosen to be 2.5 mm, and the need for the high speed to correspond to a low slip for a conventional low pole number induction machine. In a larger machine, wider ranges of pole numbers and gear ratios are feasible.

Significant dimensions and parameters are given in Table 2-II. and a schematic of the proposed magnetic gear is shown in Fig. 2-7.

Table 2-II 42/8 Magnetic Gear Parameters

Inner rotor pole pairs, p_H	42
Outer rotor pole pairs, p_L	8
Modulating ring pieces, N_S	50
Gear ratio, G	5.25
Air gap (inner and outer rotor sides)	0.5 mm
Magnet thickness	2.5 mm
Modulating ring piece thickness	2.5 mm
Outer airgap radius	59 mm
Inner airgap radius	47.5 mm
Shaft radius	40 mm
Stack length	54 mm

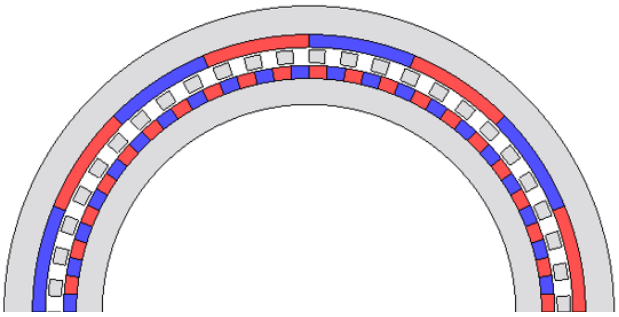

Figure 2-7 Section of 42/8 magnetic gear

At the desired rating of 1.5 kW 220 rpm, the high torque side requirement is 65.1 Nm, corresponding to 12.4 Nm at the low torque side. An investigation of the torque-angle properties is carried out using 2-D FEA. With one of the rotors stationary, the other rotor is rotated through

90 electrical degrees. The resulting data is plotted in Fig. 2-8. It can be seen that the peak torque exceeds the required maximum value, with rated torque occurring when the angle between the rotors is approximately 30 electrical degrees from the position corresponding to maximum torque.

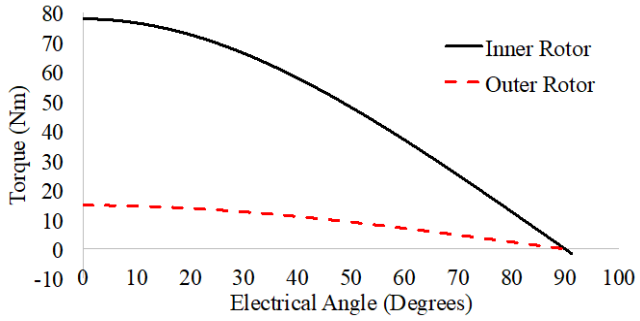

Figure 2-8 Torque – Load angle plot for 42/8 magnetic gear

The predicted torque for constant speed operation at an angle of 31.2 electrical degrees is plotted in Fig. 2-9, demonstrating a low torque ripple on the high torque output rotor. As expected, the electromagnetic torques are in the same direction, supporting the motion for one rotor and opposing the rotation for the other rotor.

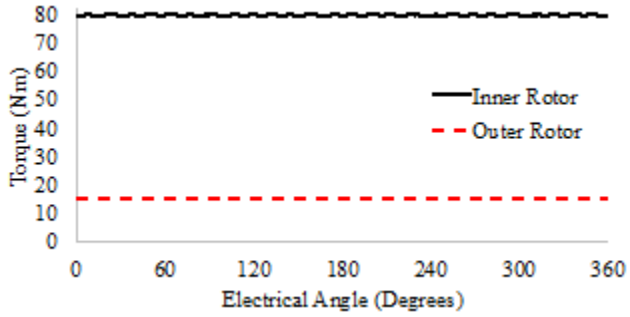

Figure 2-9 Gear torques at constant speed gear

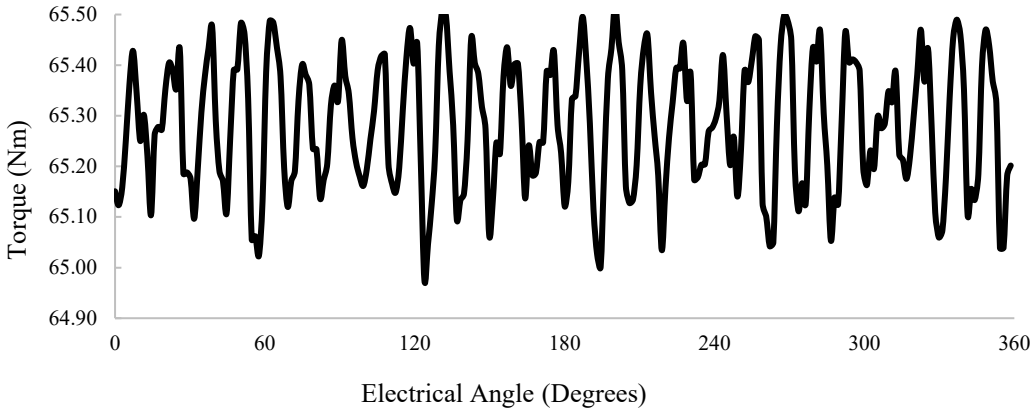

Figure 2-10 Inner rotor torque ripples

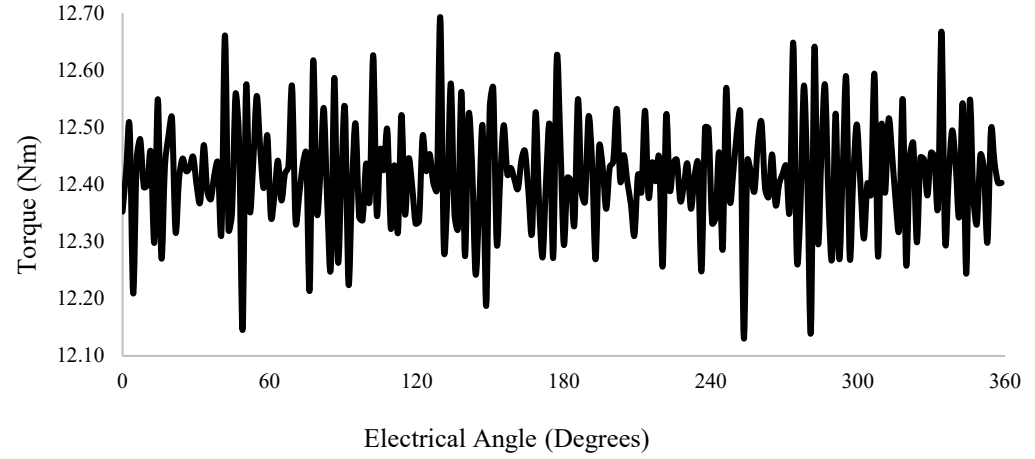

Figure 2-11 Outer rotor torque ripples

Fig. 2-10 is the inner rotor ripple content and Fig. 2-11 shows the ripples in the outer rotor.

2.3 Modulating ring designs

The construction of the three concentric rotors is challenging. The most difficult part is the modulating ring. Ideally, separate pieces of laminated steel should be gathered to form the modulating steel pieces between the two rotors. Rods may be used to keep the modulator laminations together forming modulator teeth. They are connected to a side plate and inserted in the slots between modulator teeth [80]. However, stacking separate small pieces is not reliable.

Besides, the presence of the rods may affect the magnetic circuit, results in unwanted eddy currents, and reduces the overall performance of the gear. To make the modulating ring less complicated and more reliable, this work investigates the use of full ring laminations. The use of interconnected modulating ring pieces has been implemented in previous work [34]. However, the author is not aware of work investigating the trade-off between torque transfer, flux modulation, losses, and the manufacturability of six different designs of the modulating ring laminations. Different designs for the modulating ring are suggested and shown in Fig. 2-12.

In each of the proposed designs, h is the modulating ring height, and the lamination modulating segment pieces are connected by a bridge. The thickness of three of the bridges is h/3and the thickness of the other three is h/5. The designs in Fig. 2-12 are shown such that the top of the diagram faces the high pole number, low-speed rotor and the bottom of the diagram faces the low pole number, high-speed rotor.

Six different designs are introduced, with the pole pieces interconnected by bridges at different points. For each of the designs, two different thicknesses of the interconnecting bridge pieces are studied, giving, six modulating ring designs. Comparing against the ideal case, seven simulation cases are carried out.

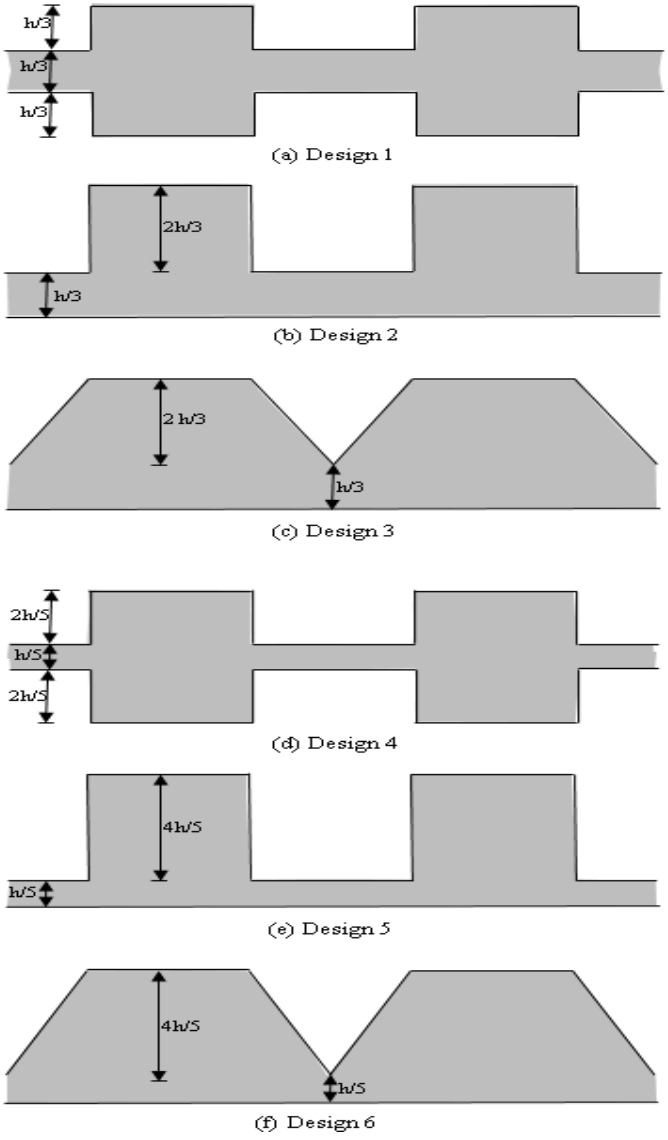

Figure 2-12 Modulating ring proposed designs

2.3.1 Design simulation

Time-domain finite element analysis (FEA) magnetic simulation of the different modulating rings within an integrated magnetic gear and induction machine is carried out using JMAG software. The dimensions of the magnets, back iron, modulating ring thickness, magnetic phase angle, and rotational speed are constant for all seven cases presented in this study. The magnetic gear in this research is an outer sun gear configuration where the inner rotor has the high number

of poles. The modulation ring has 50 modulating segments, the high-speed outer rotor has 8 pole pairs and the low-speed inner rotor has 42 pole pairs. In this configuration, the gear ratio is 42:8.

The torque capability as a function of electrical load angle is simulated for all seven designs. Time-stepped steady-state FEA simulations for each design are performed, changing the initial position from zero to ninety electrical degrees. The modulating ring alignment is such that zero electrical degrees corresponds to maximum torque. Fig. 2-13 shows the magnitude of the torque versus the initial position for the six proposed designs and the ideal modulating ring. (The two rotors are counter-rotating and experience opposing torque.) As expected the ideal design has the most modulation and so the highest peak torque capability.

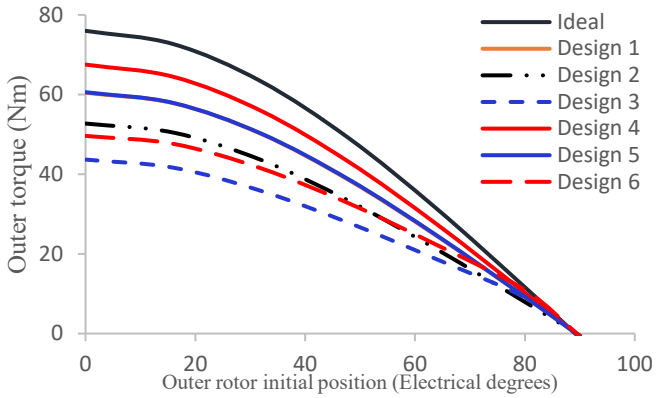

Figure 2-13 Torque – Load angle plot for different modulating ring design magnetic gears

As Fig. 2-13 shows, for the same design the thinner the bridge, the higher the gear torque. The descending order of the peak torque capability is design 4, Design 5, and Design 1 are overlapped with almost the same values for the torque for both designs, Design 2, Design 6, and at last Design 3. According to the design and the depth of the modulating waveform, this order is expected.

Flux line plots for the 7 cases are shown in Fig. 2-14. Some immediate observations may be made from Fig. 2-14: as expected the designs with a thicker bridge (d-f) between the poles see more

leakage flux than the cases with a thinner bridge (a-c); the location of the bridge in the center of the pole or at the low pole number surface does not seem to significantly impact the leakage.

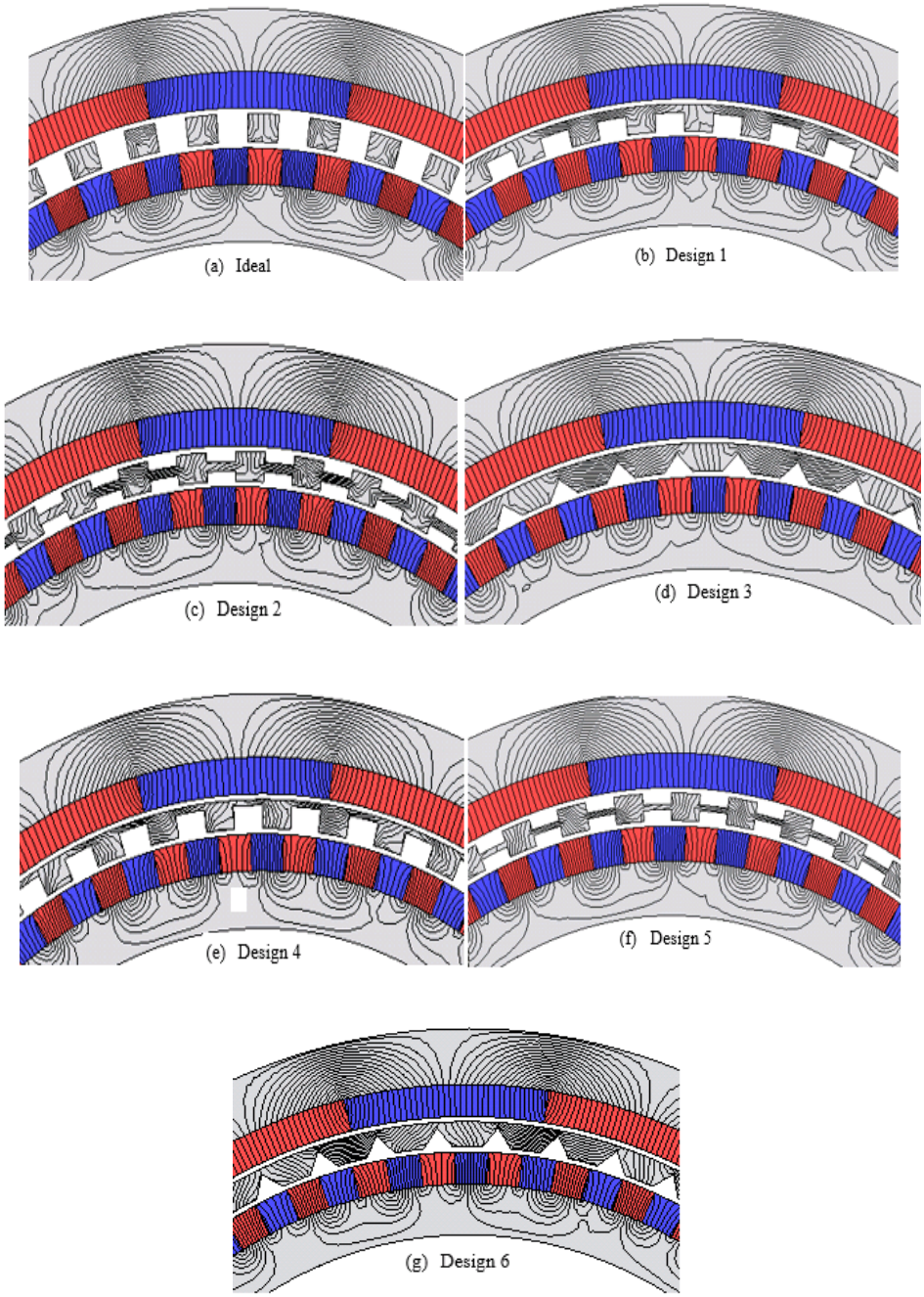

Figure 2-14 Cross-section of induction motor with integrated magnetic gear, showing flux pattern, magnets interacting with stator flux for different modulating ring designs

To have a better understanding of the performance of the different designs, eddy current losses are simulated for different designs.

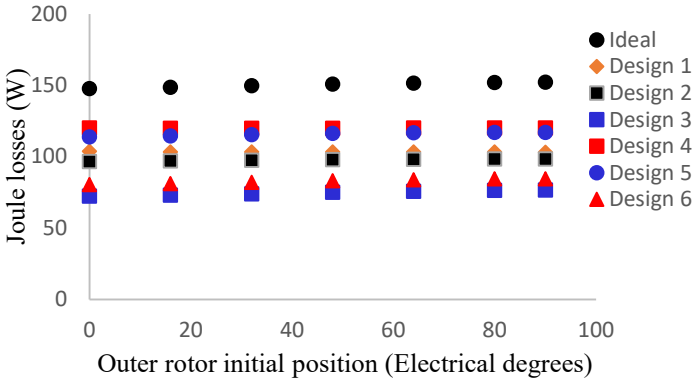

Figure 2-15 Eddy current loss for magnetic gear with different modulating ring designs

Fig. 2-15 shows that the eddy current losses are almost constant with the loading. The higher the torque the gear provides, the higher the eddy current losses. Eddy current losses predominately occur in the inner magnets. For Design 1 and Design 5, although both provide almost the same torque Design 5 has higher losses.

To test the quality of the torque for the different proposed designs, the machine is simulated with the different modulating ring at different torque angle to allow all the designs to provide the same average torque. Simulation results for transient torque under constant speed conditions are presented in Fig. 2-16 for the outer rotors and Fig. 2-17 for the inner rotors. The outer rotor torque is the net total torque on the outer rotor of an integrated machine – a torque of zero indicates the ideal case with the torque stator reaction torque passed through the modulating ring. A small positive torque represents the power loss in the outer rotor. The inner rotor torque is the output mechanical torque available to the load. Table 2-III presents the average torque and percentage total harmonic distortion (THD) for different modulating ring proposed designs.

Considering the figures and table, it can be seen that even with changing the shape of the modulating ring lamination the average torque transfer of the gear can be obtained to a certain range at different loading conditions for each design. However, the ripple content of the torque is impacted by the design of the modulating ring. The outer rotor torque simulation results show that Design 5 has the lowest torque ripple and Design 1 has the highest ripple content. For the inner rotor torque simulation results Design 3 has the lowest torque ripples and Design 4 has the highest ripple content. It should be noted that the inner rotor torque represents the output. Lower THD in power systems means higher power factor, lower peak currents, and higher efficiency.

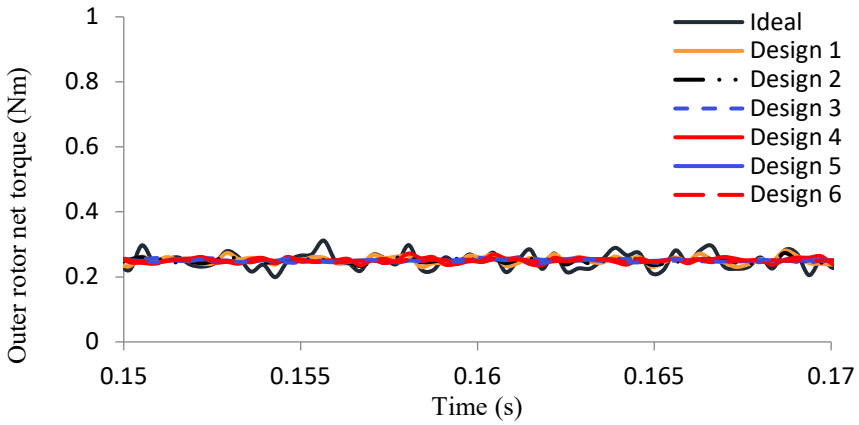

Figure 2-16 Outer rotor torque waveform

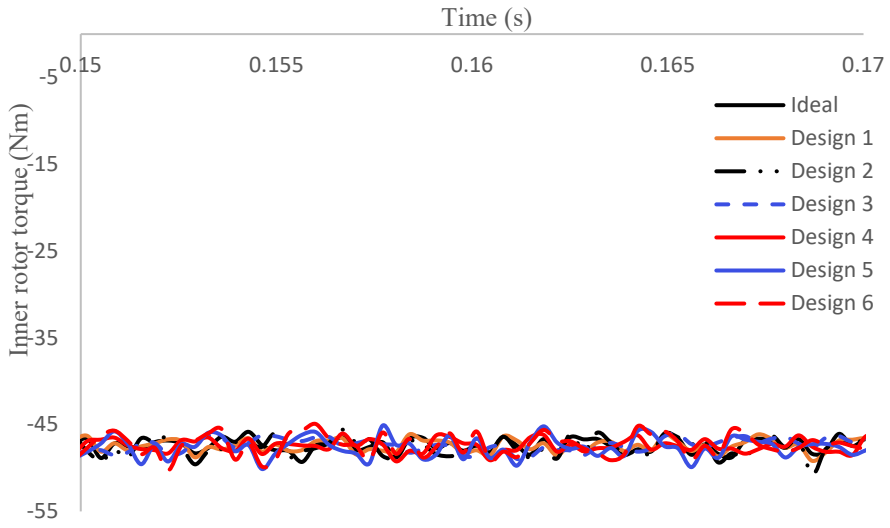

Figure 2-17 Inner rotor torque waveform

Table 2-III Average torque and %THD of different modulating ring designs

	Inner rotor		Outer rotor	
	Average	%THD	Average	%THD
Ideal	-47.41	0.073	0.25	10.36
Design 1	-47.43	0.077	0.252	4.64
Design 2	-47.65	0.53	0.25	2.94
Design 3	-47.35	0.07	0.251	1.77
Design 4	-4742	0.082	0.251	3.29
Design 5	-47.61	0.5	0.25	1.23
Design 6	-47.34	0.42	0.25	1.3

For the designs considered in this work, the modulating ring height is 2.5 mm and the minimum manufacturable interconnecting dimension happened to be h/3. For a bigger gear, the

ratio of the ring piece height and the interconnecting bridge height may be investigated in future work. More investigation is done for those three designs and compared with the ideal case.

Time-domain finite element analysis (FEA) magnetic simulation is carried out using JMAG software. As an initial step, the three proposed designs are simulated under static conditions, together with an ideal design of individual modulating pole pieces. The dimensions of the magnets, back iron, modulating ring thickness are constant for all cases. Next, the steady-state torque transfer under constant speed is investigated as a function of the initial load angle. Finally, the torque ripples, and magnet eddy current loss under steady-state operation are considered.

2.3.2 Static Analysis

The static analysis enables the modulating capability of the different designs to be investigated. It is expected that the ideal case will produce the highest coupling between the rotors. Fig. 2-18 plots the flux lines for each case. It can be seen that Design 3 results in the highest leakage flux, with similar performance between Designs 1 and 2. To better understand the modulating capability, simulations are carried out with the inner magnets replaced by air. The resulting radial flux density predictions in the inner air gap are plotted in Fig. 2-19. In this simulation case, a good modulator will result in high harmonic content at the high pole number. It can be seen that the ideal case has the highest harmonic content, and Design 3 has the lowest flux density.

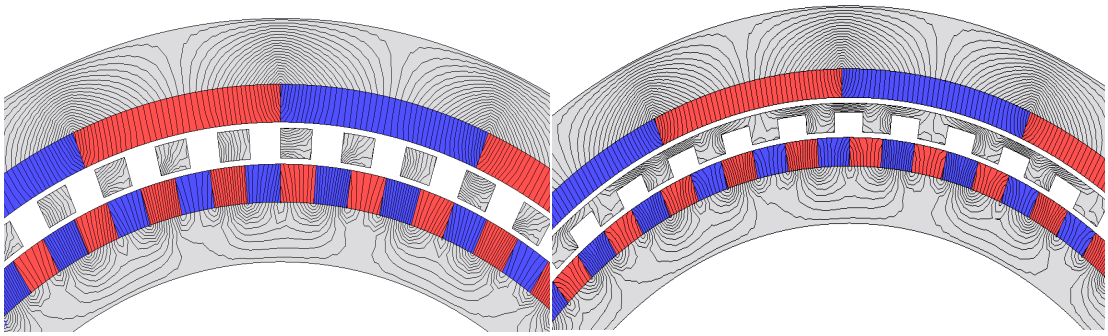

(a) Ideal (b) Design 1

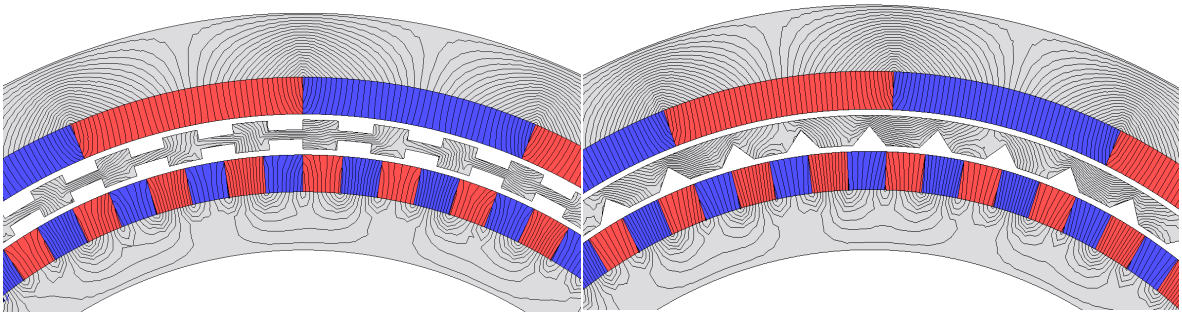

(c) Design 2 (d) Design 3

Figure 2-18 Cross-section of induction motor with integrated magnetic gear, showing flux pattern, magnets interacting with stator flux for different modulating ring designs

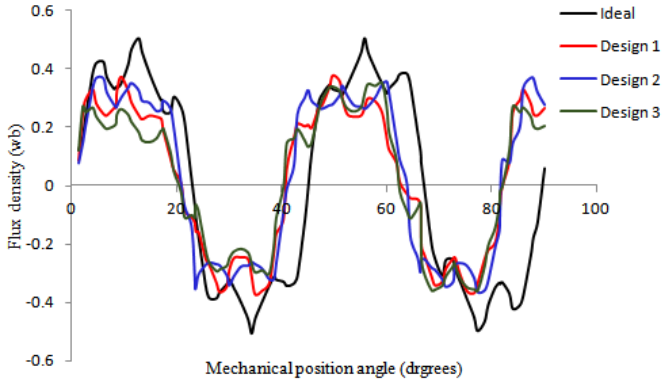

Figure 2-19 Spatial variation in flux density in the inner air gap when only the outer magnets are modeled

2.3.3 Torque capability

The torque capability as a function of electrical load angle is simulated for all four designs. Time-stepped steady-state FEA simulations for each design are performed, changing the initial position from zero to ninety electrical degrees. The modulating ring alignment is such that zero electrical degrees corresponds to maximum torque. Fig. 2-20 shows the magnitude of the torque versus the initial position for the three proposed designs and the ideal modulating ring. (The two rotors are counter-rotating and experience opposing torque.) As expected the ideal design has the most modulation and so highest peak torque capability. The descending order of the peak torque capability of the three designs is design1, design 2, and at last design 3. According to the design and the depth of the modulating waveform, this order is expected.

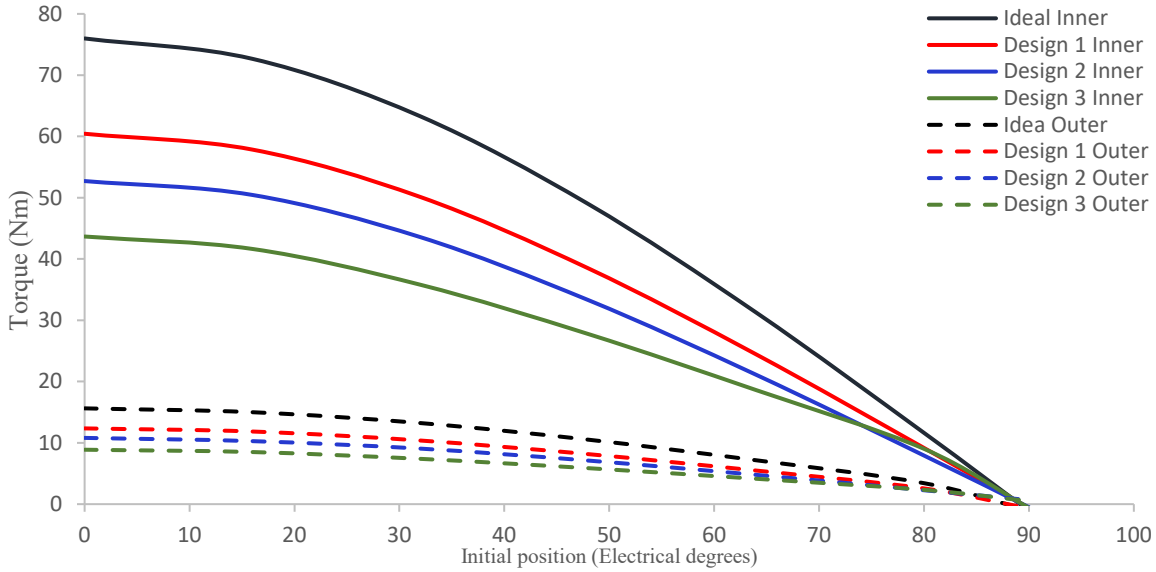

Figure 2-20 Torque – Load angle plot for different modulating ring design magnetic gears

The nominal torque gear ratio for the design is 5.25. Visual inspection Fig. 2-20 indicates that the simulation results give a ratio close to the nominal value. To verify this, Table 2-IV presents the predicted maximum torque values for each case. The predicted torque ratio is within 0.4% of

nominal for all cases.

TABLE 2-IV TORQUE MAGNITUDE PREDICTION AT 0 ELECTRICAL DEGREES

Torque (Nm)	Ideal	Design 1	Design 2	Design 3
Inner rotor	78	62	54	45
Outer rotor	14.9	11.8	10.3	8.6
Torque ratio	5.24	5.24	5.24	5.23

2.3.4 Eddy current losses

Since permanent magnets have high electric conductivity, eddy current will occur in the permanent magnet and decreases the torque transfer and efficiency of the magnetic gear. Eddy current occurs due to variations in magnetic flux density [29].

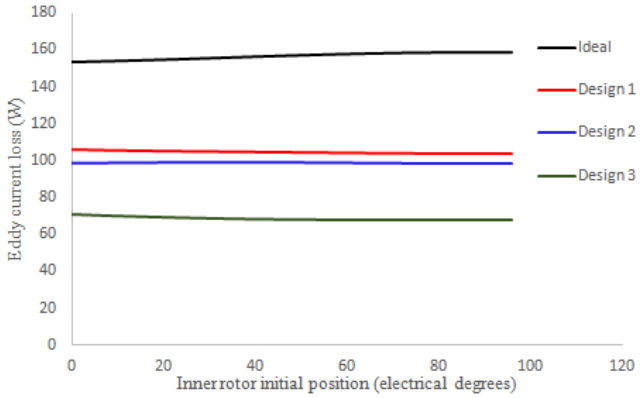

Figure 2-21 Eddy current loss for magnetic gear with different modulating ring designs

Fig. 2-21 shows that the eddy current losses are almost constant with the loading. The higher the torque the gear provides, the higher the eddy current losses. Eddy current losses predominately occur in the inner magnets. For the ideal design, the losses in the outer magnets are around 1.6 percent of the total losses. The outer magnet losses as percentages of the total losses are 1.2, 2.7,

and 2.5 for design 1, design 2, and design 3 respectively. The flux density variations within the center of an inner magnet, for different modulating ring designs, are plotted in Fig. 2-22.

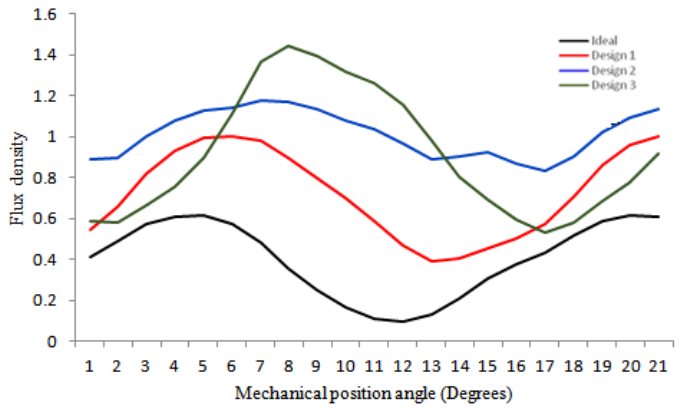

Figure 2-22 Flux density variations for different modulating ring designs

2.3.5 Torque ripple

Torque ripple causes noise, vibration, fatigue, and might reduce the lifetime of the machine. Extensive torque ripple can require measures such as skewing or changes to the machine geometry that might reduce the general performance of the machine. In addition, if these ripples have frequency coinciding with the natural mechanical frequency of the system, severe torsional oscillation will occur, and the shaft may be damaged [15].

As can be seen from Fig. 2-22 all different designs can provide a wide range of similar torque values (at different torque angles) regardless of the modulating ring design. The quality of the torque waveforms is simulated and the harmonic content is evaluated. Simulation results for transient torque under constant speed conditions are presented in Fig. 2-23. In order to have an average torque of 51 Nm from the outer rotor, the torque angle will differ from a design to another. Table 2-V presents the average torque and percentage total harmonic distortion (THD) for different modulating ring proposed designs.

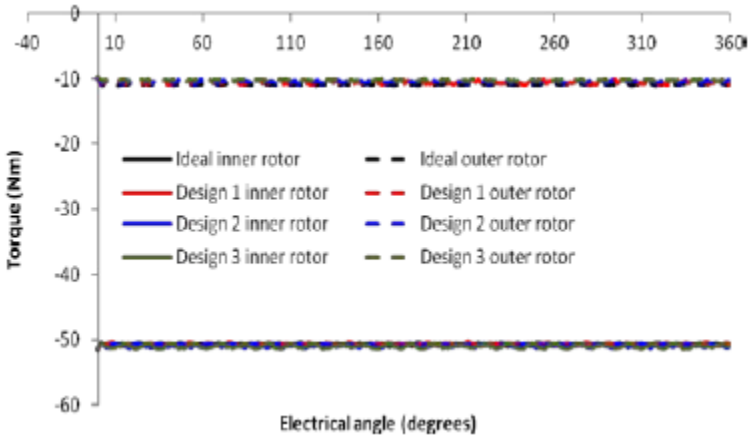

Figure 2-23 Inner and outer rotors torque waveforms for different modulating ring designs

TABLE 2-V AVERAGE TORQUE AND %THD WITH DIFFERENT MODULATING RING DESIGNS

		Ideal	Design 1	Design 2	Design 3
Inner rotor	Average	-50.7	-50.7	-50.9	-50.9
	%THD	0.3	0.27	0.31	0.38
Outer rotor	Average	-10.88	-10.48	-10.44	-10.28
	%THD	0.96	1.4	1.06	1.28

Considering Fig. 2-23 and Table 2-V, it can be seen that changing the design of the modulating ring lamination does not significantly impact the average torque transfer of the gear. However, the ripple content of the torque is impacted. For the outer rotor torque, simulation results show that among the three proposed designs design 2 has the lowest torque ripple and design 1 has the highest ripple content. For the inner rotor torque, design 1 has the lowest torque ripple and design 3 has the highest ripple content. It should be noted that the inner rotor torque represents the

output.

Different designs for the modulating ring of a magnetic gear are investigated in an attempt to simplify modulating ring manufacturability. Time stepped FEA simulation results show the ripple content of the torque may be reduced while the average torque is maintained and the modulating ring is made more robust. Peak torque capability and eddy current losses for the proposed designs are calculated and compared with the ideal design.

Considering the performance of the modulating ring designs, Design 1 and Design 2 offer substantially better torque transfer than Design 3. However, Design 3 has the potential to offer lower magnet losses. In all cases, the losses in the magnets on the high-pole number rotor are predicted to be substantially higher than those on the low pole-number magnet rotor. Assuming that magnet losses can be mitigated by appropriate use of magnet segmentation, Design 1 and Design 2 seem better potential choices. Modulating rings with designs similar to these can be found in the literature, without reference to their relative performance. The results indicate that Design 1, with the bridge on the low pole-number side rather than the center of the ring in Design 2, offers higher torque transfer, similar losses, and with lower punching requirements, simpler manufacturing. In addition, the lower the ripple content in the torque, the lower the shear stress on the modulating ring.

2.3.6 Bridge position

The modulating ring is the most complex part of fabrication. In an ideal explanation of the behavior of the modulator, there are independent pole pieces that modulate the magnet fields. In reality, these parts have to be supported and alignment constraints mean that it is preferable to have the modulating ring constructed from complete laminations, where the pole pieces are connected. For these reasons, the design of a configuration other than separate steel pieces is investigated. The

aim is to have easy to manufacture and robust design. The proposed design is to have interconnecting pieces (bridge) between the modulator teeth. In order to select the optimal position for the bridge from the torque production point of view, a gear model that has a changeable bridge position is implemented using JMAG software. The bridge is one-third of the modulating ring piece thickness and has the same width. The bridge position is changed with steps from position 1 (zero position) to position 12 as shown in Fig. 2-24. The gear performance is tested. The simulation results are showed in Table 2-VI.

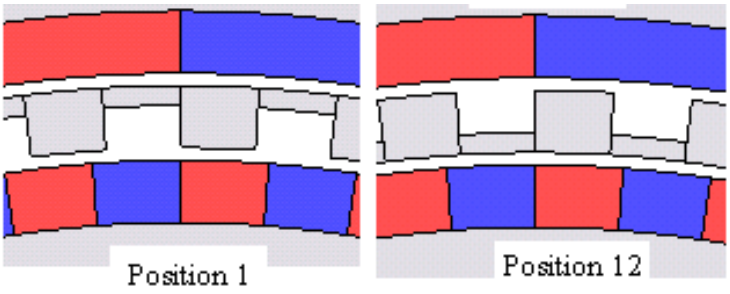

Figure 2-24 Bridge positions

Table 2-VI TORQUE FOR DIFFERENT BRIDGE POSITIONS

No.	Displacement from zero position	Average inner rotor torque	Average outer rotor torque	Torque ratio
1	0	-60.44	-11.52	5.247
2	0.05	-63.64	-12.11	5.255
3	0.1	-62.11	-11.82	5.255
4	0.15	-61.0	-11.61	5.254
5	0.3	-60.4	-11.51	5.247
6	0.5	-58.6	-11.17	5.246

7	0.7	-54.8	-10.44	5.247
8	0.85	-52.72	-10.06	5.243
9	1.1	-50.7	-9.66	5.248
10	1.3	-47.67	-9.08	5.25
11	1.5	-41.13	-7.83	5.253
12	1.7	-33.37	-6.36	5.247

From the table, the optimal position is to start the bridge 0.05 mm from the edge facing the higher number of poles.

Depending on the bridge position, the torque value depends on the amount of flux leakage and the amount of modulation. From Table 2-VI position 2 is optimal from the torque value point of view. Position 8, where the bridge is in the middle of the modulating ring, is expected to be more robust from the mechanical point of view. For position 12, the value of the torque is low and this design is excluded. Looking back to Fig. 2-24, it is obvious that position 12 is an easy leakage path than position 1.

A flux density contour plot for the optimal bridge position is shown in Fig. 2-25.

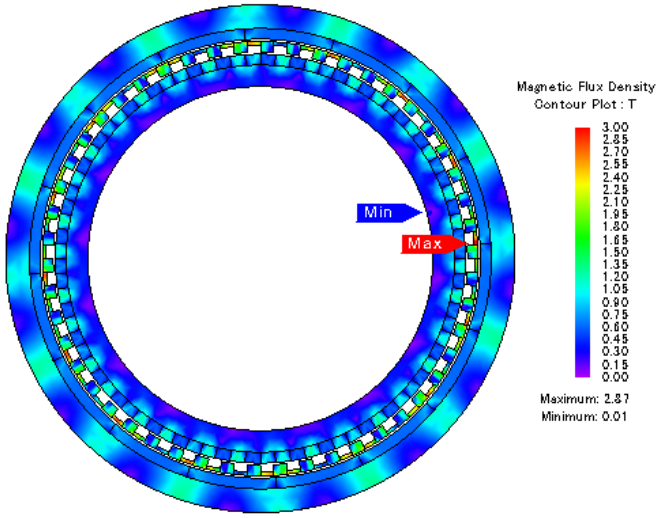

Figure 2-25 Cross-section of induction motor with integrated magnetic gear with optimal bridge position, showing flux density pattern

As expected the highest flux density occurs in the bridge area.

2.3.7 Forces on the modulating ring

The modulating ring can modulate the magnetic fields and make them have the same pole-pair number and speed of rotation in the corresponding air-gap to produce steady torque, which is the field modulation effect. Fig. 2.26 shows linear magnetic gears that represent one-quarter of the machine. Red arrows represent the magnetization direction of the permanent magnets. The magnetic fields produced by the inner and outer rotors are shown in the blue and red curves respectively.

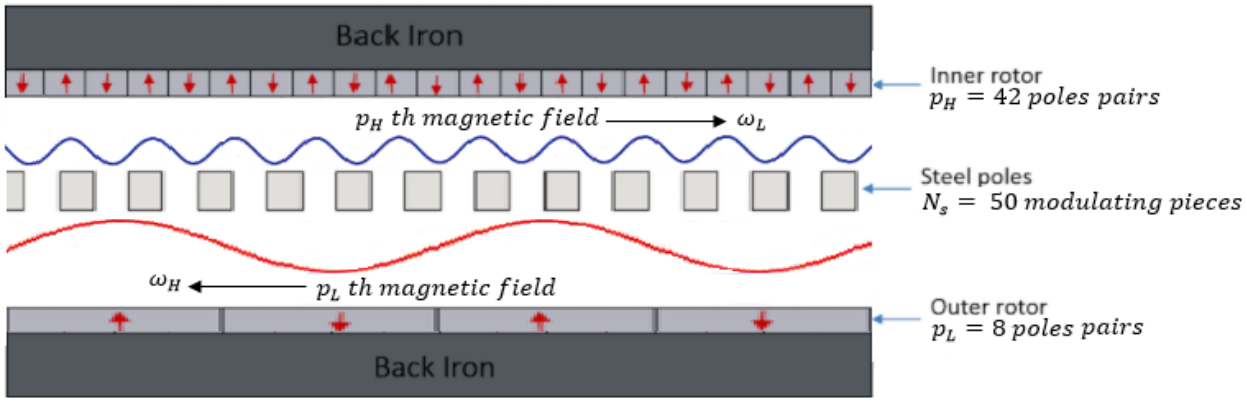

Figure 2.26 Linearized quarter of the magnetic gear

The modulating ring has two forces affecting it. The torque produced on the inner and outer rotor can be calculated, using equation 2-4 through equation 2-11, by the following equations.

$$\tau_H = \frac{{r_H}^2 l}{\mu_o} \int_0^{2\pi} B_{rH}\, B_{tH} d\theta \qquad (2\text{-}13)$$

$$\tau_L = \frac{{r_L}^2 l}{\mu_o} \int_0^{2\pi} B_{rL}\, B_{tL} d\theta \qquad (2\text{-}14)$$

Where l is the core stack length, μ0 is the permeability of the vacuum, r_H and r_L are the radius in the inner and outer air-gaps, respectively. B_{rH} in and B_{tH} in are the radial and tangential magnetic flux densities in the inner air-gap, respectively. B_{rL} out and B_{tL} out are the radial and tangential magnetic flux densities in the outer air-gap, respectively.

The modulating ring has two torques affecting it and shear and twisting forces due to different torque on both sides of the modulating ring are affecting the modulating ring.

2.4 Summary

A brief review of magnetic gear construction and design is introduced. Mathematical equations for magnetic gear design are derived. Two different magnetic gear designs are investigated and simulated. 42/8 magnetic gear is chosen to implement. Six different modulating

ring designs are investigated and their simulated performance is compared. An h/3 bridge size is chosen for implementation. The bridge position is investigated and a 0.05 mm from the edge is recommended to manufacture. Three different modulating rings laminations are used to experimentally compare their performance as will be discussed in chapter 4.

CHAPTER 3: INDUCTION MACHINE WITH INTEGRATED MAGNETIC GEAR

This chapter explores the possibility of integrating a magnetic gear with an induction machine. Induction machine design will be discussed. The integration of the magnetic gear and the induction machine, simulations, and data analysis will be introduced in details.

Low-speed high-torque electrical machines have many applications. In order to have low-speed and high-torque from an electrical machine, the machine can be designed to operate at the desired speed or the machine output can be geared to the desired speed. Satisfying the load requirements need to be done with high efficiency, low cost, minimal size, and simplicity. Since the machine size is directly proportional to the torque, a high torque machine means a large one. Direct drive machines at high torques are not promising due to size, and mass [1-4].

Low-speed, high-torque machines are significant problems in an application where size and mass are big concerns. To have a high torque machine with a smaller size and a lower cost, electrical motors were been integrated with magnetic gears [1, 2].

Due to its high torque density, permanent magnet (PM) machines were integrated with magnetic gears and resulted in a high-torque low-speed drive which eliminates mechanical gearbox with all its related concerns and has high reliability, low maintenance, low cooling requirements, inherent torque overload protection and low NVH (Noise, Vibration, and Harshness) [7-13].

PM machines integrated with magnetic gears have been used in many applications such as electric vehicle traction, wind turbines, ship propulsion systems, aerospace actuation, and industrial applications that require a high-torque, low-speed drive [1-13].

However, there remain several applications where low speed, high torque characteristics are required, but the industrial system to be driven is well suited to an induction machine drive.

Examples may include systems with a long cable an isolation transformer between drive and motor; or systems that may exhibit significant backlash, windup, or potential for jamming. In these cases, an induction machine with integrated magnetic gear may be a good solution. In order to develop a high-power-density high-efficiency motor at a lower cost; integrating a three-phase induction machine with a magnetic gear is being investigated.

Induction motors are simple, robust, rugged in construction, and can operate in any environmental condition such as polluted, and explosive environments. A three-phase induction motor will have self-starting torque, easy operation, durability, low cost, maintenance-free, and high starting torque. [7], [8]. In addition, induction machines offer simplified open-loop control or simple 'sensorless' closed-loop control and lower cost.

Potential applications for an induction motor with integrated magnetic gear are those where high torque density is desirable and the operating environment may make conventional gearing undesirable. Relative to PM machines, a clear advantage is the case where the machine is remote from the control. Such cases may require transformers or filtering between the drive and the machine, making sensorless control difficult. The combination of an induction machine with magnetic gearing also has the potential to be lower cost than a PM machine with integrated gear. Potential applications include as an alternative to hydraulic motors, such as in oilfield applications; mechanical crushers, drilling motors, or wind generation.

This work discusses an investigation into the potential of a cage induction motor with an integrated internal magnetic gear. While the target application may typically be a large machine, the potential of such a system is investigated at a reduced scale, with a target of 1.5kW, and speed in the 220 rpm range. This chapter presents the design process, initial design, and the simulation of the performance of an induction motor with an integrated magnetic gear at different loading

conditions.

3.1 Induction motor design

As described in the previous chapter, the magnetic gear design is carried out assuming integration with a 6-pole induction motor. To balance the gear load on the outer rotor, a design torque of 12.4 Nm is required at 1155rpm. The design process for the induction machine is a conventional one, beginning with basic assumptions for electric and magnetic loadings. However, to integrate a magnetic gear with the induction machine, modifications from conventional designs rapidly become apparent. To fully utilize the torque potential from a given force density, the magnetic gear performance is improved with a large radius. The resulting magnetic gear design has a relatively short stack length compared to the diameter. While this work describes the induction machine design and gear design separately, in reality, an iterative process is required to define parameters about which to finalize designs. Additionally, constraints that may normally be placed on an induction machine design process may be relaxed. Starting current, pull-up, and pull-out torque constraints are not required as the motor is intended for operation from a variable speed drive. The pull-out torque requirement is reduced as the magnetic gear will pull-out before the induction machine reaches maximum torque.

Without the use of a gear system, the design target of 220 rpm at 60 Hz would require a machine with 32 poles. This may be possible with a concentrated winding PM machine, but a number of papers, e.g. [64] have shown the difficulty of implementing high pole number induction machines. As an initial starting point for a system with a magnetic gear, a 6-pole induction motor is used as a base design. The design process to develop an integrated machine requires analysis of a synchronous system, the magnetic gear, plus an asynchronous machine. While the final system

may result in linked magnetic fields from the two sub-systems, in this work, the design process is: to first develop a suitable magnetic gear design; secondly, design an induction machine that uses the magnetic gear size to define its interior parameters; finally, investigate any unwanted cross-coupling effects and modify the design accordingly. This process has been used to ensure that the magnetic gear components may be physically realized.

It can be seen from chapter 2 that the magnetic gear design that meets the torque and speed requirements has an aspect ratio with a relatively short shaft and large diameter. To enable an integrated magnetic gear, the induction motor must have a stack length of 54 mm with an inside diameter of 118 mm. However, during the design process, constraints that may normally be placed on an induction machine design are relaxed as the motor is not intended to be required to operate under direct on-line starting. A conventional induction motor design process is used, together with commercial motor design software (JMAG Express). Parameters for a candidate 6-pole design that meets the requirements are shown in Table 3-I, with a schematic cross-section in Fig. 3-1. Note that the combination of an 8 –pole outer rotor magnetic gear with a 6-pole induction machine design requires a full machine model with no periodic boundary.

When simulating a steady-state speed of 1172 rpm, the induction motor predicted torque is 12 Nm. Therefore it can be seen that at close to 1172 rpm, the induction torque on the rotor will be equal to the torque from the magnetic gear.

TABLE 3-I. INDUCTION MACHINE PARAMETERS

Rated voltage	120 V
Rated frequency	60 Hz
Number of stator poles	6 poles
Number of turns	17 turns
Number of stator slots	36 slot
Tooth width	8 mm
Core back width	14 mm
Stator outer radius	115 mm
Stator inner radius	80.6
Air gap	0.6 mm
Length	54 mm
Number of rotor bars	40 bars
Distance between bar edge centers	6 mm
Bar outer radius	3 mm
Bar inner radius	3 mm

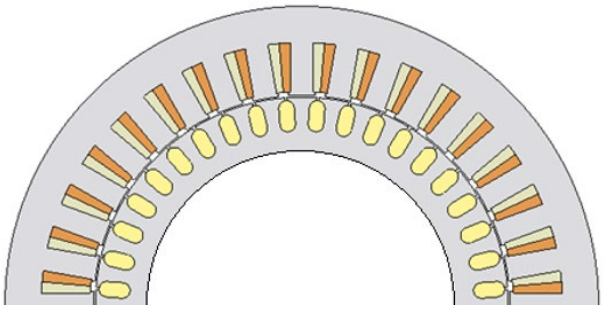

Figure 3-1 Induction motor cross-section

The torque-speed characteristic of the induction motor is evaluated by means of a series of time-stepped finite element simulations at a constant speed. Simulations of induction motor operation under constant speed operation are carried out for a number of slips, and the resulting torque – speed curve for low slips is plotted as shown in Fig. 3-2. It can be seen that the induction machine is capable of producing almost double the desired torque at the initial design speed of 1155rpm. The required torque is obtained at a speed of 1172rpm. When simulating a steady-state speed of 1172 rpm, the induction motor predicted torque is 12 Nm, as shown in Fig. 3-3. The plot of the variation of slip with time indicates that although the rotor is not skewed, the torque ripple is not significant. Based on this analysis it can reasonably be assumed that that at close to 1172 rpm, if the induction machine is integrated with the magnetic gear, the induction torque on the rotor will approximately be equal and opposite to the torque from the magnetic gear.

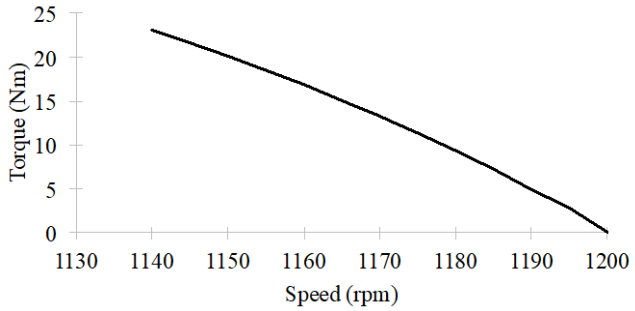

Figure 3-2 Induction motor torque-speed curve

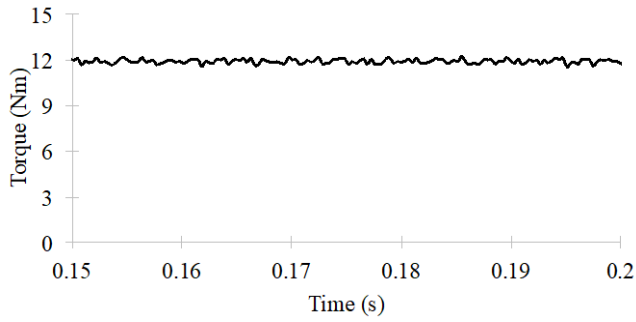

Figure 3-3 Induction machine torque at 1172 rpm

3.2 Induction machine integrated with magnetic gear

The design process to develop an integrated machine requires analysis of an asynchronous machine coupled with a synchronous gear, with two rotors interacting to produce torque across three air gaps. In order to simulate this set of conditions in a reasonable time but with accuracy to understand harmonic torques, time stepped FEA simulations are carried out under constant speed conditions. The combination of a 3-pole pair induction machine with an even pole pair gear means that the machine has no magnetic symmetry and simulations must consider the whole machine.

As an initial simulation point, the torque-speed characteristics of both the magnetic gear and the induction motor may be compared to find a load angle and outer rotor speed that should result in two equal and opposite torques applied to the outer rotor. However, the flux path in the induction machine may interact with that of the magnetic gear. Flux line plots, showing the interactions of the two magnetic devices are shown in Fig. 3-4 and Fig. 3-5. In Fig. 3-4, the flux lines passing through the central two magnets can be seen to follow a closed path that does not cross the rotor-stator air gap.

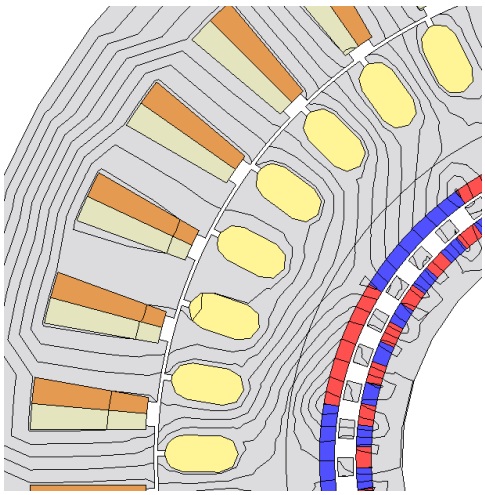

Figure 3-4 Cross-section of an induction motor with an integrated magnetic gear, showing flux pattern, magnets interacting with the stator flux

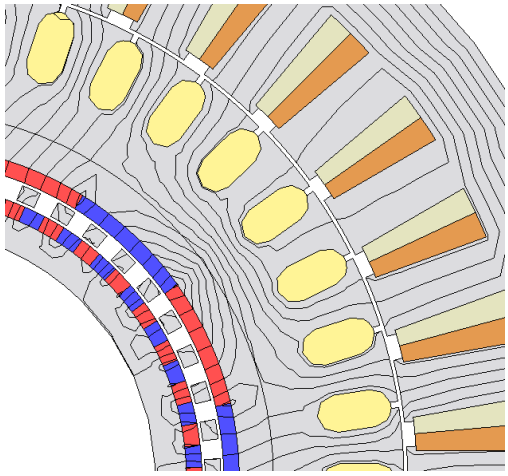

Figure 3-5 Cross-section of an induction motor with an integrated magnetic gear, showing flux pattern, magnets not interacting with the stator flux

However, in Fig. 3-5, the flux lines passing through the magnets can clearly be seen crossing the air gap and interacting with the stator. Due to this interaction, a time stepped FEA simulation of the integrated machine at a speed and a load angle that appear to balance the outer rotor torques, does not result in a balanced operation. Table 3-III presents the results of 4 simulations at a constant speed of 1176 rpm as the load angle is adjusted until the net outer rotor torque is close to zero. In the data in table 3-III, the torques are positive in a counter-clockwise direction. The stator torque is the reaction torque, where a negative value indicates a positive torque applied to the outer rotor. The outer rotor torque is the net torque applied to the outer rotor. The inner rotor torque is the net torque applied to the inner rotor, where negative torque indicates support for the motion in the negative (clockwise) direction. It is clear from the data in the table that the torque transmitted between the stator and the outer rotor is not significantly affected by changes to the gear load angle. However, a simulation that only considers the inner rotor torque is not balanced, there is a negative torque on the outer rotor, indicating that the outer rotor is trying to slow down, changing the load angle and output torque. To accurately model the case with net-

zero torque on the outer rotor, multiple simulation cases are required to iteratively adjust the load angle until the balance is found. An alternative approach to estimate steady-state torque performance can be found by considering the net airgap power of the two rotors. Summing to find the net inner and outer rotor torques return a net output power that is close to the balanced case, enabling fast analysis of the overall performance characteristics.

TABLE 3-II. STEADY STATE ESTIMATION OF OPERATING CONDITIONS AT 1176 RPM, DIFFERENT LOAD ANGLES

Case	**Torque (Nm)**			**Airgap Power (W)**				**Torque**
	Inner	***Outer***	***Stator***	***Inner***	***Outer***	***Stator***	***Net***	***Estimate***
A	-69.1	-2.5	-10.9	1622	-313	1344	1309	-55.8
B	-66.9	-2.1	-10.9	1570	-263	1344	1307	-55.8
C	-65.2	-1.8	-10.9	1529	-222	-1344	1307	-55.8
D	-53.4	0.1	-10.6	1266	7.4	1308	1274	-54.3

While the above estimation technique proves useful to understand the overall performance capabilities of the integrated machine, a detailed simulation of the case with balanced outer rotor torque and output power close to 1.5kW is carried out. Under this condition, the outer rotor speed is 1172 rpm, the inner rotor speed is 223.2 rpm and the electrical load angle between gear rotors is 31.2 degrees. The resulting simulated torques are plotted in Fig. 3-6. The mean induction torque is 12.2 Nm and the outer rotor torque 65.3Nm, giving an output power of 1.52kW. In this case, the steady-state error for the outer rotor torque is -0.5Nm.

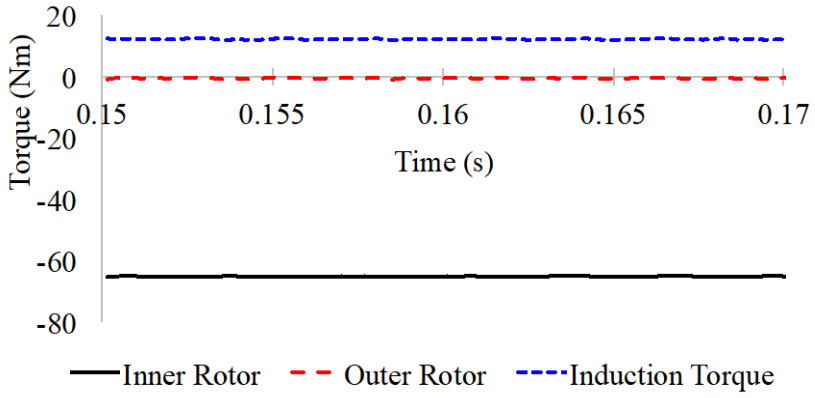

Figure 3-6 Torque of the induction machine integrated with magnetic gear

The design process to develop an integrated machine requires analysis of a synchronous system, the magnetic gear, and an asynchronous machine. While the final system may result in linked magnetic fields from the two sub-systems, in this work, the design process initially addresses each of the sub-systems individually. The first step is to develop a suitable magnetic gear design; the second is to design an induction machine that uses the magnetic gear size to define its interior parameters. The final stage of the design process is to, investigate any unwanted cross-coupling effects and modify the design accordingly. This process has been used to ensure that the magnetic gear components may be physically realized.

The final stage of the design process is to integrate the motor and gear. Since the induction machine action and outer magnetic gear share back-iron, it is expected that the fields from these components will cross-saturate and may interact. The net effect of this interaction is minimized by the pole combinations chosen earlier. The induction machine is a 6-pole system, while the outer rotor has 16 poles. The reluctance of the magnetic gear is similar to a large air gap, as seen from the stator, while the high outer gear pole number will limit the penetration of the gear flux through the outer rotor. A negative impact of this, from the investigation and simulation perspective, is that there is no magnetic symmetry in the system and a full machine model is required. A schematic

showing the assembly is shown in Fig. 3-7 and a flux density pattern is shown in Fig. 3-8.

The machine under investigation is an integration of a 6 pole induction machine and a magnetic gear with a gear ratio of 5.25, corresponding to 42 inner poles and 8 outer poles. The construction of the machine integrated with magnetic gear requires four concentrically aligned parts: an outer stator; an outer rotor; a modulating ring and an inner rotor. The outer stator and modulating ring are stationary, while the outer rotor and modulating ring only transfer torque, they are not externally connected.

Considering a general radial flux magnetic gear assembly, the gear consists of three mechanically centered rotors. In one possible configuration, one rotor contains an array of a large number of permanent magnets and rotates slowly; the other rotor contains an array of a low number of permanent magnets and rotates at a high speed; the middle rotor contains an array of modulating steel poles. The inner and outer rotors that contain PMs interact with the middle ferromagnetic pole pieces to create space harmonics and modulate the magnetic flux generated by the two rotors to create a stable gear ratio [10].

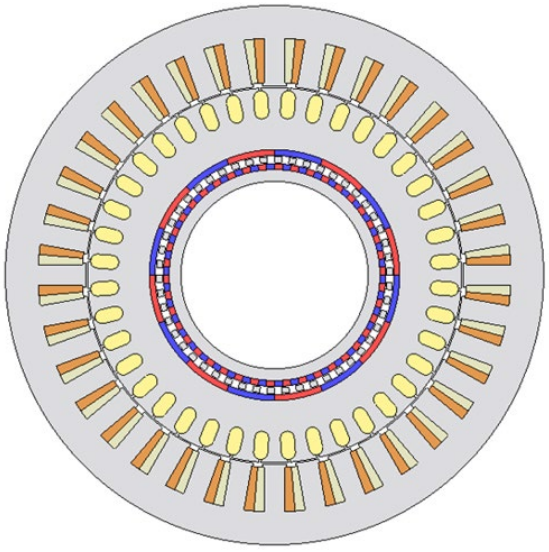

Figure 3-7 Cross-section of an induction motor with an integrated magnetic gear

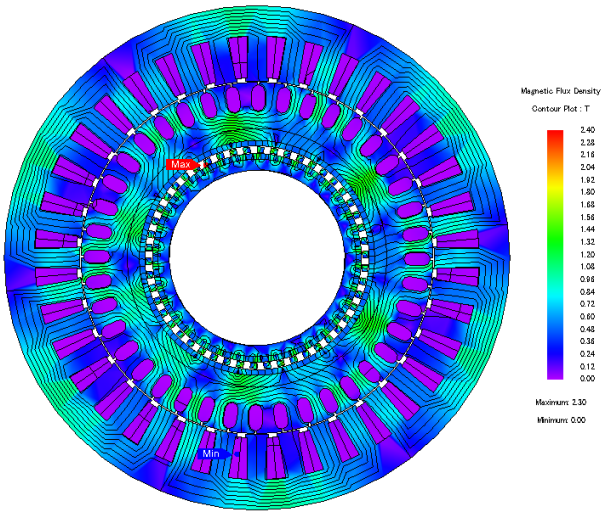

Figure 3-8 Cross-section of an induction motor with an integrated magnetic gear, showing the flux density pattern

The interaction of the magnetic fields in the outer rotor requires either a full mechanical dynamic simulation to balance torques, or an iterative set of constant speed, constant load angle simulations. The latter option is used in this work. In the FEA tool used for this work (JMAG Designer), the torque is calculated as the total torque exerted on a component. In steady-state for the magnetic gear system, the net torque on the outer rotor should be zero. The torque transmitted from the stator to the outer rotor may be evaluated by calculating the reaction torque exerted on the stator.

Simulation of operation at 1172 rpm for the outer rotor, 223.2 rpm for the inner rotor, and initial electrical angle of 31.2 degrees gives the torque data plotted in Fig. 3-6. In this diagram, induction torque is shown as positive, supporting the counter-clockwise rotation of the outer rotor. The inner rotor torque is calculated as having a negative value, supporting a clockwise rotation of the inner rotor. For the period shown in Fig. 3-6, the mean induction torque is calculated to be 12.2 Nm, the mean torque transmitted to the inner rotor is 65.3Nm, corresponding to an output power

of 1.52kW. The calculation also indicates that the net outer rotor torque is -0.5Nm. This illustrates the impact of the interaction of the magnetic fields of the two subsystem components, the ideal linear sum of components at this condition should give zero net torque to the outer rotor. However, the result is considered acceptable to begin a prototype investigation.

The torque density of the proposed prototype may be calculated in terms of total volume and active volume, neglecting end winding overhang. The applications envisaged for this type of machine are expected to be at higher power levels than the 1.5kW target in this paper. At low power, the stack length is relatively short due to the limits on magnet size that have been imposed to facilitate assembly, (the induction machine is short with a large diameter when compared to a commercial 1.5kW 6-pole motor). The end winding overhang is expected to exceed the stack length in the prototype. The total net torque density for the system including an allowance for end windings is expected to be 15.6kNm/m^3 rated, 19.1kNm/m^3 peak. Using active volume as a guide for scaling to larger machines, the torque density values are 33kNm/m3 rated, 40.5kNm/m3 peak.

3.3 Loading

To show the overall machine performance Fig. 3-9 plots the torque-speed characteristics of the machine under investigation.

Simulation of torque-speed characteristic shows that it is complicated to combine asynchronous and synchronous torque mechanisms. An iterative process is required at each load condition, in order to identify the exact speed and load angle combination such that the net torque on the outer rotor is zero. If this torque is non-zero, the outer rotor is effectively a second mechanical output port, complicating efficiency calculations from input power and inner rotor output power. To enable rapid calculations of the potential performance in the initial design stage

this reason, the efficiency is calculated by subtracting calculated losses from the simulation input power.

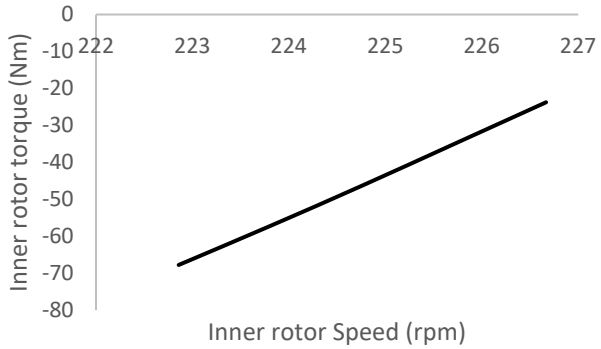

Figure 3-9 Torque-speed of the induction machine integrated with magnetic gear

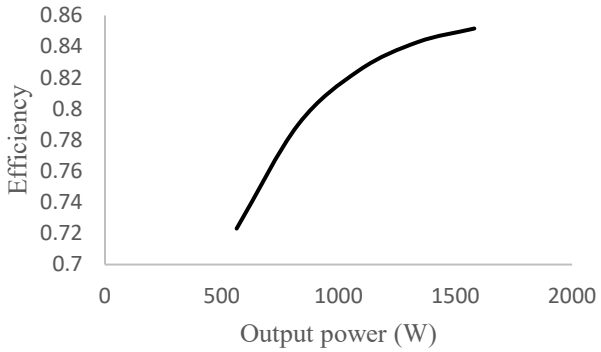

Figure 3-10 Efficiency –output power

The efficiency curve is shown in Fig. 3-10. A commercial 1.5kW 6-pole motor has an efficiency of around 82%; the simulated efficiency of the proposed machine is more than 85% and also has the ability to run at low speed and has high torque due to the presence of the magnetic gear.

3.4 Loss analysis

Torque transmission of a magnetic gear is based on the modulation of the magnetic field using ferromagnetic pole pieces between the outer rotor and the inner rotor. However, because of

the modulation effect, the magnetic fields produced by either the outer or the inner permanent magnets have many sub-harmonics. These unwanted harmonics lead to undesirable effects, such as high permanent magnet eddy current loss and iron core loss, low efficiency, noise, and vibration. Due to the significant amount of heat caused by the losses, partially irreversible demagnetization of the magnets may occur.

3.4.1 Joule loss

These losses occur due to the current flowing in stator and rotor windings. As the load changes, the current flowing in rotor and stator winding also changes, and hence these losses also change.

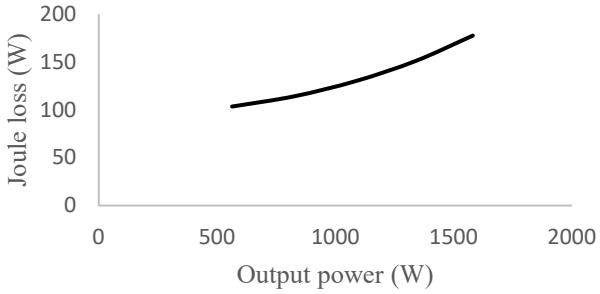

Figure 3-11 Joule loss –output power

Fig. 3- 11 shows how the joule loss changes at different load output power.

3.4.2 Iron loss

Iron loss is calculated in two components: eddy current loss and hysteresis. The eddy current losses are assumed to be proportional to the square of frequency and the hysteresis losses proportional to frequency. The frequency of the field in the stator is always the supply frequency, f and the fundamental frequency in the rotor is slip times the supply frequency, (sf) which is always less than the stator frequency. Hence the rotor core loss is very small as compared to stator core loss.

Hysteresis and eddy current losses in each part of the machine are shown in Fig. 3-12, and Fig. 3-13 respectively.

As expected the losses in the moving parts are less than the losses in the stator.

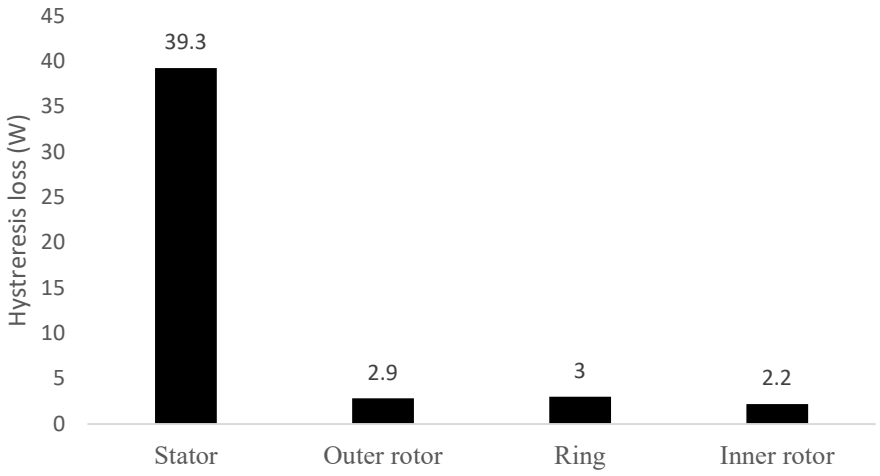

Figure 3-12 Hysteresis loss distribution in the different machine parts

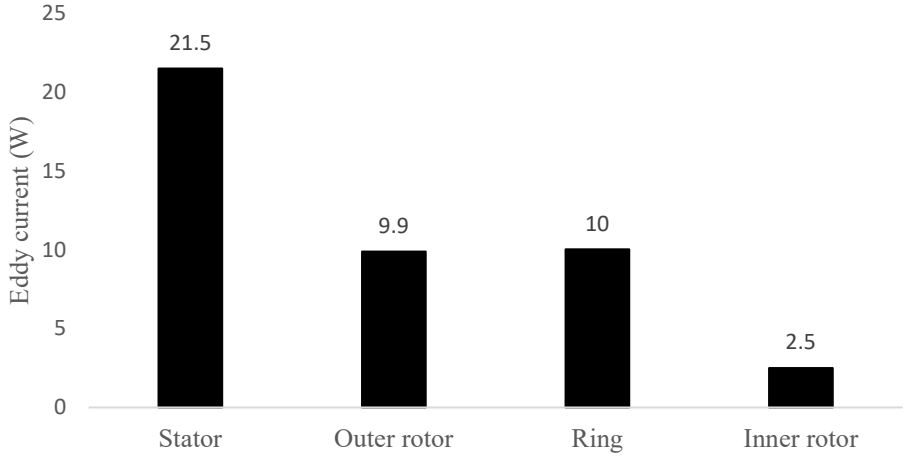

Figure 3-13 Eddy current distribution in the different machine parts

The harmonic orders can be expected from the interaction between magnetomotive force M and permeance P as follow:

$$M = M\cos(p\theta - \omega_1 t) \qquad (3-1)$$

$$P = P_o + P_{ss}\,(\cos N_s\,\theta) \qquad (3-2)$$

Slotting frequency seen by the rotor is:

$$1 - \frac{p \pm N_s}{p}(1-s) \times \text{supply frequency} \qquad (3-3)$$

For 6 poles, and 36 slot stator the expected harmonic orders in the rotor are $s \pm 12n(1-s)$ where n is an integer. When the motor is running at 1170 rpm so the slip s = 0.025 so the expected harmonic orders in the rotor are $|0.025 \pm n11.7|$ which can be seen in Fig. 3-12.

The harmonic content of the joule loss component of iron loss in the different machine parts is shown in Fig. 3-14, Fig 3-15, and Fig. 3-16. Induction rotor losses are at the frequencies given by (10), stator loss occurs primarily at fundamental supply frequency, plus 11th and 13th harmonics. Losses in the ring and inner rotor are substantially lower than in the other parts of the machine.

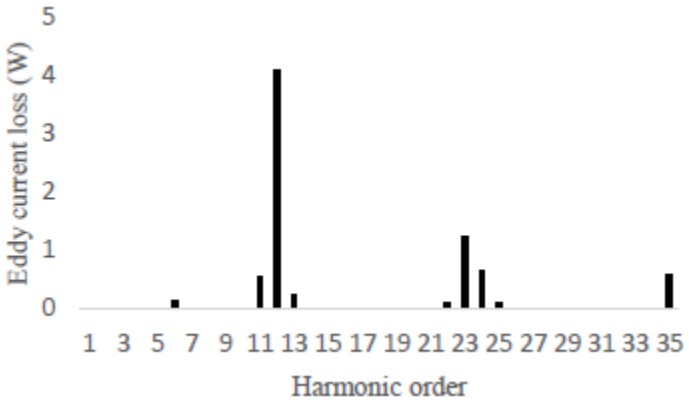

Figure 3-14 Spectrum of joule loss (iron loss) in the induction motor rotor

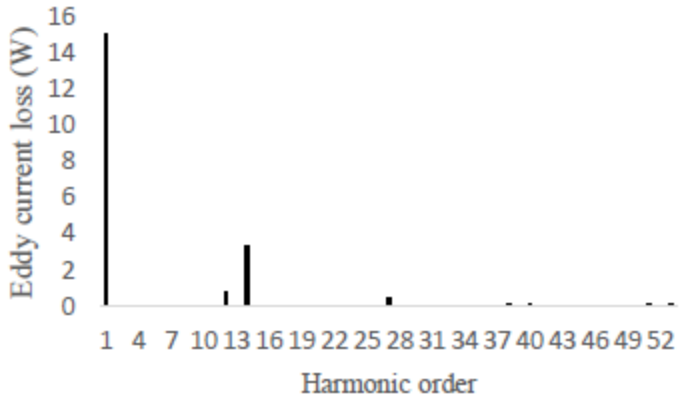

Figure 3-15 Spectrum of joule loss (iron loss) in the induction motor stator

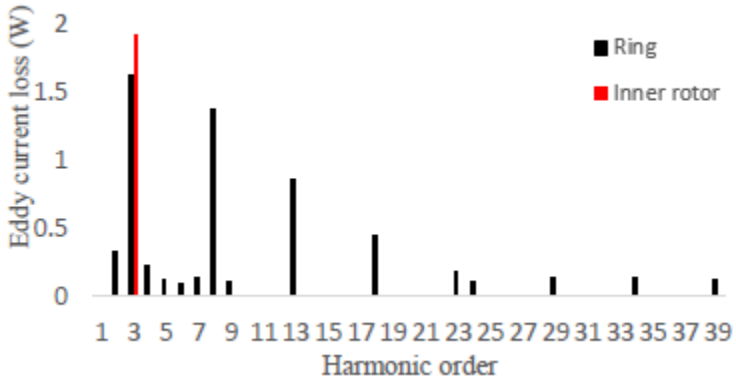

Figure 3-16 Spectrum of iron loss in the ring and inner rotor

The iron loss could be separated into two combinations: eddy current loss and hysteresis loss. The first one is thermal loss by current circulation and depends on the type of steel and the thickness of the laminations. The second one is the loss in the magnetization process and the demagnetization process. The total iron loss is only in one frequency, as the hysteresis loss does not have harmonic components. In this plot, the iron loss of the induction motor stator is the highest as expected and discussed earlier, losses in the induction motor rotor and modulating ring almost the same, and iron loss in the gear rotor is the lowest.

3.5 Summary

This Chapter presented an investigation into the feasibility of incorporating a magnetic gear into an induction machine system. The resulting machine offers high-torque low-speed output at high torque density and may enable simple sensorless operation, either from grid connection or from open-loop control. The combination of high torque density and low-to-no control complexity is attractive for many applications. Machine design and simulation are been discussed. The simulation results so far have demonstrated the feasibility of implementing this machine.

CHAPTER 4: PROTOTYPE MOTOR AND TEST FACILITY

This chapter provides detailed steps of the machine prototype manufacturing process such as lamination design and manufacturing, winding of the stator, and assembly of all the machine parts. A squirrel cage induction motor with an integrated internal magnetic gear is designed at a reduced scale, with a target of 1.5kW, and speed in the 220 rpm range is designed and built. This chapter presents the assembly process and shows the machine fabrication progress. An open-loop V/F controller -used to drive the machine- will be discussed.

4.1 Induction machine with integrated magnetic gear

The machine under investigation is an integration of a 6-pole induction machine and a magnetic gear with a gear ratio of 5.25, corresponding to 42 inner poles and 8 outer poles. A schematic showing the assembly is shown in Fig. 4-1 and Fig. 4-2. Table 4-I shows the induction machine and the magnetic gear parameters.

The construction of the machine integrated with magnetic gear requires four concentrically aligned parts: an outer stator; an outer rotor; a modulating ring and an inner rotor. The outer stator and modulating ring are stationary, while the outer rotor and inner rotor are free to run. Modulating ring only transfer torque, they are not externally connected.

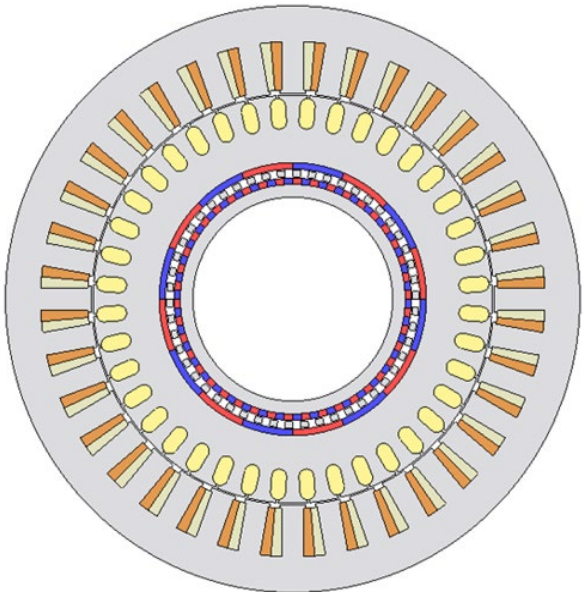

Figure 4-1. Cross-section of induction motor with an integrated magnetic gear

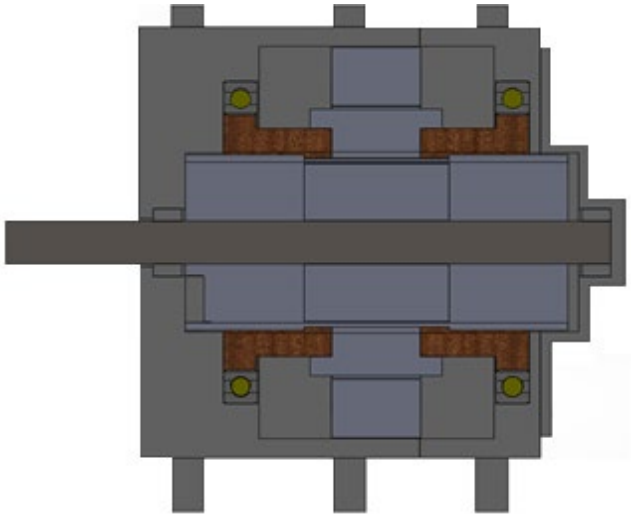

Figure 4-2. Longitudinal cross-section assembly drawing of induction motor with an integrated magnetic gear

TABLE 4-I Induction machine and magnetic gear parameters

Induction machine		Magnetic gear	
Rated voltage	120 V	Inner rotor pole pairs, p_H	21
Rated frequency	60 Hz	Outer rotor pole pairs, p_L	4
Number of stator poles	6 poles	Modulating ring pieces, N_S	25
Number of turns	17 turns	Gear ratio, G	5.25
Number of stator slots	36 slot	Air gap (inner and outer rotor sides)	0.5 mm
Tooth width	8 mm	Magnet thickness	2.5 mm
Core back width	14 mm	Modulating ring piece thickness	2.5 mm
Stator outer radius	115 mm	Outer airgap radius	59 mm
Stator inner radius	80.6	Inner airgap radius	47.5 mm
Air gap	0.6 mm	Shaft radius	40 mm
Length	54 mm	Stack length	54 mm

Number of rotor bars	40 bars		
Distance between bar edge centers	6 mm		
Bar outer radius	3 mm		
Bar inner radius	3 mm		

4.2 Outer stator

The stator of the machine is a conventional stator of an induction machine with the parameters shown in Table I. The stator pole number is chosen to ensure that stray magnet flux from the outer gear mechanism does not link the coils to produce unwanted harmonics in the stator voltage.

4.2.1. Laminations

The prototype final design using JMAG designer is discussed in Chapter 3. The stator laminations have been drawn using AutoCAD software and have been sent to an external manufacturer company Proto Laminations Inc. [81]. Based on the AutoCAD designs, stator and modulating rings laminations are laser cut and delivered by the manufacturer company.

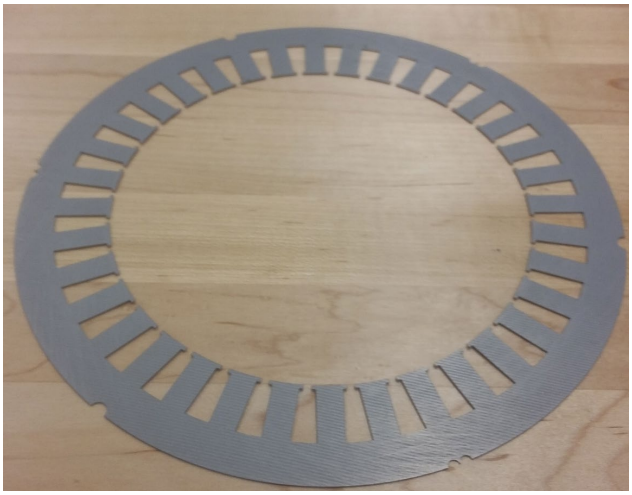

Figure 4-3 Stator lamination

The stator laminations have been attached and welded together to make the 54 mm stator stack in the machine shop of the University of Calgary. With laminations thickness of 0.45 mm, around 120 laminations are used.

4.2.2. Windings

The stator is wound with 6-pole three-phase single layer fully-pitched windings in an external electrical shop Bata's Electric [82]. The windings specifications are as follows,

a) Turns per coil: 34 turn

b) Slot/pole/phase : 2

c) Conductor size: AWG 15

Figure 4-4 Wound stator

The wound stator is shown in Fig. 4-4.

The casing for the machine is made in the machine shop of the University of Calgary and Fig. 4-5 shows the stator inside the casing.

Figure 4-5 Machine stator

4.3 Outer rotor

The rotor has been manufactured at National Cheng Kung University in Taiwan [83]. An AutoCAD drawn lamination is sent along with the rotor specifications in Table 4-I and the end ring details shown in Fig. 4-7. The machine's outer rotor is made. The rotor lamination has a thickness of 0.34 mm so the stack length is made using about 160 laminations.

Figure 4-6 Rotor lamination

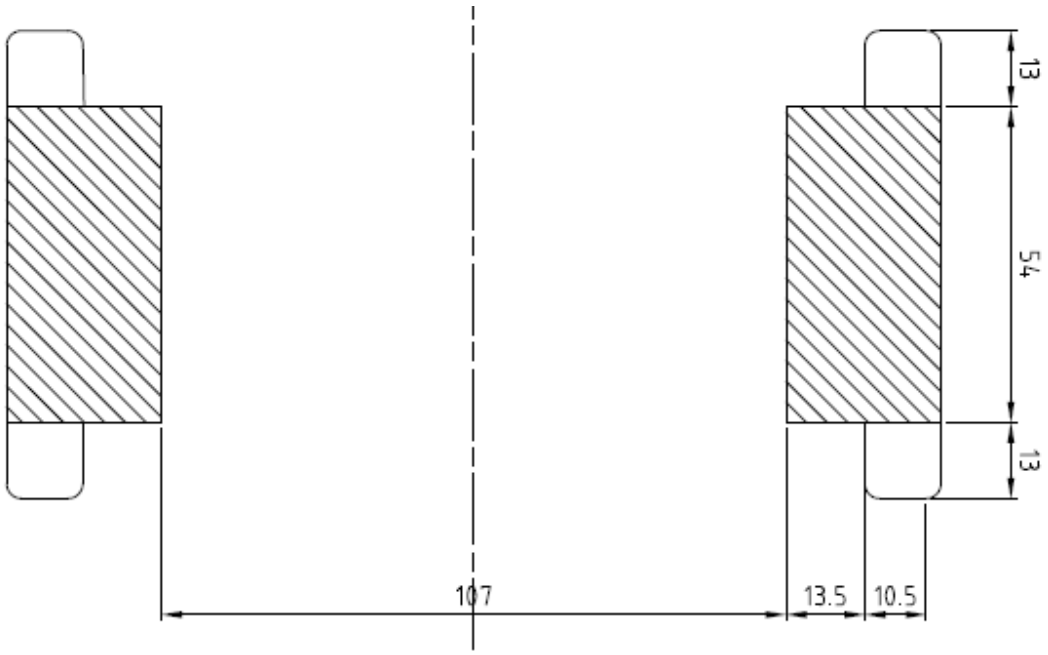

Figure 4-7 AutoCAD drawing of the outer rotor with end ring

The finished rotor is shown in Fig. 4-8.

Figure 4-8 Outer rotor

In order to evaluate the performance without stray effects due to structural steel, micarta parts - a non-magnetic and easily machinable for prototyping – are used to hold the induction machine rotor and provides a mount for the ring bearings which suspends this rotor from the outside of the stator housing. Fig. 4-9 shows the outer rotor of the machine after sticking the micrata.

Figure 4-9 Outer rotor with micrata parts

The outer rotor is a shaft-less structure, with a cage rotor to the outside of the rotor and a low pole-number permanent magnet assembly for the magnetic gearing on the inner surface. The rotor cage is cast aluminum, parameters of the cage and the magnet are summarized in Table 4-1. The magnets used are NdFeB, Grade N42. As shown in Figure 4-1, the magnets should be 16 arc magnets. In order to keep the cost of prototyping reasonable these arc magnets are replaced by

rectangular prism magnets with dimensions of 1" x 1/8" x 1/8" thick, (25.4 mm x 3.175 mm x 3.175 mm). Each pole is made by two rows of six magnets. Fig. 4-10 shows the inside of the outer rotor with the magnets and micrata parts.

Figure 4-10 The inner side of the inner rotor with magnets

Each of the two endplates has a bearing for the outer rotor.

4.4 Modulating ring

The modulating ring is the most complex part of fabrication. In an explanation of the behavior of the ideal modulator, there are independent pole pieces that modulate the magnet fields. In reality, these parts have to be supported and alignment constraints mean that it is preferable to have the modulating ring constructed from complete laminations, where the pole pieces are connected. For these reasons, the design of a configuration other than separate steel pieces is investigated. The aim is to have easy to manufacture and robust design. The proposed design is to have interconnecting pieces (bridge) between the modulator teeth. Three different designs are simulated and manufactured.

4.4.1. Laminations

Three modulating rings laminations have been drawn using AutoCAD software and have been sent to an external manufacturer company Proto Laminations Inc. [81]. Based on the AutoCAD designs, stator and modulating rings laminations are laser cut and delivered by the manufacturer company. Fig. 4-11 shows the three different designs laminations.

4.4.2. Laminations stacking

A 3D printed frame is used to align the laminations. Epoxy is used to glue the laminations

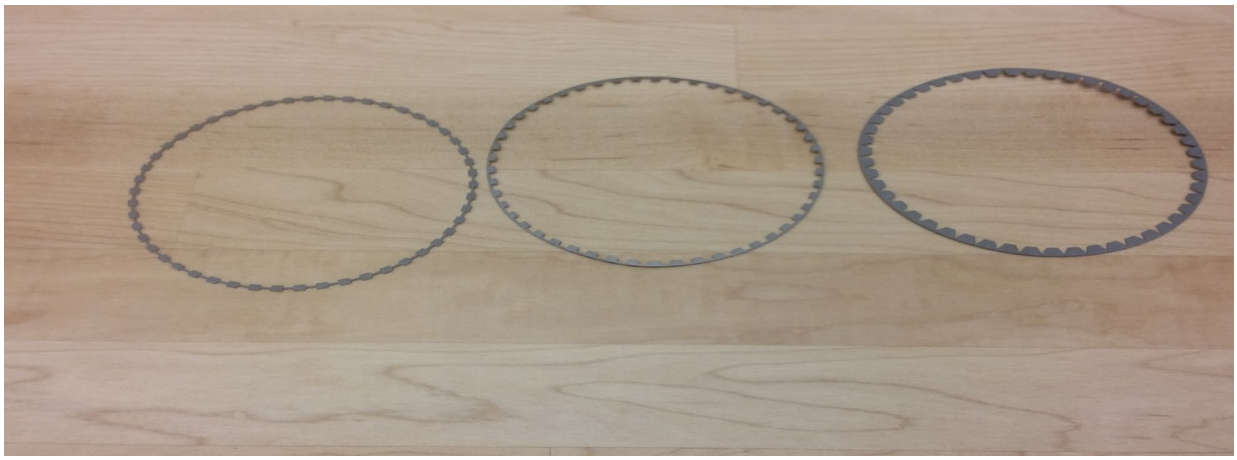

Figure 4-11 Modulating rings laminations

together and clamps are used to tighten the laminations without air between the laminations. Fig. 4-12 shows the laminations clamped after putting epoxy between every two of them. After the laminations stack is dry, the slots are filled with epoxy to strengthen the modulating ring. Fig. 4-13 shows the modulating ring. The modulating rings are assembled with reinforcements between the pole pieces, embedded in epoxy, and connected to an external nylon assembly. This assembly is mounted to the stator end bell housings to prevent the modulating ring from rotating. Fig. 4-14 shows the modulating ring attached to two nylon bases.

Figure 4-12 Modulating rings laminations stack

Figure 4-13 Modulating ring

Figure 4-14 Modulating ring with nylon bases

4.5 Inner rotor

The inner rotor is a solid mild steel assembly that is integrated with the motor output shaft. In order to securely place the rectangular magnets, this surface of the inner rotor is machined with 84 flats. The inner rotor magnets are identical to those used on the outer rotor. Fig. 4-15 shows the inner rotor with the magnets mounted on its outer surface.

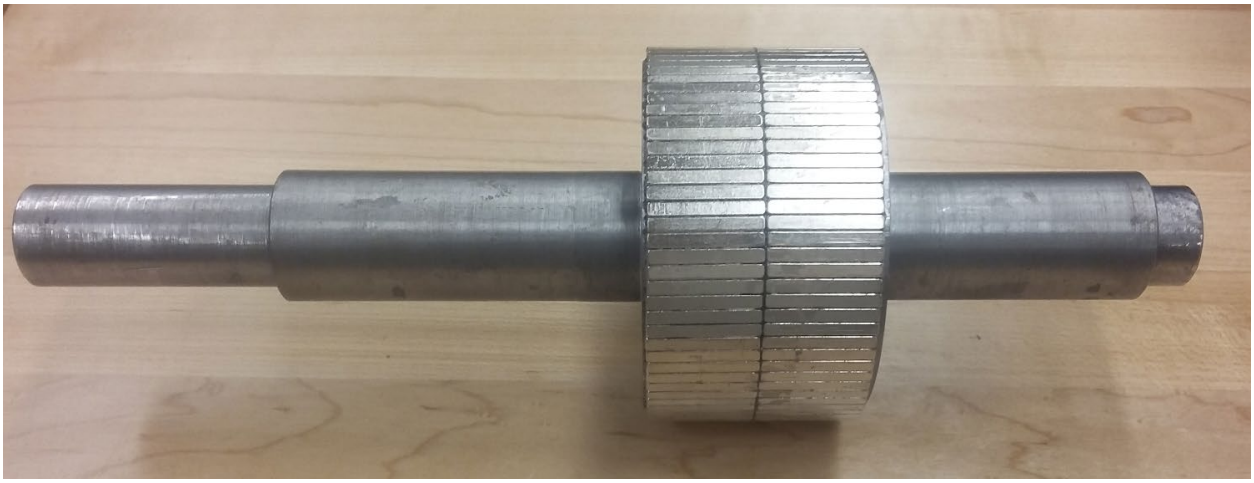

Figure 4-15 Inner rotor

4.6 Machine assembly

The prototype assembly is somewhat more complex than a production machine should require. The modulating ring and outer rotor micarta assembly and bearing structure is developed to enable the investigation of different modulating ring performances, and are designed to enable easy disassembly and re-assembly. The full arrangement of the parts is shown in Fig. 4-16 before assembly.

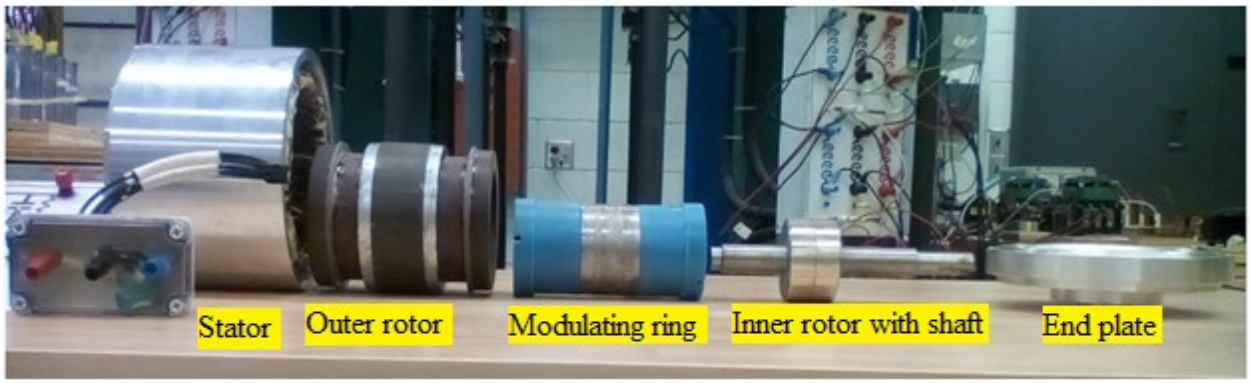

Figure 4-16 Machine parts

The next step is to fastidiously assemble the different parts of the machine: wound stator and casing are assembled, outer rotor bearings are assembled with the endplates in the machine shop of the

University of Calgary. Assembling stator, outer rotor, modulating ring, and inner rotor with the shaft is done in corresponding to SolidWorks design that is shown in Fig. 4-17.

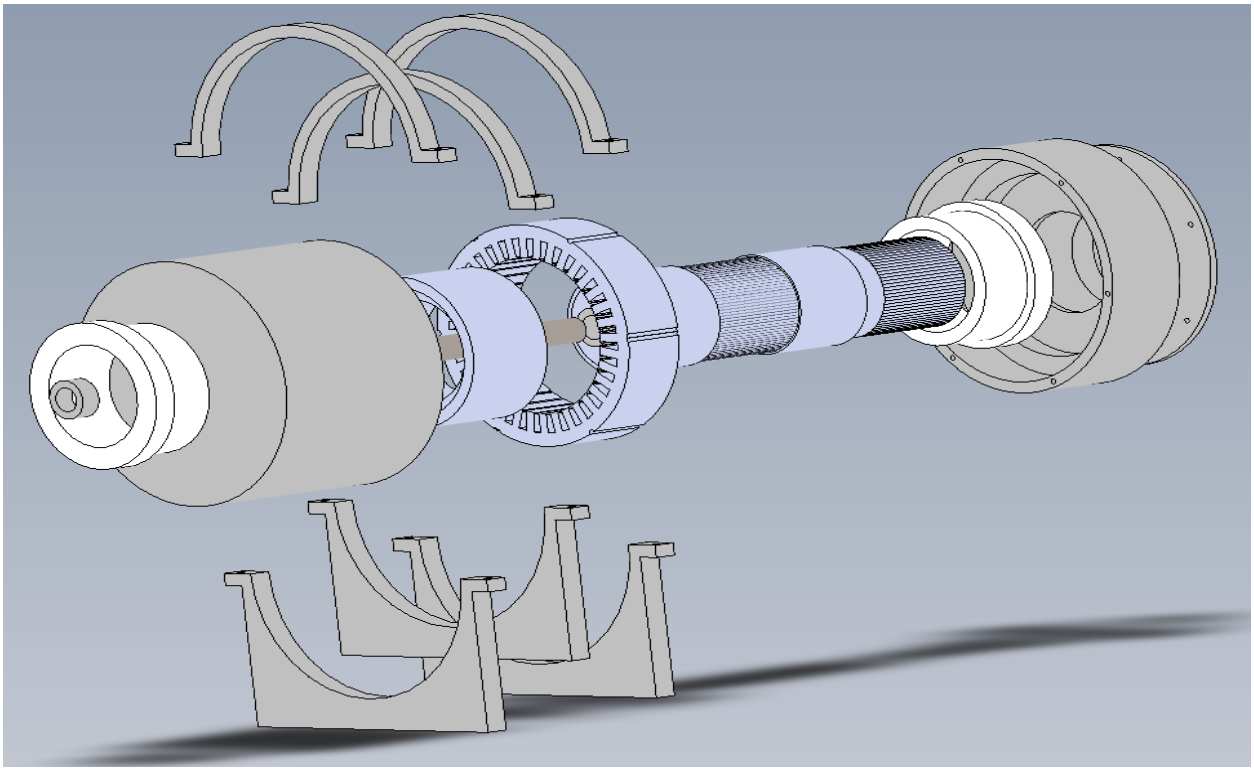

Figure 4-17 Different parts of machine assembly designed in SolidWorks software

[Courtesy: Machine Shop, Schulich School of Engineering, University of Calgary]

The machine is assembled or dissembled in the Lab. when needed.

4.7 Test rig

In order to be able to test the high torque machine, the machine is coupled to a 100 Nm 100:1 gearbox to reduce its output torque so it can be loaded with an existing 3hp permanent magnet synchronous machine.

On the steel base, the induction machine integrated with magnetic gear is coupled with the gearbox that is coupled with a load machine. The coupled machines on the steel base are shown in Fig. 4-18 where the torque transducer and the couplers are also visible.

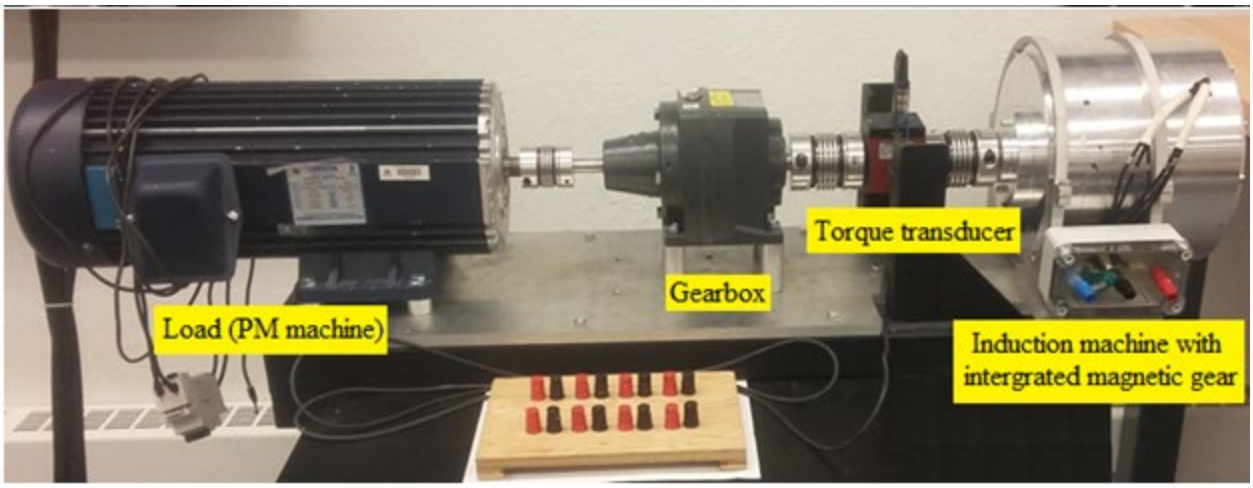

Figure 4-18 Machine coupled with gearbox and load mounted on the steel base

The proposed converter based open-loop motor drive system consolidating the machine has been implemented by using the SWITCHGEAR system from Denkinetic Pty Ltd. [84] which is a Digital Signal Processor (DSP) based system and uses a Texas Instruments TMS320F28335 microcontroller. The SWITCHGEAR system and TMS320F28335 microcontroller are programmed in C++ language. TMS320F28335 is actually a 32-bit floating-point microcontroller with an operating frequency up to150 MHz. It is equipped with 6-channel Direct Memory Access (DMA) Controller (for ADC, ePWM etc.), a maximum of 18 PWM outputs, up to 88 shared General-Purpose Input/output (GPIO) pins, and a 12-bit 16-channel ADC module. Besides, it has 256K×16 Flash and 34K×16 SARAM on-chip memory [85].

The complete implemented motor drive setup in the lab is visualized in Fig. 4-19. In this motor drive, Space Vector Pulse Width Modulation (SVPWM) control and signal interfacing are carried out by the SWITCHGEAR DSP system whereas the stator windings of the machine are fed from a 750 V (DC max), 20 KW, IGBT based newer version Semikron Semiteach three-phase rectifier-inverter systems with 4400 μF capacitance DC link. The microcontroller receives an actual motor speed signal from an encoder SWITCHGEAR system peripheral boards.

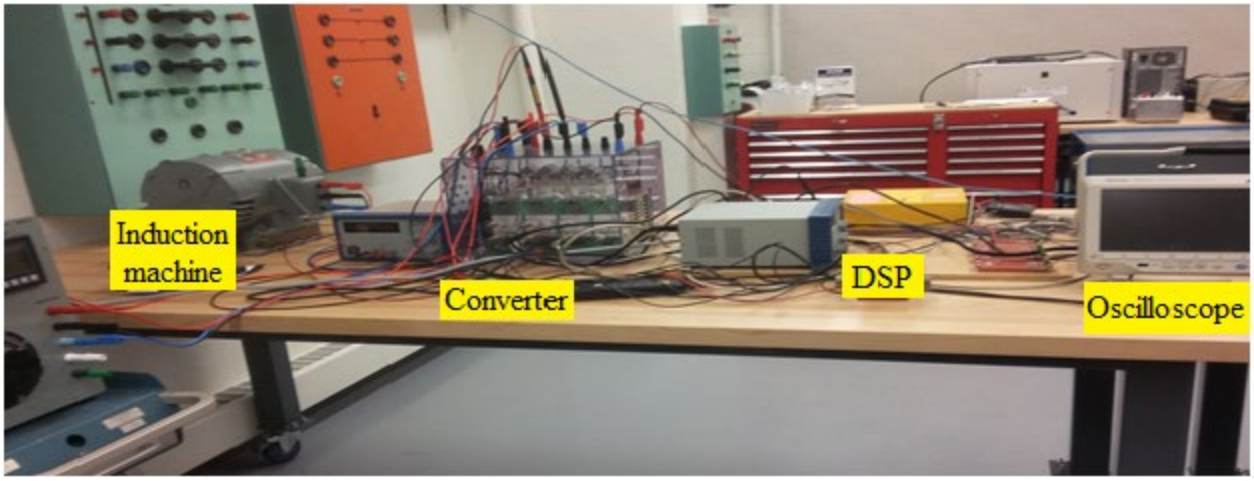

Figure 4-19 Drive setup

This drive is used with a conventional three-phase, 5 hp, 1745 rpm induction machine. An oscilloscope and a power analyzer are used to monitor the machine's performance.

4.8 Summary

Details of all the parts of the machine, steps of the real machine building process, and assembly of the machine were introduced. Test rig components, and motor drive were presented.

CHAPTER 5: EXPERIMENTAL TESTING

This chapter presents the experimental test results of the induction motor integrated with the magnetic gear. Challenges and failures that are faced during testing the machine will be introduced and analyzed. Alternative design for the failed part will be described, built, and tested. The corresponding test results have been discussed accordingly.

5.1 Induction machine parameters

The experimental work started with testing the drive. A conventional induction motor is controlled by the drive circuit and efficiently follows the commanded performance.

The induction machine under investigation is assembled without the modulating ring or the inner rotor in order to determine the induction machine's equivalent circuit parameters. Conventional tests are performed: a DC test, a no-load test, and a locked rotor test.

5.1.1 DC test

The induction machine windings are connected as a star four wires connection. A variable DC voltage source is connected on two terminals of the stator and an ammeter is inserted in the current path and a voltammeter is connected across the terminals. Fig. 5-1 shows the voltage-current plot from which the resistance value can be calculated.

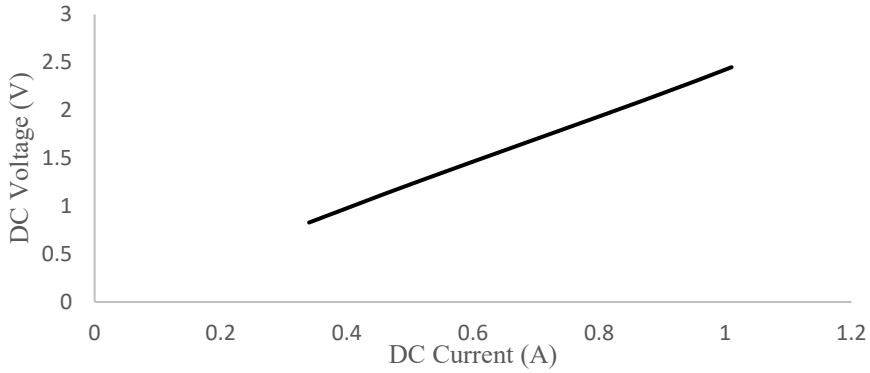

Figure 5-1 DC test

From fig. 5-1, the DC resistance is calculated to be 2.43 Ω. As the stator is Y- connected, the calculated resistance is the value of two-phase resistance and so the DC phase resistance is 1.22 Ω.

5.1.2 Locked rotor test

The rotor is held stationary and the source voltage is increased until the current reaches the rated current of the machine. A screenshot of the power analyzer for the locked rotor test is shown in fig. 5-2. The rotor resistance and the leakage reactances can be calculated.

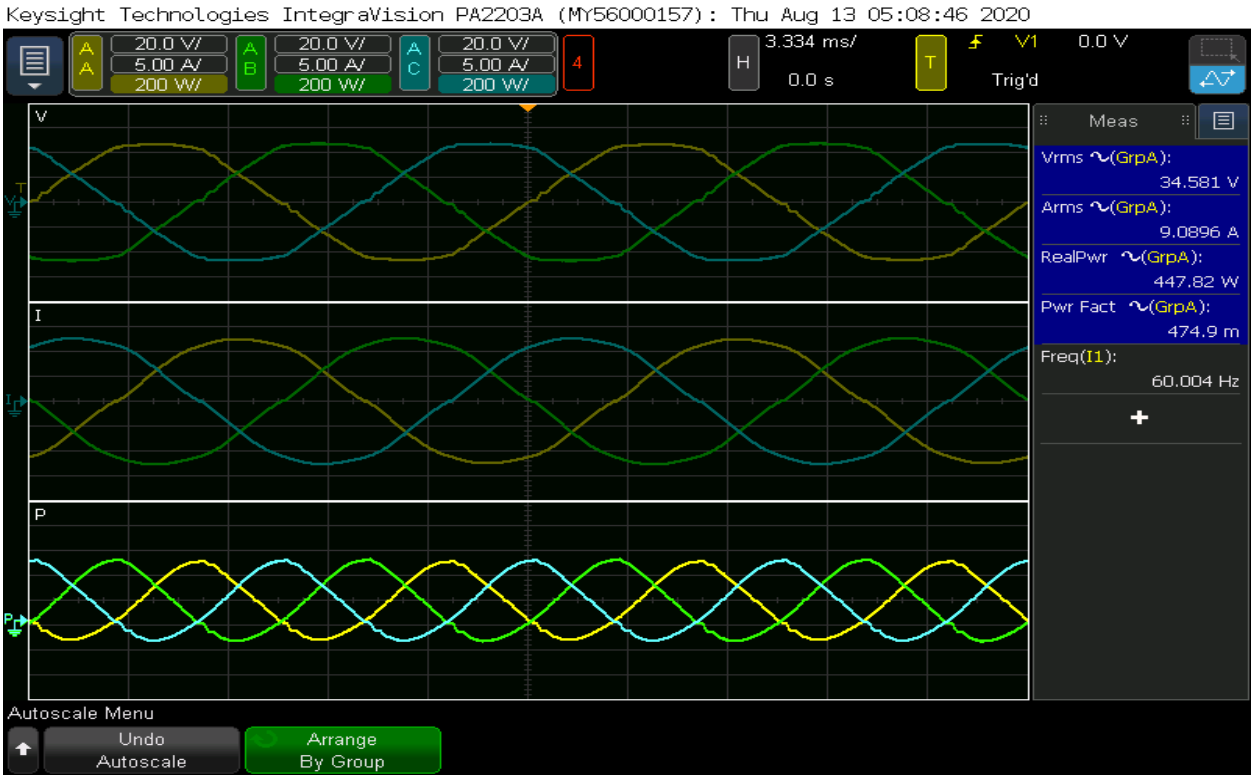

Figure 5-2 Power analyzer screenshot of locked rotor test

At locked rotor;

$$P_{LR} = 3I_1^2\ (R_1 + R_2)$$

$$Q_{LR} = 3I_1^2\ (X_1 + X_2)$$

5.1.3 No-load test

The no-load test is performed to obtain the magnetizing reactance, core loss resistance, and windage and friction losses. To separate the no-load losses into core losses and mechanical losses, a no-load test is performed at different voltage values. Fig. 5-3 shows the iron loss at different voltage values.

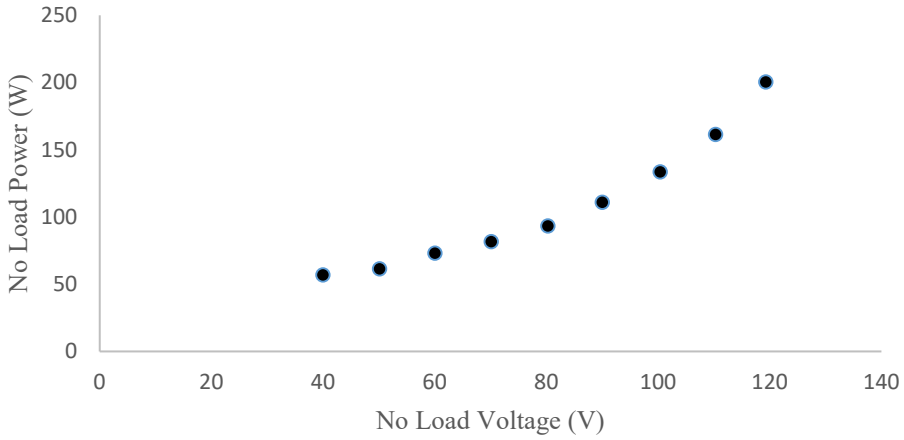

Figure 5-3 Iron losses

From fig. 5-3 and at zero voltage, friction and windage losses are around 52 W.

At rated voltage, the no-load test readings and waveforms are shown in fig. 5-4 which is a screenshot from the power analyzer.

At no load;

$$E = V_1 - I_1 Z_1$$

$$\mathrm{P_{nl}} = 3\, I_1^2 R_1 + 3\frac{E^2}{R_c} + P_{F+W}$$

$$Q_{nl} = 3I_1^2\, X_1 + 3\frac{E^2}{X_m}$$

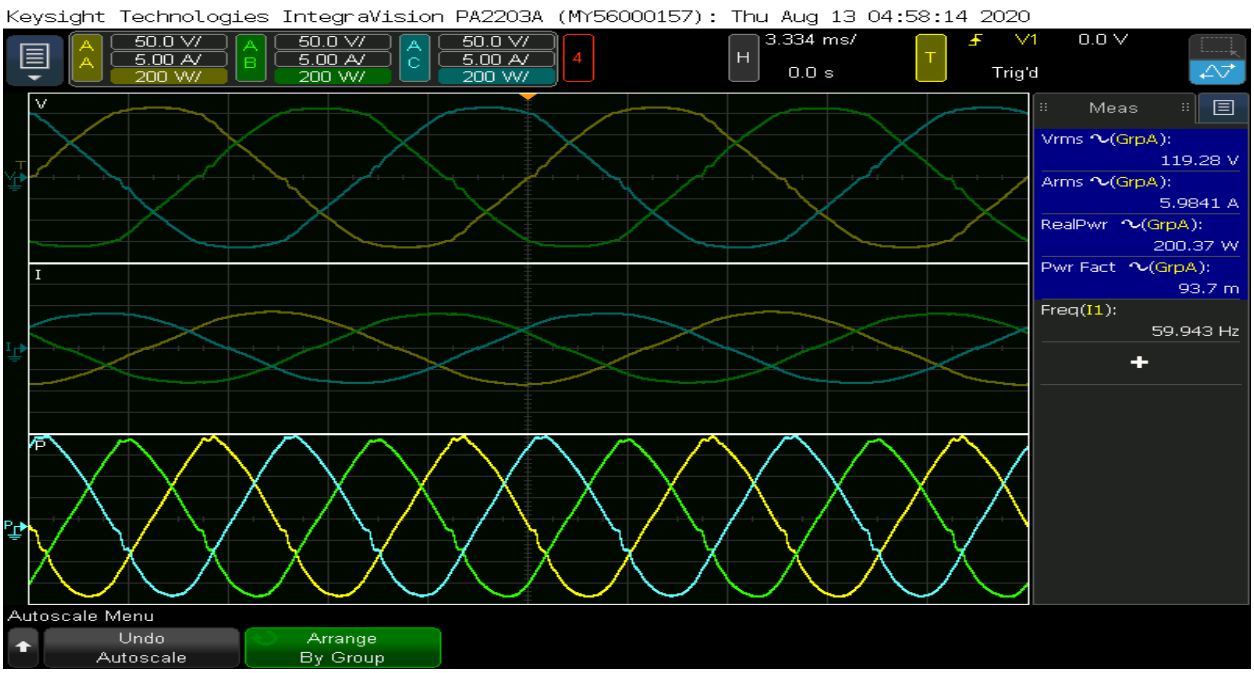

Figure 5-4 Power analyzer screenshot of the no-load test

Table 5-I shows the induction machine parameters.

Table 5-I Induction machine parameters

Rated phase voltage	120 V
Rated current	9.09 A
Frequency	60 Hz
Stator resistance R_1	1.22 Ω
Rotor resistance R_2	0.587 Ω
Stator reactance X_1	1.674 Ω
Rotor reactance X_2	1.674 Ω
Magnetizing reactance X_m	18.22 Ω
Iron losses resistance R_C	2051.86 Ω
Windage and friction losses	52 W

The induction machine performance is simulated using the actual machine parameters. Different performance characteristics are shown in the following curves. Fig. 5-5 shows the torque-speed characteristics of the machine.

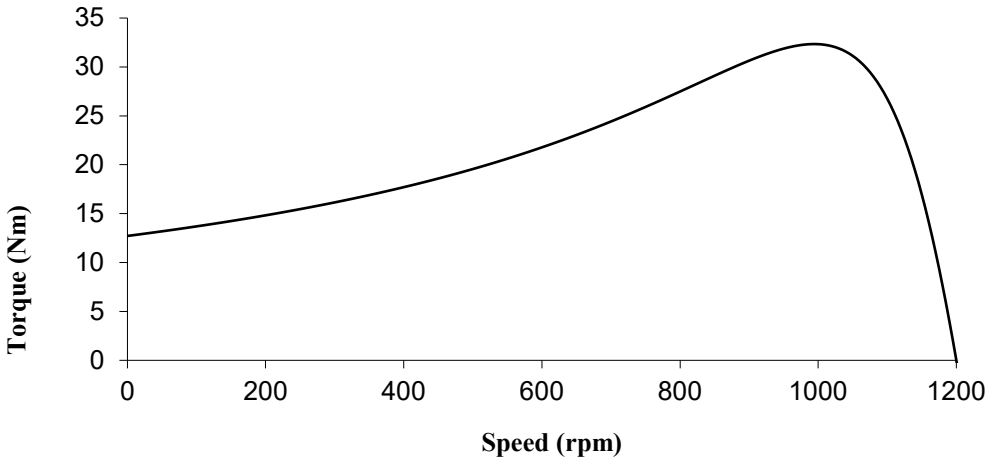

Figure 5-5 Torque–speed characteristics from equivalent circuit parameters

The starting torque is around 13 Nm and the maximum torque is around 33 Nm. Fig. 5-6 is comparing the torque-speed characteristics using the actual machine parameters with the characteristics presented in chapter 3 which represents the FEA simulation for the induction machine.

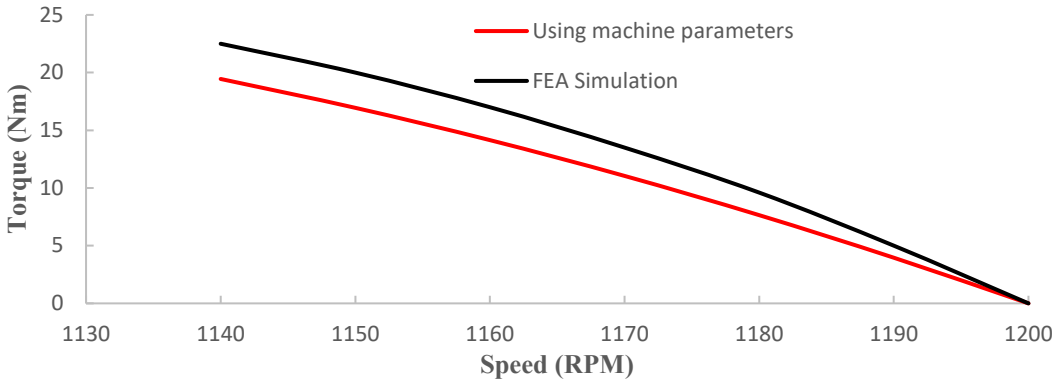

Figure 5-6 Torque–speed characteristics

As shown in Fig. 5-6 the calculation from the actual machine parameters are close to the FEA simulation results.

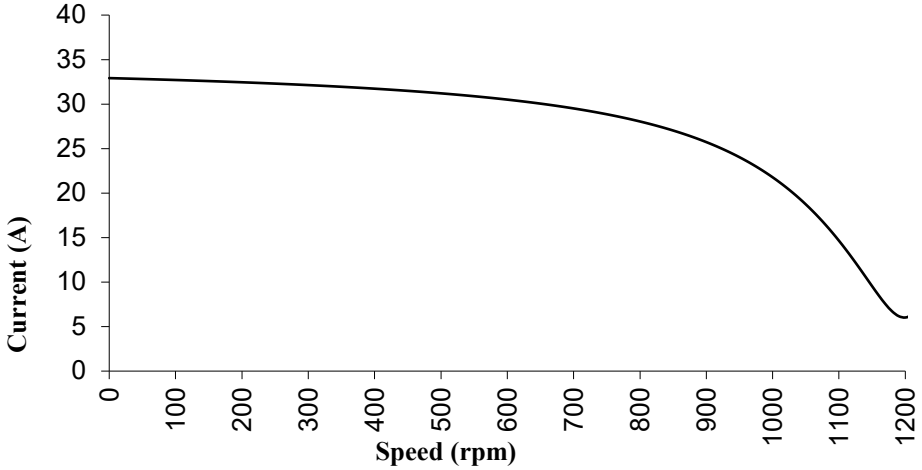

Figure 5-7Current–speed characteristics from equivalent circuit parameters

Fig. 5-7 shows the current – speed characteristics of the induction machine. The starting current is 33 A which is around 3.6 times the rated current.

Fig. 5-8 shows the efficiency change with speed and the maximum efficiency is 83%.

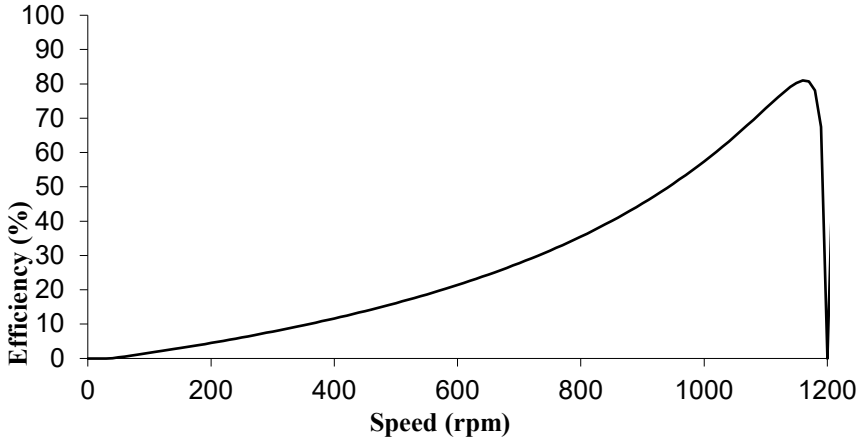

Figure 5-8 Efficiency–speed characteristics from equivalent circuit parameters

5.2 Induction machine integrated with a magnetic gear

The machine casing is made in a way to be able to take the machine apart and change the modulating ring. The first modulating ring is used and the gear is assembled without the induction machine stator. Then the gear is tested by rotating the outer rotor (high-speed rotor) by hand which resulted in the rotation of the inner rotor (low-speed rotor). The outer rotor needed to rotate 5.25 revolution in order to rotate the inner rotor one full rotation which showed the modulation occurred. The whole machine is again assembled with the stator. Then the machine was energized through the drive circuit. The machine ran for a few minutes and then rotated both ways and then stopped and acted as it is blocked. The power is turned off and the machine is taken apart to find that unfortunately, this modulating ring failed to withstand the shear forces and twisting torques of the machine. As the modulating ring laminations are glued together with epoxy, the laminations are apart from each other, and middle laminations are damaged as shown in fig. 5-9.

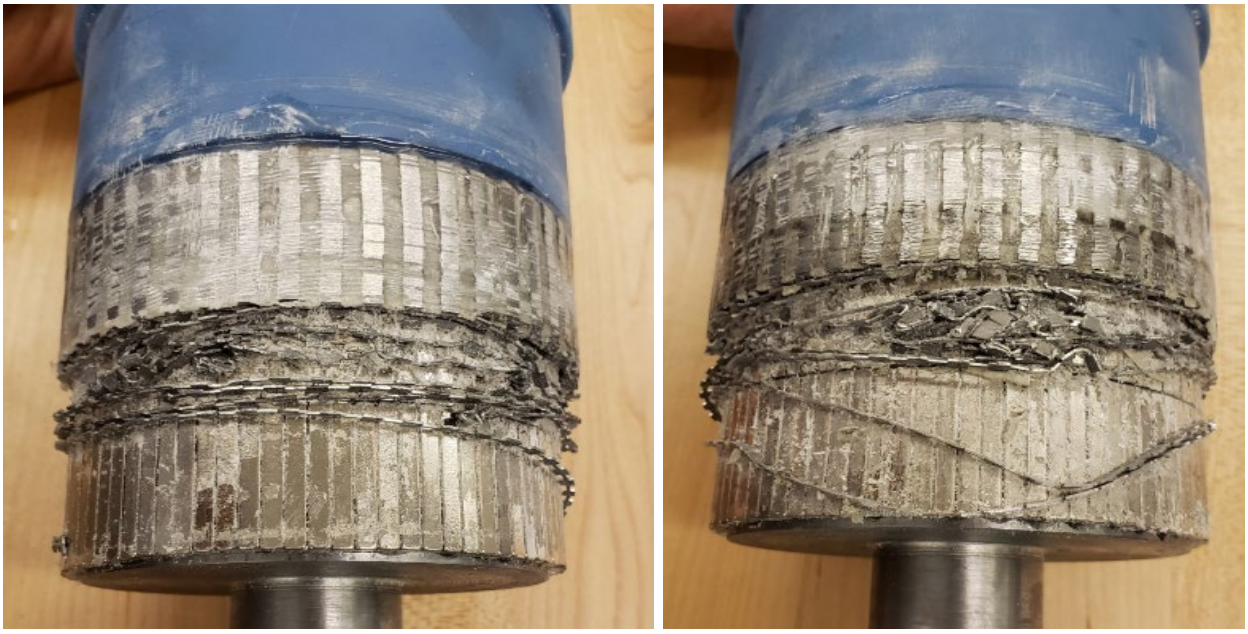

Figure 5-9 Damaged modulating ring

As the air gap is very small (0.5 mm) on both sides of the modulating ring, there is no room for any layer of epoxy to cover the laminations. The only thing that is gathering the laminations together is a thin film of epoxy between the laminations and the epoxy that is filling the slots.

After investigating the failure and looking into the possible alternatives that can be used to replace the broken modulating ring, three options were suggested. First, a trial to cut the modulating ring as one solid piece by water jet. The machine shop was not able to cut the modulating ring with the required length. When it was tried to cut it as a sheet in order to weld it as a cylinder; it did not work either. Fig. 5-10 shows the water jet cut modulating rings. Second option is to cut it with laser but after contacting different companies it was found that cutting the 54 mm length modulating ring with laser is expensive.

Figure 5-10 Water-jet cut modulating ring

Third suggestion was to design a 3D printed rotor with slots to act as an envelope closure to the modulating ring pieces. The enclosure was designed and in order to keep the modulating ring pieces with the same dimensions, the air gap size was doubled as the slots have walls and a clearance both sides of the modulating ring is needed to be able to the rotors to rotate inside and outside the modulating ring. The value of the torque is expected to decrease to around one-fourth of the simulated value. This was the valid option to be able to prove the concept not the best alternative but the fast economic one. Fig. 5-11 shows the 3D printed enclosure. A laminated sheet

with a thickness of 0.3 mm is cut into 2.5 mm × 6mm pieces to act as the modulating ring piece. Fig. 5-12 shows the modulating ring pieces. Each slot was filled with 8 pieces of laminations to form a modulating ring piece.

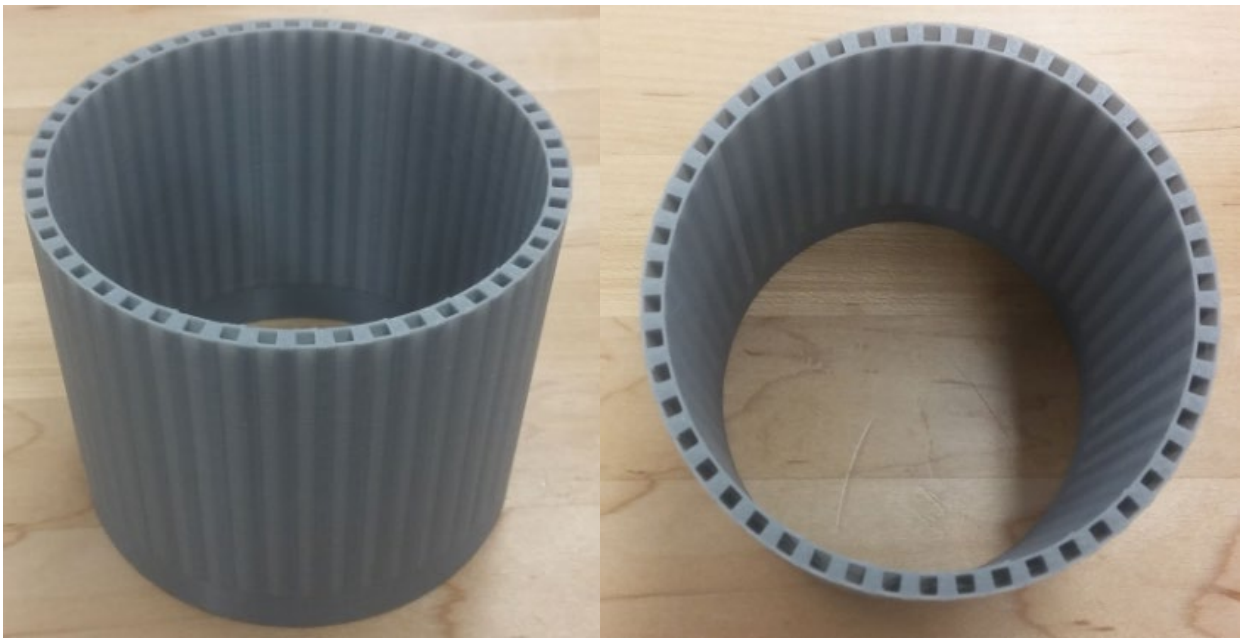

Figure 5-11 3D printed modulating ring enclosure

Figure 5-12 Modulating ring pieces

After printing the enclosure, the laminations were inserted in the slots at radial direction orientation and the opening was closed with epoxy filling.

The gear is assembled again without the induction machine stator. Then the gear is tested by rotating the outer rotor (high-speed rotor) by hand which resulted in the rotation of the inner rotor (low-speed rotor). The outer rotor needed to rotate 5.25 revolution in order to rotate the inner rotor one full rotation which showed the modulation is occurred. The machine is energized through the drive circuit but the current is high without running which indicate the machine was blocked. When the machine was taken apart, I found cracks in the modulating ring as shown in fig. 5-13 and some laminations were out of the enclosure and blocked the machine.

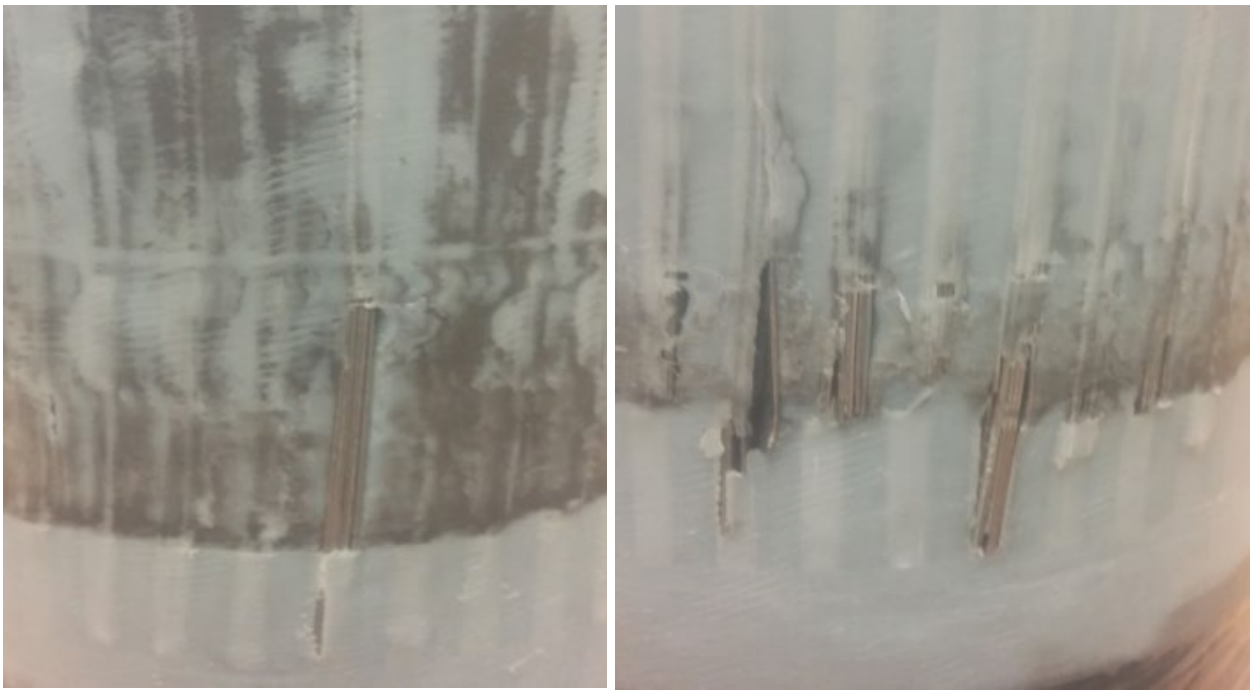

Figure 5-13 Cracked modulating ring

As shown in fig. 5-13, there are signs of unbalanced friction, which means that the modulating ring is not centrally suspended. A bearing on the inner rotor shaft on both sides is suggested to

ensure the center placement of the modulating ring. The printed enclosure was not strong enough to bear the shear and twisting forces on the modulating ring.

The modulating steel pieces inside the modulating ring envelop were taken out. A new envelop enclosure is printed with finer 3D printing settings to have a more dense, and robust enclosure.

The gear is assembled again without the induction machine stator. Then the gear is tested by rotating the outer rotor (high-speed rotor) by hand which resulted in the rotation of the inner rotor (low-speed rotor). The outer rotor needed to rotate 5.25 revolution in order to rotate the inner rotor one full rotation which showed the modulation is occurred. The whole machine was assembled and tested. The outer rotor was locked to measure the pull-out torque. The inner rotor was moved by hand as slow as possible and the waveform from the torque transducer is shown in fig. 5-14 and fig 5-15. The inner rotor was rotated both clockwise and counter-clockwise directions.

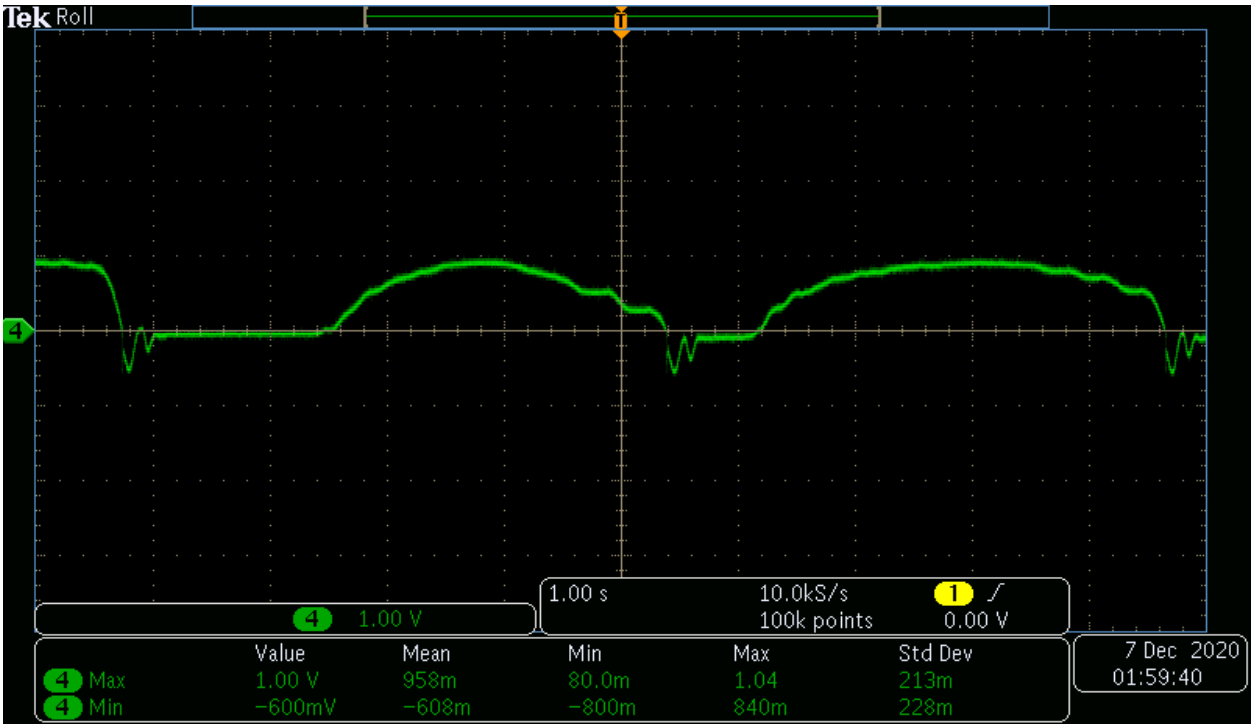

Figure 5-14 Oscilloscope screenshot of pull-out torque (clockwise rotation)

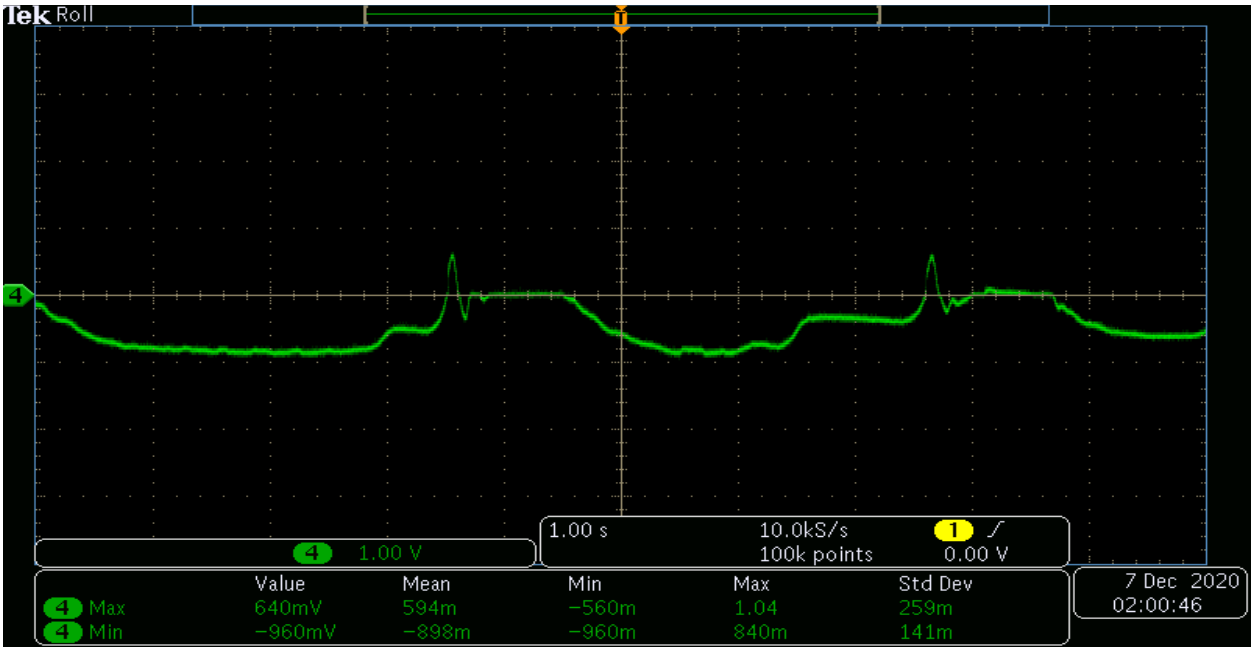

Figure 5-15 Oscilloscope screenshot of pull-out torque (counter-clockwise rotation)

From fig 5-14 and fig 5-15, the pull-out torque is around 1 V which is equivalent to 20 Nm (5V = 100 Nm). Giving the fact that with this design the airgap is doubled which makes the expected torque go to one-fourth of the simulated torque with the small airgap as the torque is directly proportional with the flux density twice and the flux density is inversely proportional to the air gap length. Compared to the simulation results, this is accepted and expected value for the torque. Keeping in mind that if the machine was executed the same way it was designed, 4 times this torque will be gained from 1.5 kW machine.

With the outer rotor free to rotate, the outer rotor was rotated by hand 5.25 revolutions resulting in one revolution for the inner rotor which verifies the gear ratio of 5.25.

Then the machine was energized through the drive and given the order to rotate at a frequency of 10 Hz with the electric load disconnected. Then the electric load was connected and the frequency was increased in 5 Hz increments. The following screenshots show the input and output sides of the machine.

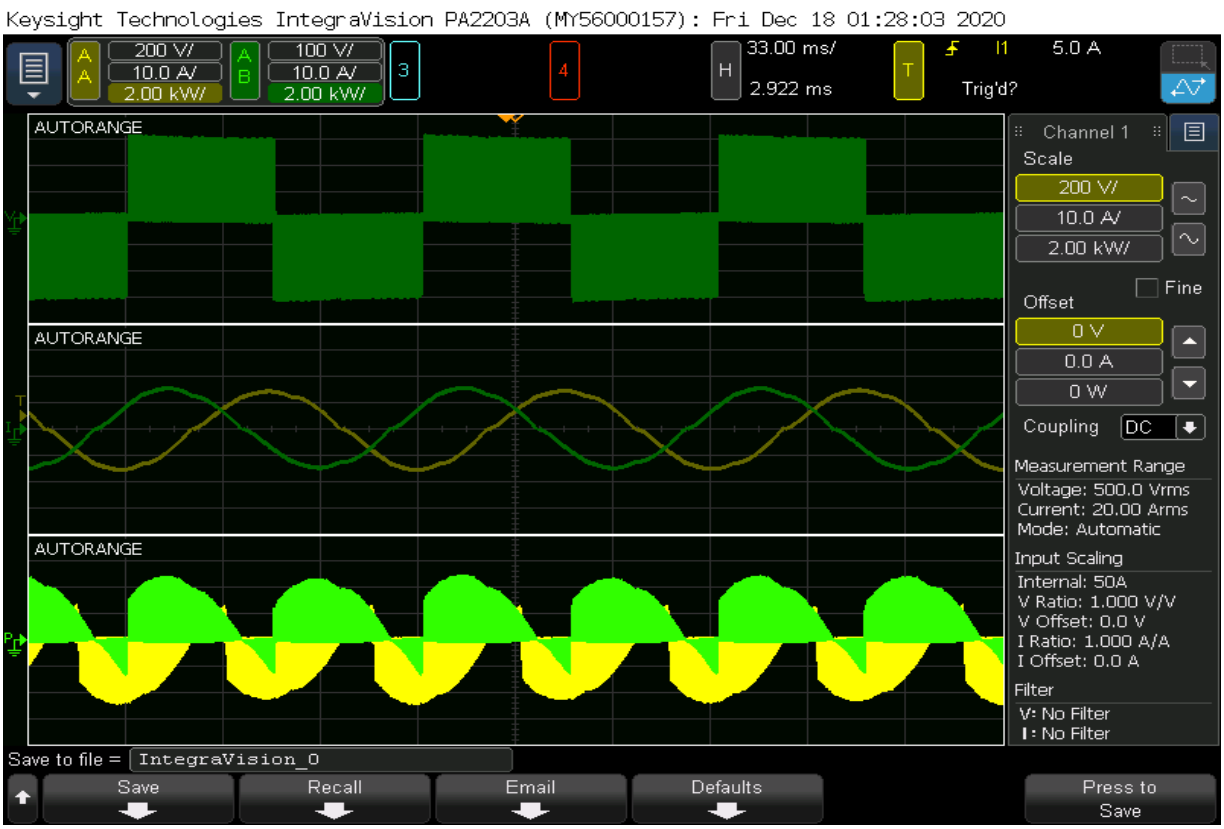

Figure 5-16 Power analyzer screenshot of machine input (10 Hz & load 1)

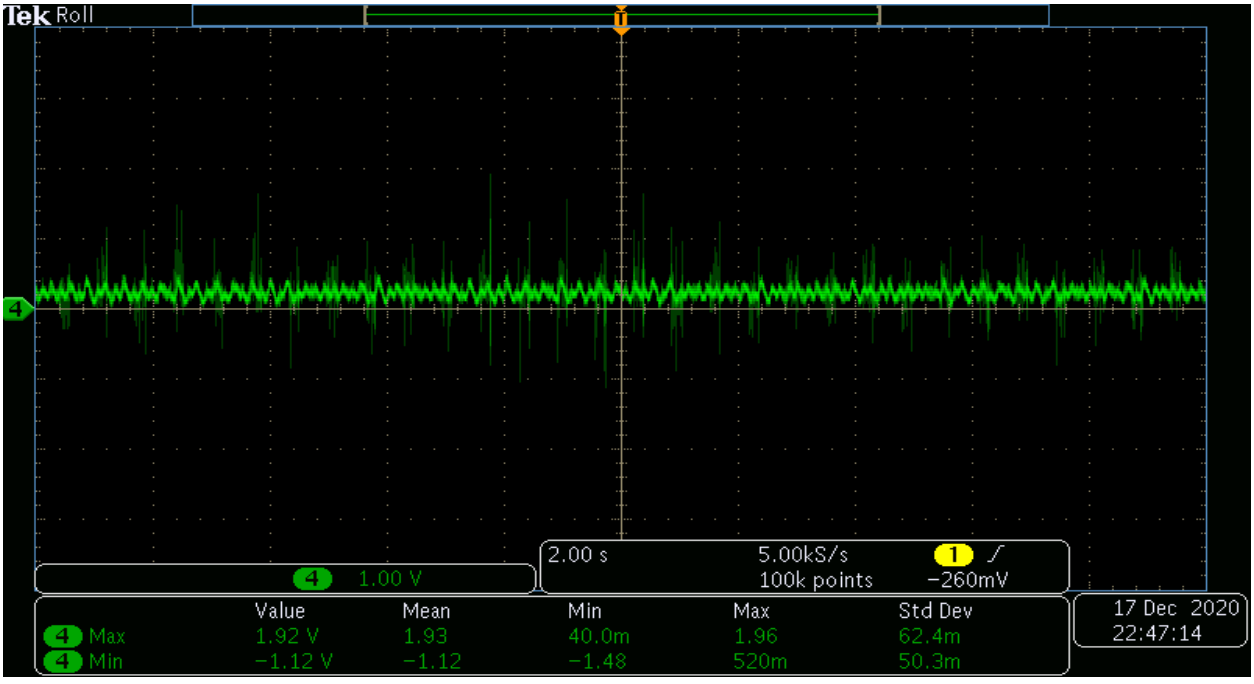

Figure 5-17 Oscilloscope screenshot of an average output torque of 4 Nm (10 Hz & load 1)

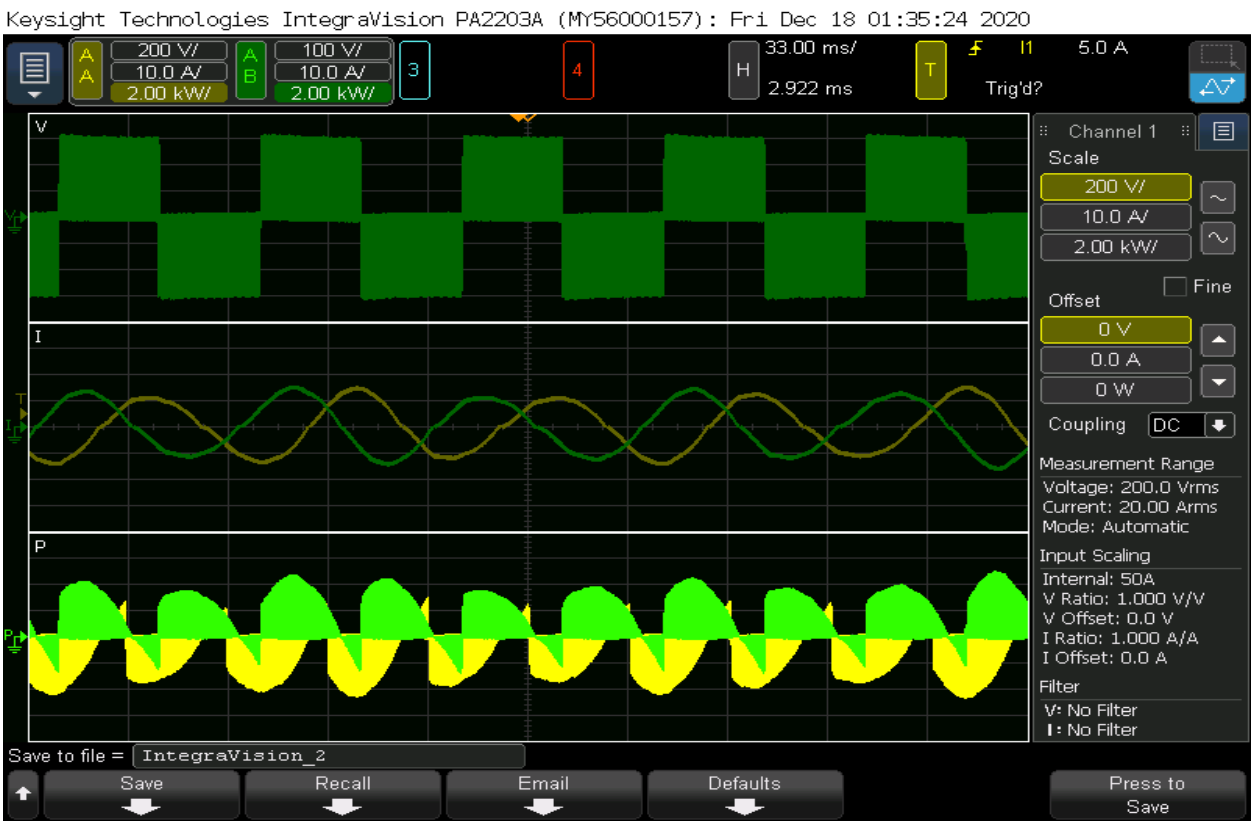

Figure 5-18 Power analyzer screenshot of machine input (15 Hz & load 1)

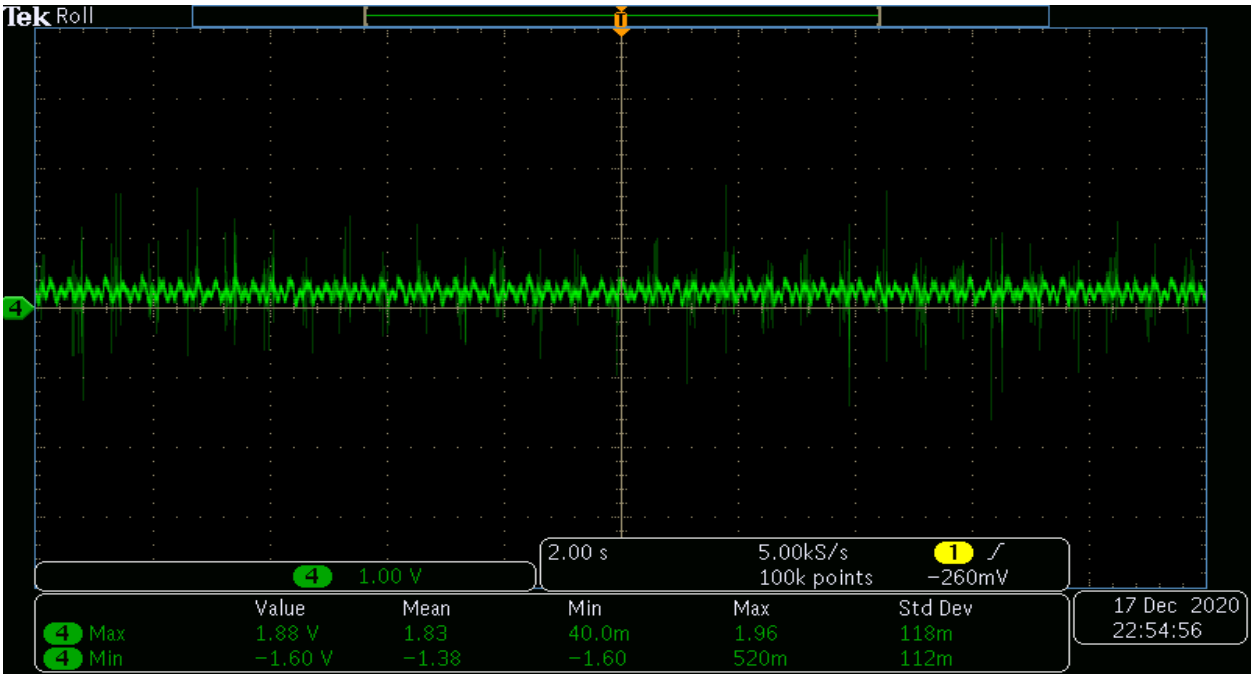

Figure 5-19 Oscilloscope screenshot of an average output torque of 4 Nm (15 Hz & load 1)

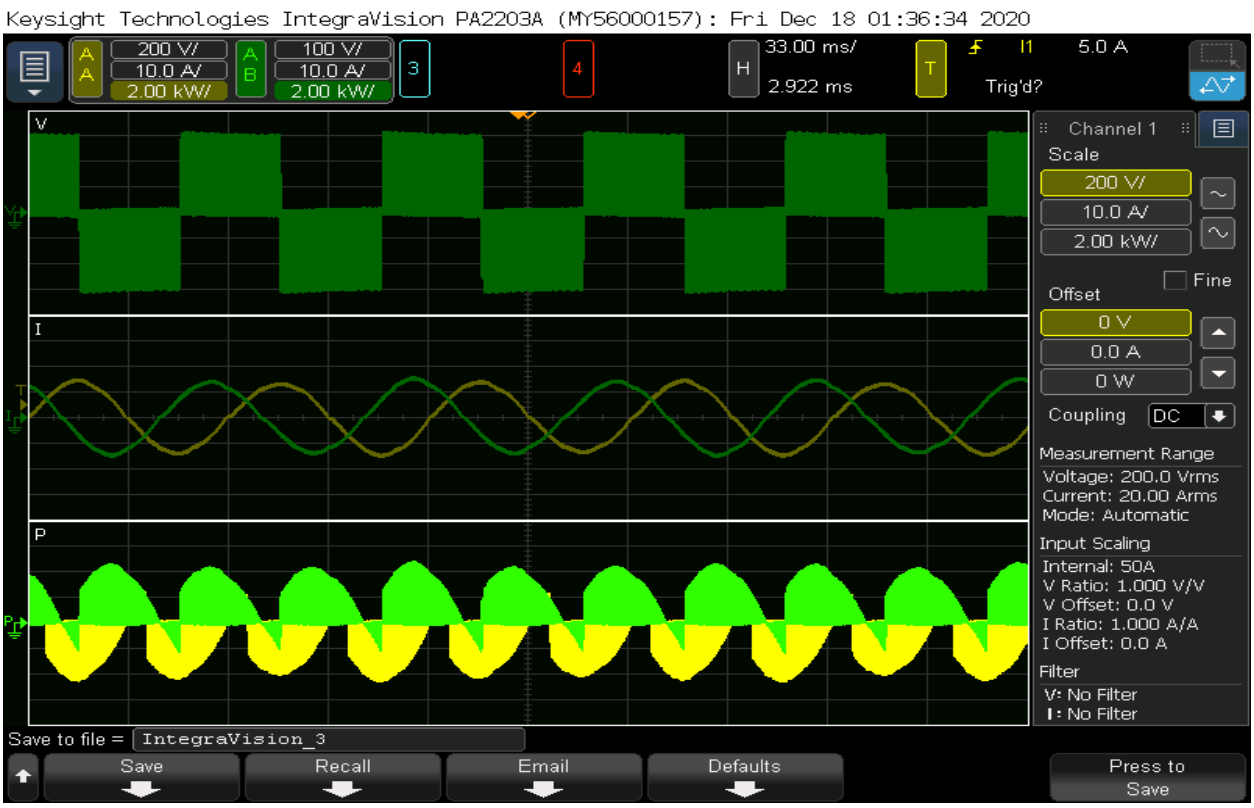

Figure 5-20 Power analyzer screenshot of machine input (15 Hz & load 2)

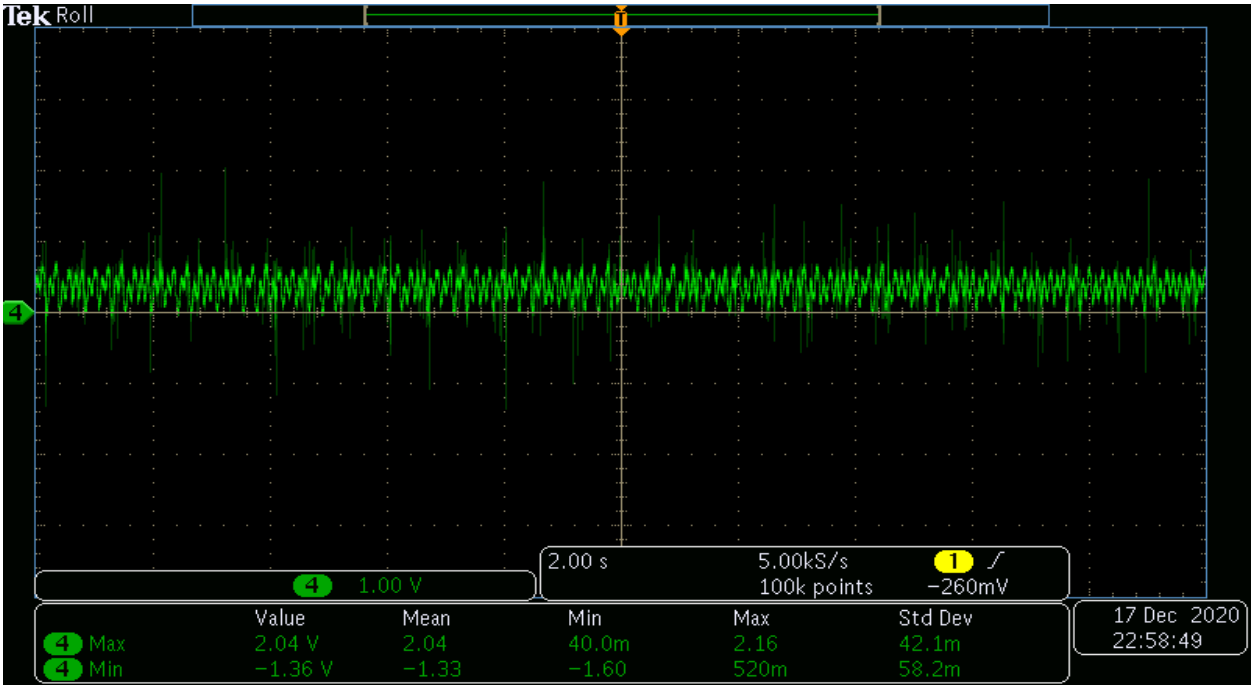

Figure 5-21 Oscilloscope screenshot of an average output torque of 8 Nm (15 Hz & load 2)

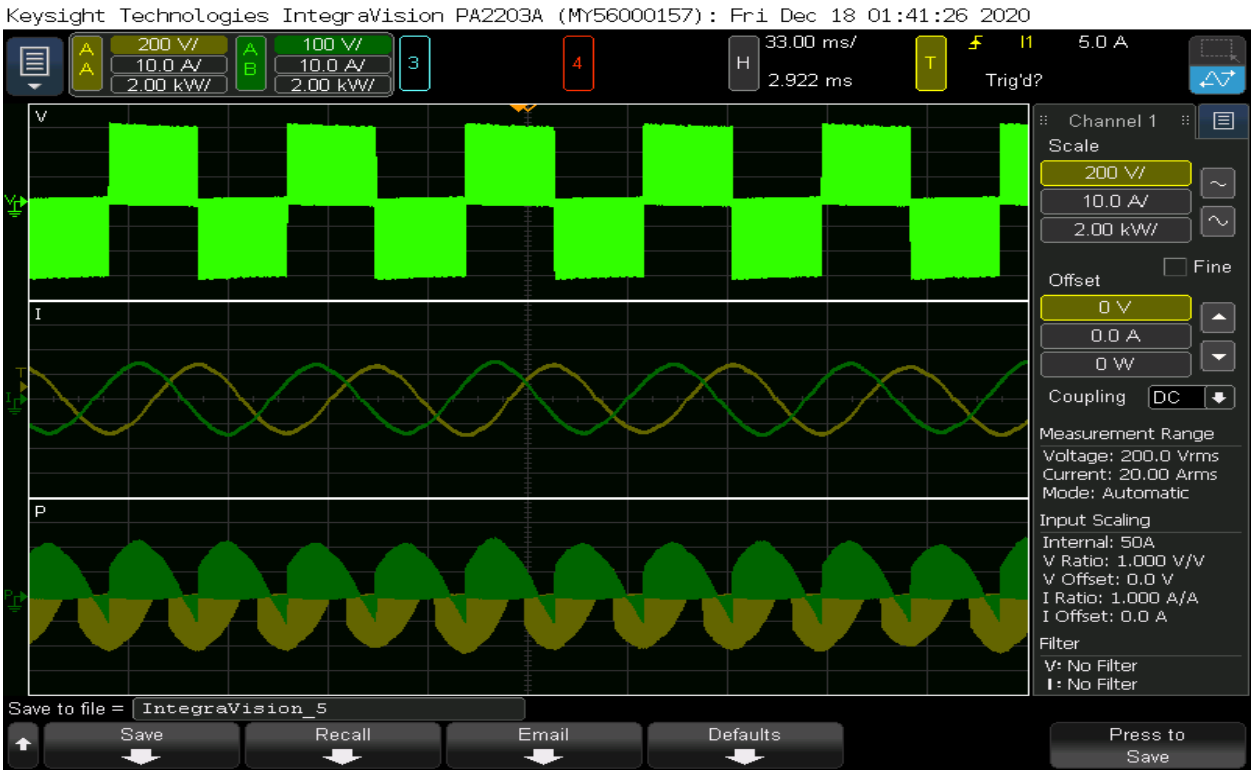

Figure 5-22 Power analyzer screenshot of machine input (20 Hz & load 3)

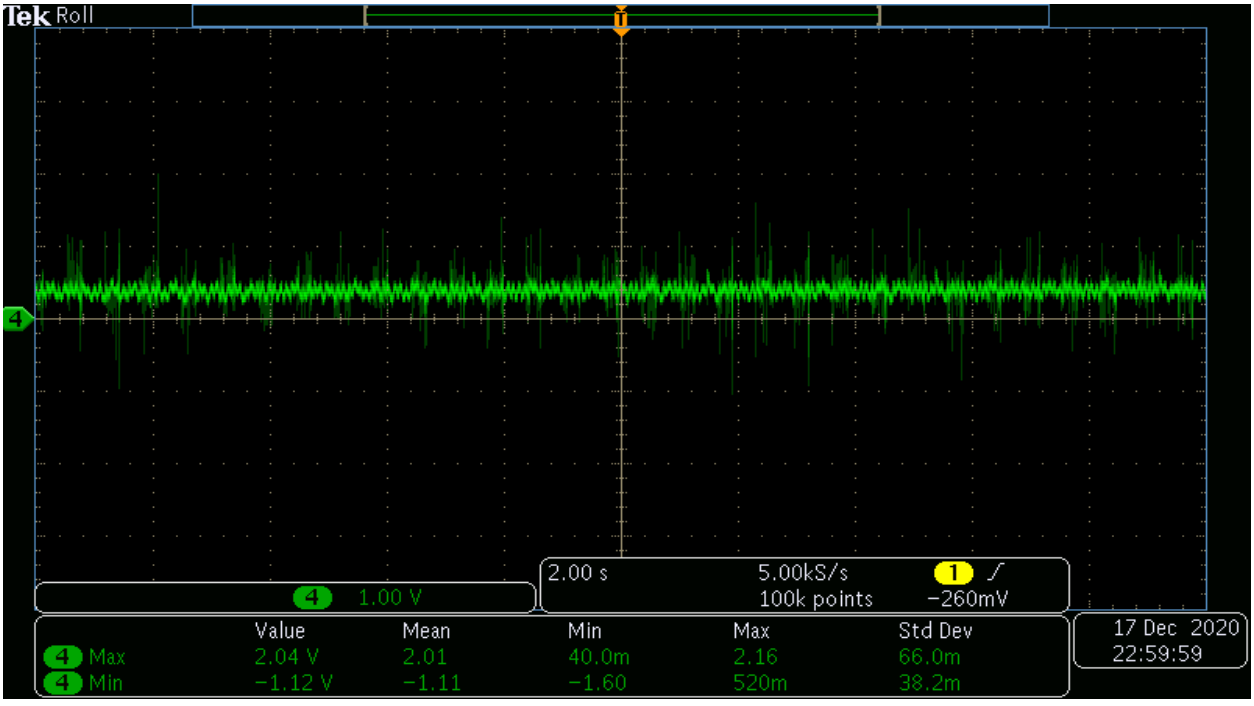

Figure 5-23 Oscilloscope screenshot of an average output torque of 10 Nm (20 Hz & load 3)

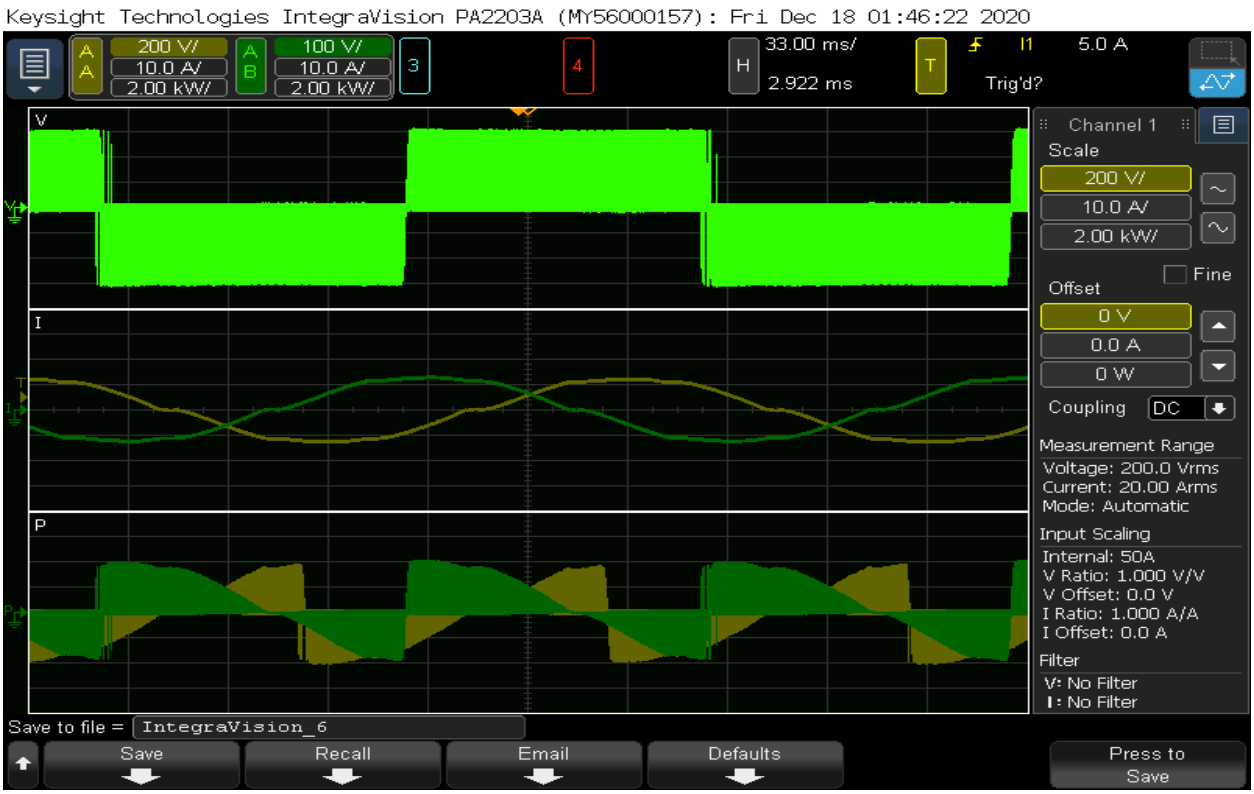

Figure 5-24 Power analyzer screenshot of machine input (5 Hz & load 3)

Fig 5-16 though Fig 5-24 are the screenshots of the power analyzer and oscilloscope which show different operating points of the machine during the machine start-up with the load. As the machine was in the start-up stage to reach the full speed and full load, it was accelerated and loaded in steps to avoid magnetic gear slipping. Then the machine was supposed to run at full speed and with the full load and then the load will be decreased to check torque-speed characteristics of the machine. Unfortunately, the modulating ring failed and needed to be replaced. Although the modulating ring broke, the machine was loaded to half the pull-out torque which is the normal loading of the machine.

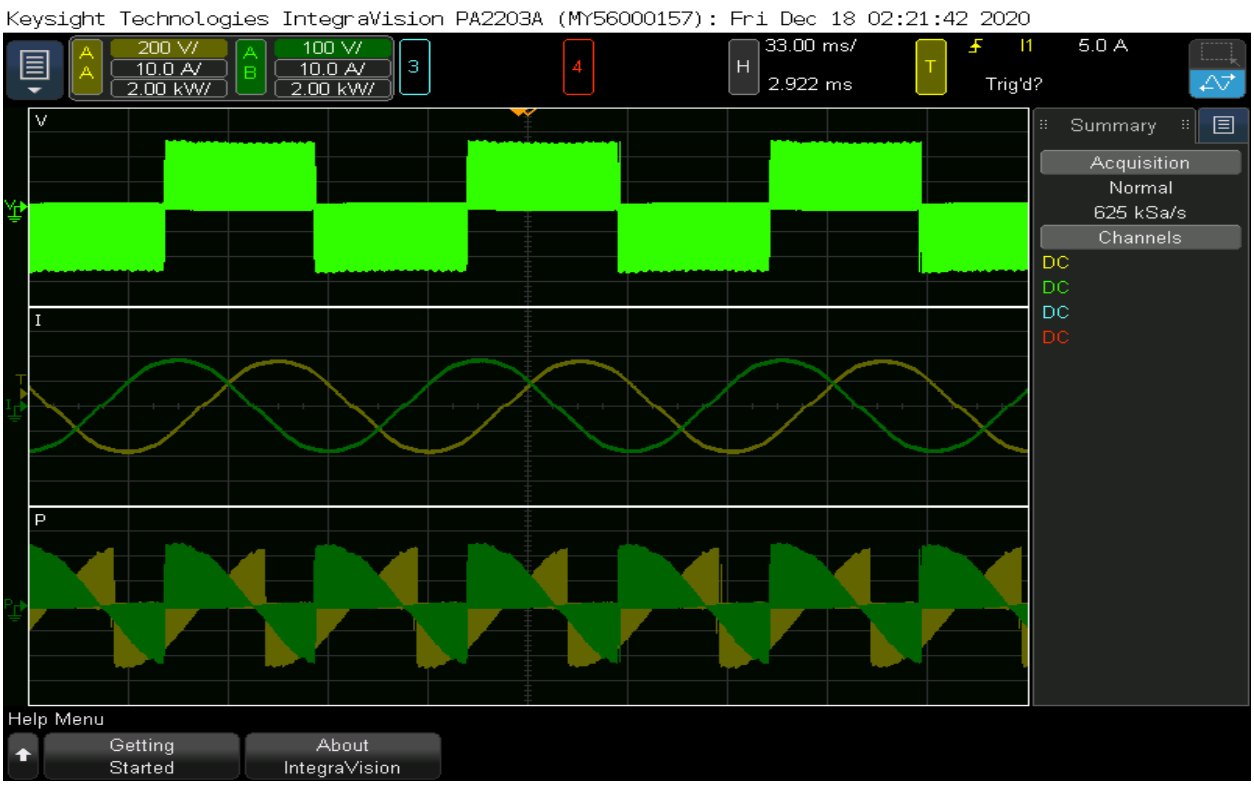

Figure 5-25 Power analyzer screenshot of machine input locked rotor

At this point, the machine was blocked. The machine was de-energized and taken apart to found that two of the slot walls were broken and the steel laminations are out blocking the outer rotor. Fig 5-26 shows the modulating ring damage from all the sides. The damage is believed to be caused by friction because of the laminations that got outside the slot and looks also to be heat damaged. The modulating ring enclosure is redesigned to have thicker walls from the outer rotor side and planned to use another material that can withstand higher temperatures.

Figure 5- 26 The modulating ring damage from all the sides

At this point, the machine is working as expected following the gear ratio, and with stronger material, the modulating ring can withstand the forces and heat.

After everything was finalized, a new simulation is done with the new parameter. Air gap was doubled, arc magnets were replaced with two rows of square magnets, the magnets are a bit shorter than the active length of the machine as the magnet length is 1 inch, using two sets of magnets means the total magnet length is 50.8 mm and the active machine length is 54 mm, and the magnet is 3.175 mm rather than 2.5 mm.

Another 3 D printed enclosure is made. The machine was assembled and coupled to the gearbox. The outer rotor was locked to measure the pull-out torque. The inner rotor was moved by hand as slow as possible and the waveform from the torque transducer is shown in Fig 5-27 and Fig 5-28.

The inner rotor was rotated both clockwise and counter-clockwise directions. From fig 5-27 and fig 5-28, the pull-out torque is around 1.14 V which is equivalent to 22.8 Nm (5V = 100 Nm).

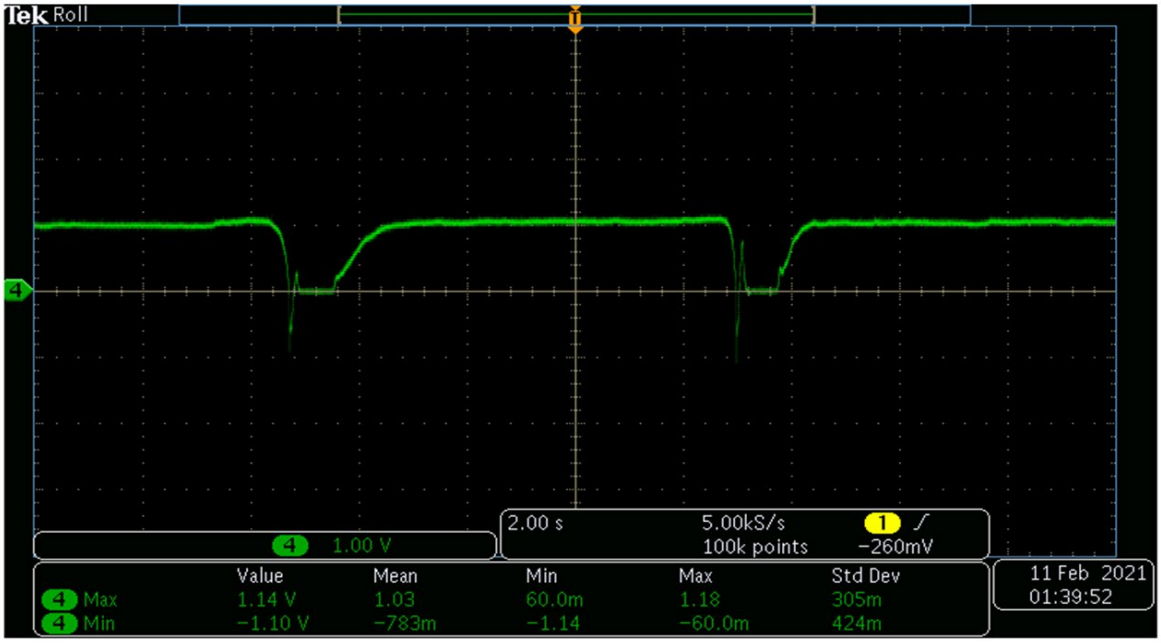

Figure 5-27 Oscilloscope screenshot of pull-out torque (clockwise rotation)

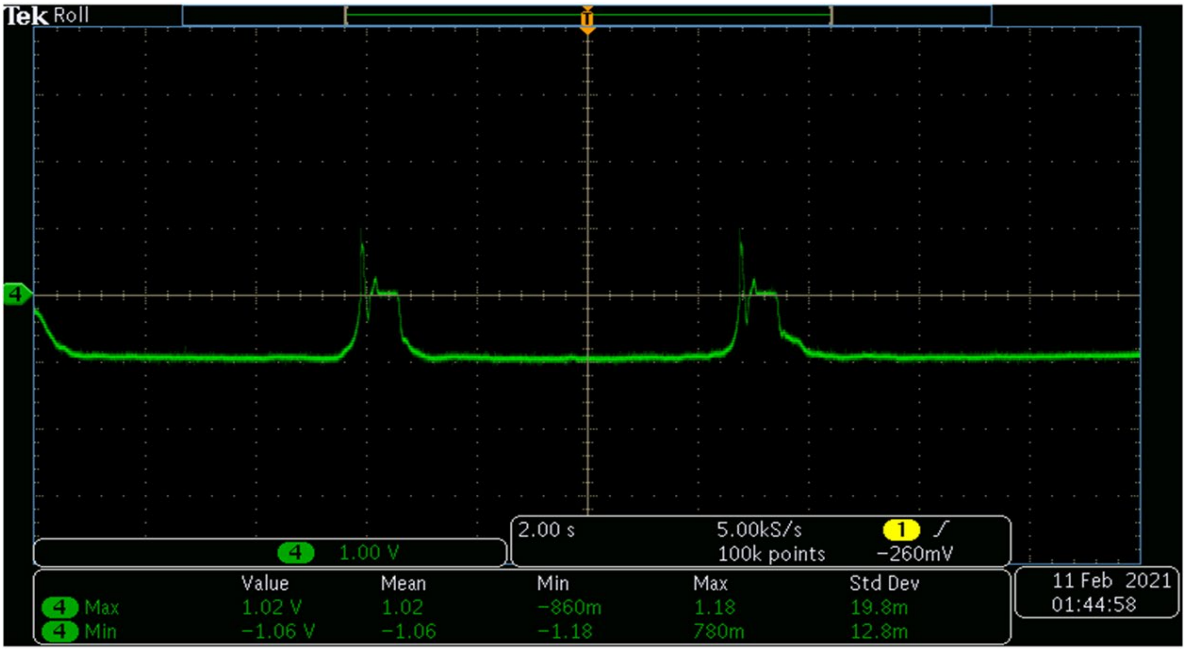

Figure 5-28 Oscilloscope screenshot of pull-out torque (counter-clockwise rotation)

Fig 5-29 shows the simulated torque – load angle characteristics of the magnetic gear with the new parameters and the experimental reading for the pull – out torque.

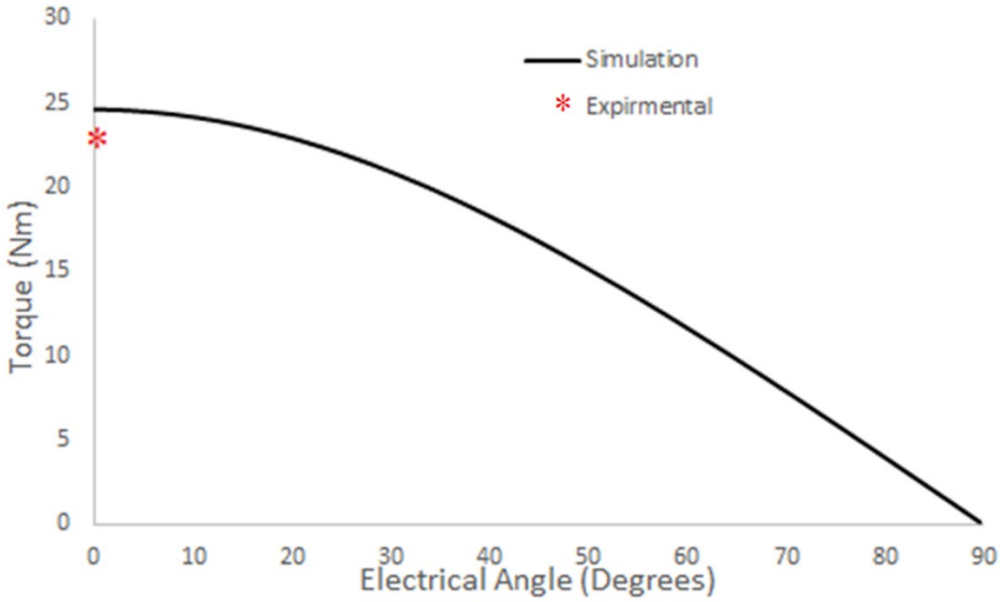

Figure 5-29 Simulated and experimental torque – load angle characteristics

Fig 5-29 shows that the experimental value of the pull – out torque is close to the simulation keeping in mind that the simulation is developed value without mechanical friction.

The machine was energized through the drive and accelerated by increasing the frequency in steps until the rated machine frequency of 60 Hz was reached. The electric load was then turned on and different loads were applied.

Fig 5-30 shows the simulated and experimental torque speed characteristics at different load values. The experimental readings are close to the simulated performance.

Table 5-II shows the values of the mechanical output of the machine (torque, power, and speed), the electrical input power, and the efficiency at each load.

The induction machine was designed to have a full load torque of 12.2 Nm, which is 64.05 Nm at the high torque side of the machine. The machine was loaded to 10 Nm, which is less than one-

sixth of the rated load so the efficiency was expected to be low. Even with this small partial load the efficiency values are good.

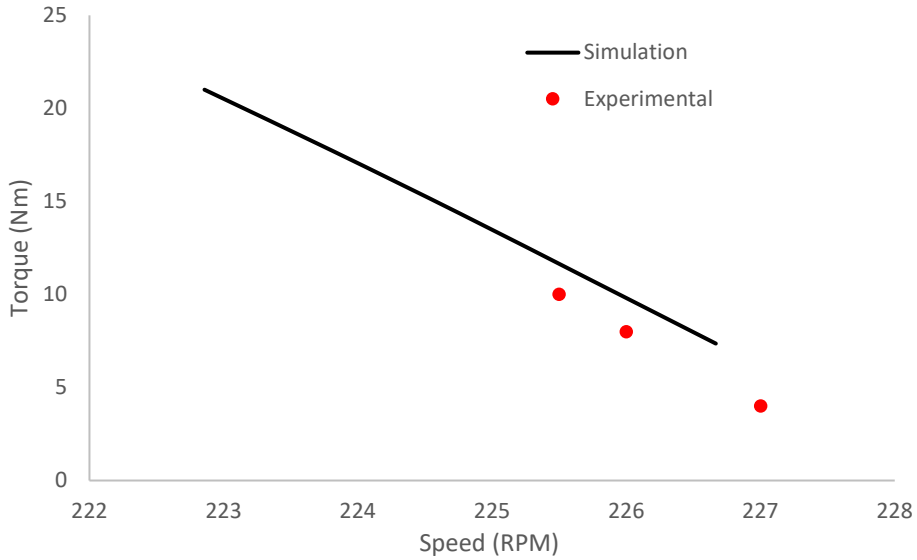

Figure 5-30 Simulated and experimental loading torque – speed characteristics

Table 5-II Loading performance

Speed (RPM)	Torque (Nm)	Output power (W)	Input power (W)	Efficiency
225.5	10	236	322	73.3%
226	8	190	260	73%
227	4	95	132	72%

5.3 Design modifications for performance improvement

The current design is criticized in order to suggest improvement to upgrade the machine performance. The current machine has four parts:

5.3.1 Stator

The machine windings have a high overhang that is almost the same length as the effective length of the machine on both sides. High overhang means more copper and higher cost, higher resistance, and more copper losses. From the overall machine specifications point of view, high overhang increases the machine gross length and so size and decreases the torque density. Furthermore, a long machine results in a longer modulating ring and makes the ring suspension and alignment more difficult.

5.3.2 Outer rotor

The current machine does not have access to the outer rotor. Fig 5-27 shows the suggested design in order to have two shafts: one high speed is connected to the outer rotor and one low speed is connected to the inner rotor.

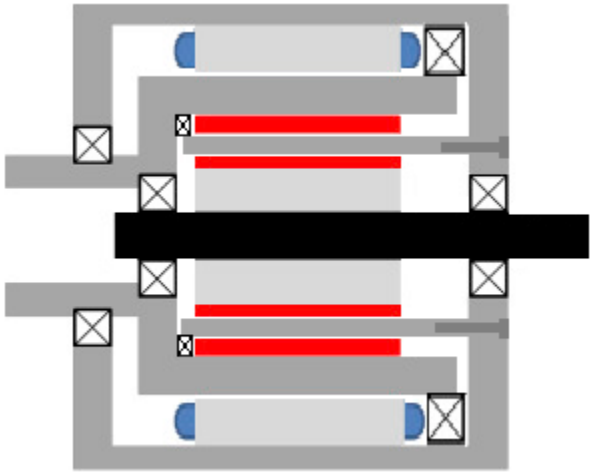

Figure 5-31 Two shaft machine

5.3.3 Inner rotor

The current inner rotor is a solid rotor. The solid rotor increases the core loss. To improve machine performance, a laminated rotor can be used.

5.3.4 Magnets

In order to save time and lower the cost, standard on-shelf small magnets bar are ordered. For the outer rotor, the same polarity five bars are forced to form a pole. Because of similar polarity and repulsion forces, there is a gap between some of these magnets. These gaps affect the uniformity of the magnetic field. In addition, these magnets are used as two sets to cover the stack length of the machine. Another issue arises which is the magnet alignment which also causes the field deformation. Instead customized long arc magnets should be used. For the outer rotor, each pole is formed using one bar but because it is short, two sets are used. Again the possibility of misalignment can affect the torque value and machine performance as the pole arc is around three mm which means only one mm misalignment is equivalent to 60 electrical degrees. Fig 5- 28 shows the value of the torque if the magnets are one mm misaligned. The torque dropped to almost half its value from 0 degrees torque angle to 60 degrees torque angle. Long magnets should be used for the inner rotor.

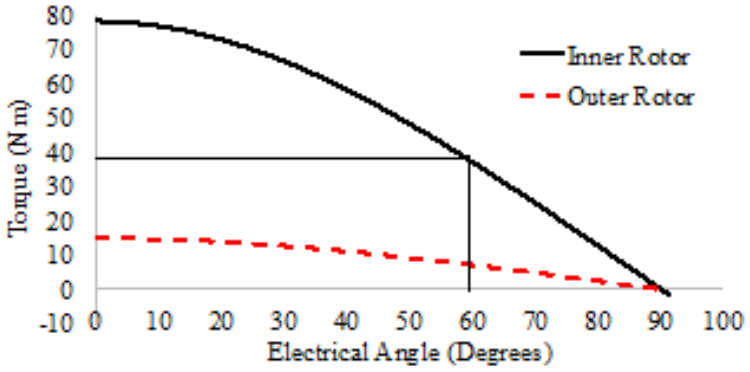

Figure 5-32 Torque – Load angle plot for magnetic gear

5.3.5 Modulating ring

This research work introduced two different designs for the modulating ring. Laminations stacked together to form the modulating ring and a 3D printed envelope enclosure for longitudinal laminations. Modulating ring is the weakest part of the machine and it suffers from shear forces and twisting torques. In addition to these forces, the current machine may have issues with the field uniformity and distribution as discussed before. Each lamination has a part of the torque which is calculated as shown in Table 5-II.

Table 5-III Torque per lamination calculations

Lamination thickness	0.4 mm
Stack length	54 mm
No of laminations	135 lamination
Peak torque for design 1	60 Nm
Torque/ lamination assuming uniform torque distribution	0.44 Nm

From Table 5-II each lamination is carrying a torque of 0.44 Nm which is a considerable amount of torque to be carried by one lamination.

For the current machine, the dimensions of the modulating ring are small in a thickness of 2.5 mm which doesn't allow a lot of options to strengthen the structure.

For the first design, in order to make the modulating ring stronger, fiberglass can be added in the slots to enforce the ring structure. Stronger material can be used to glue the laminations together.

For the second design, stronger material and finer 3D printing modulating ring envelope can be used.

To ensure the ring is precisely aligned, a bearing on the inner rotor shaft on both sides to align the modulating ring.

Also, a bigger machine will result in a bigger modulating ring. In addition, a bigger pole pitch results in a thicker modulating ring that will allow more options of how to stack the laminations in a way it can withstand all the forces.

The possibility of misalignment can affect the torque value and machine performance as the pole arc is around three mm which means only one mm misalignment is equivalent to 60 electrical degrees. Fig. 5-29 shows the value of the torque if the magnets are one mm misaligned. The torque dropped to almost half its value from 0 degrees torque angle to 60 degrees torque angle.

As a result of the 1mm misalignment of the magnets, two adjacent laminations may have a local torque variation. If lamination one has a torque corresponding to a torque angle zero electrical degrees torque angle which corresponding to a torque of 80 Nm, the torque per lamination will be around 0.6 Nm. Lamination 2 has a torque corresponding to a torque angle sixty electrical degrees torque angle and the value of the torque at this torque angle is 40, the torque per lamination is 0.3 Nm. this will lead to a torque variation of 0.3 Nm local torque variation between two adjacent laminations. If the misalignment is repeated with all the magnets, the modulating ring will see the two sets of magnets as two different machines with different torques. One end of the modulating ring will see a torque of 80 Nm and the other end will see a torque of 40 Nm and this torque variation may cause the breakdown of the modulating ring laminations. It is not easy to ensure the alignment of the magnets in the lab. Also, it is not easy to handle and place long magnets in the lab without the proper tools but in an industrial facility, this would be executable.

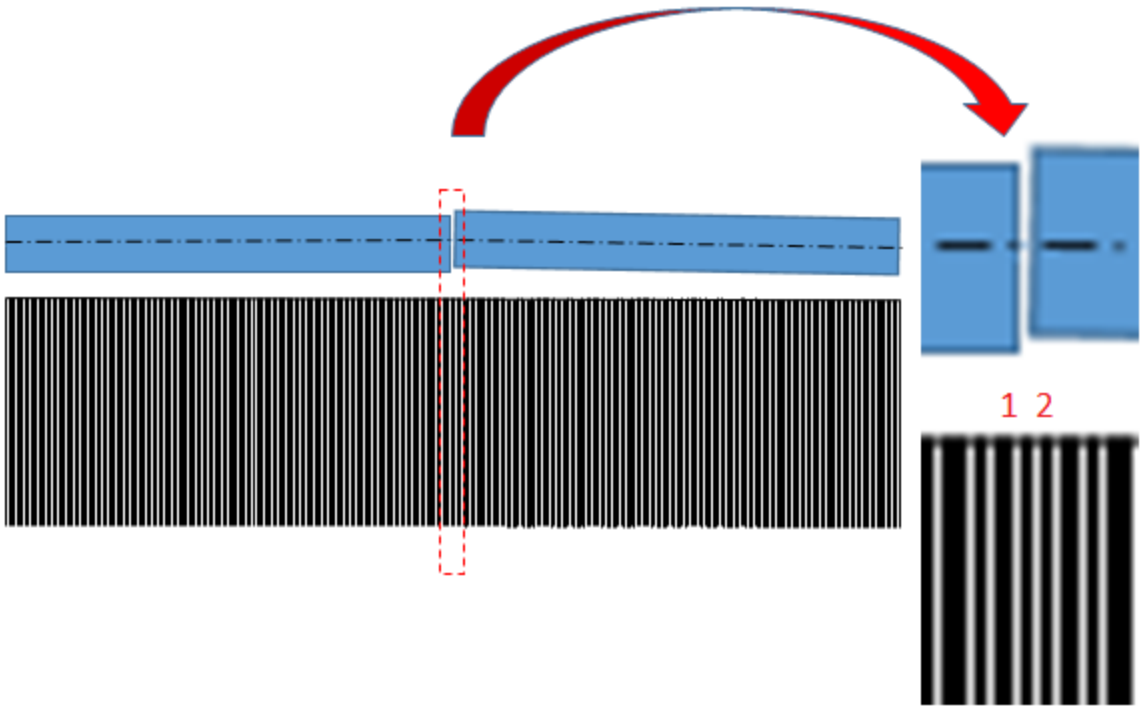

Figure 5-33 Magnet misalignment and modulating ring laminations

5.4 Summary

The experimental readings for the machine were introduced. The modulating ring challenges and solutions were discussed. The visibility of the machine design is validated. The ability of gearing, following the gearing ratio, generating the expected torque, and loading is proved.

CHAPTER 6: CONCLUSION

The work in this thesis presents one of the first investigations into the feasibility of incorporating a magnetic gear into an induction machine system. The approach used in the paper has been patented and is the first known successful attempt at integrating an induction machine with an inner magnetic gear. The resulting machine offers high-torque low-speed output at high torque density and may enable simple sensorless operation, either from grid connection or open-loop control. The combination of high torque density and low-to-no control complexity is attractive for many applications. Machine design, FEA simulation of its performance, efficiency, and losses analysis for operation across a range of operating points are discussed. The simulation results and experimental results in the thesis show good agreement.

The difficulties of integrated machine design and FEA simulation are discussed, together with guidance to mitigate some of the initial design complexities. Two different gears were introduced and investigated for integration with the induction machine. A simplified analysis is shown to be suitable for determining pole combinations that provide good torque ripple performance, but more complex models may be necessary to fully account for tangential flux. The simulation results so far have demonstrated the feasibility of implementing this machine. A promising machine is expected to provide high-torque low-speed easy-control direct drive which will be a good fit for many systems.

Different designs for the modulating ring of a magnetic gear are investigated in an attempt to simplify modulating ring manufacturability. Time stepped FEA simulation results show the ripple content of the torque may be reduced while the average torque is maintained and the modulating ring is made more robust. Optimization analysis has been done to investigate the optimal position of the bridge. Considering the performance of the modulating ring designs, the

thinner the thickness of the bridge the better the performance. In all cases, the losses in the magnets on the high-pole number rotor are predicted to be substantially higher than those on the low pole-number magnet rotor. Modulating rings with designs similar to these can be found in the literature, without reference to their relative performance.

Three sets of modulating ring designs were manufactured to justify the simulations and compare the performance with the induction machine integrated with magnetic gear with three different ring designs. However, in all cases the original modulation ring designs failed. And the possible causes of failure are discussed. A novel 3-D printed modulation housing is implemented and demonstrated. At the time of writing, I am not aware of any other successful modulating ring construction using a 3D-printed housing.

The After reconstruction of the machine with the new housing, the new gear parameters were simulated. The measured performance of the machine closely matches the expected performance

Future Work

This work has demonstrated a proof of concept, future work should focus on reliable manufacturability. The prototype in this thesis proves the concept but makes a breakdown of experimental losses difficult. Investigations of similar machines should focus on access as a 3-port machine, enabling the interaction of the two rotors to be studied. An assembly that allowed the modulation ring and inner rotor to be easily added to /removed from the outer rotor would be beneficial. Considering the novel modulating ring structure presented in this thesis and used in the final prototype, an investigation of high strength materials is recommended.

REFERENCES

[1] A. Penzkofer, K. Atallah, "Magnetic Gears for High Torque Applications," in Magnetics, IEEE Transactions on , vol.50, no.11, pp.1-4, Nov. 2014.

[2] K.K. Uppalapati, W. Bomela, J.Z. Bird, M. Calvin, J. Wright, "Construction of a low speed flux focusing magnetic gear," in Energy Conversion Congress and Exposition (ECCE), 2013 IEEE, vol., no., pp.2178-2184, 15-19 Sept. 2013.

[3] S. Hazra, S. Bhattacharya, K. K. Uppalapati and J. Bird, "Ocean energy power take-off using oscillating paddle," *2012 IEEE Energy Conversion Congress and Exposition (ECCE)*, Raleigh, NC, 2012, pp. 407-413.

[4] K. K. Uppalapati, J. Z. Bird, D. Jia, J. Garner and A. Zhou, "Performance of a magnetic gear using ferrite magnets for low speed ocean power generation," *2012 IEEE Energy Conversion Congress and Exposition (ECCE)*, Raleigh, NC, 2012, pp. 3348-3355.

[5] K. Atallah, S. Calverley, R. Clark, J. Rens, D. Howe, "A new PM machine topology for low-speed, high-torque drives," in Electrical Machines, 2008. ICEM 2008. 18th International Conference on, vol., no., pp.1-4, 6-9 Sept. 2008.

[6] K. Li, J. Wright, S. Modaresahmadi, D. Som, W. Williams and J. Z. Bird, "Designing the first stage of a series connected multistage coaxial magnetic gearbox for a wind turbine demonstrator," *2017 IEEE Energy Conversion Congress and Exposition (ECCE)*, Cincinnati, OH, 2017, pp. 1247-1254.

[7] K. K. Uppalapati, J. Z. Bird, J. Wright, J. Pitchard, M. Calvin and W. Williams, "A magnetic gearbox with an active region torque density of 239Nm/L," 2014 IEEE Energy Conversion Congress and Exposition (ECCE), Pittsburgh, PA, 2014, pp. 1422-1428.

[8] M. Bouheraoua, J. Wang, K. Atallah,."Influence of Control Structures and Load Parameters

on Performance of a Pseudo Direct Drive." Machines 2, no. 3: 158-175, 2014.

[9] V. M. Acharya, J. Z. Bird and M. Calvin, "A Flux Focusing Axial Magnetic Gear," in *IEEE Transactions on Magnetics*, vol. 49, no. 7, pp. 4092-4095, July 2013.

[10] K. Atallah, J. Rens, S. Mezani, D. Howe. "A novel "Pseudo" direct-drive brushless permanent magnet machine." Magnetics, IEEE Transactions on 44, no. 11 (2008): 4349-4352.

[11] L. Mathe, N.I. Berg, R.K. Holm, T.N. Matzen, P.O. Rasmussen, K.K. Jensen, "Motor Integrated Permanent Magnet Gear in a Battery Electrical Vehicle" IEEE Trans Industry Applications Vol 51, No 2, 2015, pp 1516 – 1525.

[12] K. K. Uppalapati, M. D. Calvin, J. D. Wright, J. Pitchard, W. B. Williams and J. Z. Bird, "A Magnetic Gearbox With an Active Region Torque Density of 239 N·m/L," in IEEE Transactions on Industry Applications, vol. 54, no. 2, pp. 1331-1338, March-April 2018.

[13] Y. Fan, L. Zhang, S. Member, J. Huang, and X. Han, "Design , Analysis , and Sensorless Control of a Self-Decelerating Permanent-Magnet In-Wheel Motor," vol. 61, no. 10, pp. 5788–5797, 2014.

[14] D. Som *et al*., "Analysis and Testing of a Coaxial Magnetic Gearbox With Flux Concentration Halbach Rotors," in *IEEE Transactions on Magnetics*, vol. 53, no. 11, pp. 1-6, Nov. 2017, Art no. 8112206.

[15] N. Frank and H. Toliyat, "Gearing ratios of a magnetic gear for wind turbines," in Electric Machines and Drives Conference, 2009. IEMDC '09. IEEE International, pp. 1224 –1230, may 2009.

[16] K. K. Uppalapati and J. Z. Bird, "An Iterative Magnetomechanical Deflection Model for a Magnetic Gear," in IEEE Transactions on Magnetics, vol. 50, no. 2, pp. 245-248, Feb.

[17] N. Frank and H. Toliyat, “Analysis of the concentric planetary magnetic gear with strengthened stator and interior permanent magnet inner rotor,” Industry Applications, IEEE Transactions on, vol. 47, no. 4, pp. 1652–1660, 2011.

[18] K. Atallah and D. Howe, “A novel high-performance magnetic gear,” Magnetics, IEEE Transactions on, vol. 37, pp. 2844 –2846, jul 2001.

[19] Armstrong, C., “Power transmitting device,” US Patent # 687,292, 1901.

[20] A. H. NEULAND, “Apparatus for transmitting power,” US Patent 1,171,351A, Feb. 8, 1916.

[21] H.T. Faus, “Magnet gearing,” U.S. Patent 2,243,555, May 27, 1941.

[22] C. Lewis, "The Advanced Induction Motor," Power Engineering Society Summer Meeting, 2002 IEEE, Chicago, IL, USA, 2002, pp. 250-253 vol.1.

[23] J. M. Crider and S. D. Sudhoff, “An Inner Rotor Flux-Modulated Permanent Magnet Synchronous Machine for Low-Speed High-Torque Applications,” IEEE Trans. Energy Convers., vol. 30, no. 3, pp. 1247–1254, 2015.

[24] L. Jian, K. T. Chau, and J. Z. Jiang, “An integrated magnetic-geared permanent magnet in-wheel motor drive for electric vehicles,” 2008 IEEE Veh. Power Propuls. Conf. VPPC 2008, pp. 1–6, 2008.

[25] P. O. Rasmussen, H. H. Mortensen, T. N. Matzen, T. M. Jahns, and H. A. Toliyat, “Motor integrated permanent magnet gear with a wide torque-speed range,” in 2009 IEEE Energy Conversion Congress and Exposition, ECCE 2009, 2009.

[26] Y. Fan, X. Han, Z. Xue, and H. Jiang, “Design, analysis and control of a permanent magnet in-wheel motor based on magnetic-gear for electric vehicles,” 2011 Int. Conf. Electr. Mach.

Syst., pp. 1–6, 2011.

[27] T. V. Frandsen, P. O. Rasmussen, and K. K. Jensen, “Improved motor integrated permanent magnet gear for traction applications,” 2012 IEEE Energy Convers. Congr. Expo. ECCE 2012, pp. 3332–3339, 2012.

[28] T. V. Frandsen, L. Mathe, N. I. Berg, R. K. Holm, T. N. Matzen, P. O. Rasmussen, and K. K. Jensen, “Motor integrated permanent magnet gear in a battery electrical vehicle,” 2013 IEEE Energy Convers. Congr. Expo., pp. 2170–2177, 2013.

[29] T. V. Frandsen, L. Mathe, N. I. Berg, R. K. Holm, T. N. Matzen, P. O. Rasmussen, and K. K. Jensen, “Motor integrated permanent magnet gear in a battery electrical vehicle,” 2013 IEEE Energy Convers. Congr. Expo. ECCE 2013, vol. 9994, no. c, pp. 2170–2177, 2013.

[30] T. V. Frandsen and P. O. Rasmussen, “Loss investigation of Motor Integrated Permanent Magnet Gear,” in 2014 17th International Conference on Electrical Machines and Systems, ICEMS 2014, 2015, pp. 2673–2679.

[31] M. P. Motor, G. Liu, Y. Jiang, J. Ji, Q. Chen, and J. Yang, “Design and Analysis of a New Fault-Tolerant,” Ieee Trans. Appl. Supercond., vol. 24, no. 3, 2014.

[32] K. Atallah, J. Wang, S. D. Calverley, and S. Duggan, “Design and Operation of a Magnetic Continuously Variable Transmission,” Ind. Appl. IEEE Trans., vol. 48, pp. 1288–1295, 2012.

[33] Y. Fan, L. Zhang, S. Member, J. Huang, and X. Han, “Design , Analysis , and Sensorless Control of a In-Wheel Motor,” vol. 61, no. 10, pp. 5788–5797, 2014.

[34] T. V Frandsen and P. O. Rasmussen, “Slip Torque Investigation and Magnetic Redesign of Motor Integrated Permanent Magnet Gear,” *2015 18th International Conference on Electrical Machines and Systems (ICEMS)*, Pattaya, Thailand, 2015, pp. 929-935.

[35] P. O. Rasmussen, T. V. Frandsen, K. K. Jensen, and K. Jessen, “Experimental evaluation of a motor integrated permanent magnet gear,” IEEE Energy Convers. Congr. Expo. Energy Convers. Innov. a Clean Energy Futur. ECCE 2011, Proc., pp. 3982–3989, 2011.

[36] P. O. Rasmussen, T. V. Frandsen, K. K. Jensen, and K. Jessen, “Experimental evaluation of a motor-integrated permanent-magnet gear,” IEEE Trans. Ind. Appl., vol. 49, no. 2, pp. 850–859, 2013.

[37] Y. Zhang, K. Lu, and Y. Ye, “Permanent magnet eddy current loss analysis of a novel motor integrated permanent magnet gear,” IEEE Trans. Magn., vol. 48, no. 11, pp. 3005–3008, 2012.

[38] Y. Fan, H. Jiang, M. Cheng, and Y. Wang, “An improved magnetic-geared permanent magnet in-wheel motor for electric vehicles,” in 2010 IEEE Vehicle Power and Propulsion Conference, VPPC 2010, 2010.

[39] L. Jian, G. Xu, Y. Wu, Z. Cheng, and J. Song, “A novel power-train using coaxial magnetic gear for power-split hybrid electric vehicles,” 2011 Int. Conf. Electr. Mach. Syst. ICEMS 2011, 2011.

[40] K. T. Chau, C. C. Chan, and C. Liu, “Overview of permanent-magnet brushless drives for electric and hybrid electric vehicles,” IEEE Trans. Ind. Electron., vol. 55, no. 6, pp. 2246–2257, 2008.

[41] K. T. Chau, D. Zhang, J. Z. Jiang, C. Liu, and Y. Zhang, “Design of a magnetic-geared outer-rotor permanent-magnet brushless motor for electric vehicles,” IEEE Trans. Magn., vol. 43, no. 6, pp. 2504–2506, 2007.

[42] L. L. Wang, J. X. Shen, Y. Wang, and K. Wang, “A novel magnetic-geared outer-rotor permanent-magnet brushless motor,” Power Electron. Mach. Drives, 2008. PEMD 2008. 4th

IET Conf., pp. 33–36, 2008.

[43] Y. Fan, J. Huang, X. Han, X. Fu, and H. Wei, “Design, analysis and sensorless control of a new self-decelerating permanent-magnet motor,” in IECON Proceedings (Industrial Electronics Conference), 2012.

[44] L. L. Wang, J. X. Shen, and M. J. Jin, “Design of a multi-power-terminals permanent magnet machine with magnetic field modulation,” in 2011 International Conference on Electrical Machines and Systems, ICEMS 2011, 2011.

[45] S. L. Ho, S. Niu, and W. N. Fu, “Transient analysis of a magnetic gear integrated brushless permanent magnet machine using circuit-field-motion coupled time-stepping finite element method,” IEEE Trans. Magn., vol. 46, no. 6, pp. 2074–2077, 2010.

[46] K. Atallah, J. Rens, S. Mezani, and D. Howe, “A novel ‘pseudo’ direct-drive brushless permanent magnet machine,” IEEE Trans. Magn., vol. 44, no. 11, pp. 4349–4352, 2008.

[47] J. W. J. Wang and K. A. K. Atallah, “Modeling and control of ‘pseudo’ direct-drive brushless permanent magnet machines,” 2009 IEEE Int. Electr. Mach. Drives Conf., pp. 870–875, 2009.

[48] D. J. Powell, S. D. Calverley, F. de Wildt, and K. Daffey, “Design and analysis of a pseudo direct-drive propulsion motor,” 5th IET Int. Conf. Power Electron. Mach. Drives (PEMD 2010), pp. MO253–MO253, 2010.

[49] M. Bouheraoua, J. Wang, and K. Atallah, “Observer Based State Feedback Controller Design for Psuedo Direct Drive using Genetic Algorithm,” Power Electron. Mach. Drives (PEMD 2012), vol. 6, p. 1,6, 2012.

[50] M. Bouheraoua, J. Wang, and K. Atallah, “A complex frequency domain analysis of a closed loop controlled pseudo direct drive,” Proc. - 2012 20th Int. Conf. Electr. Mach. ICEM

2012, pp. 2428–2434, 2012.

[51] M. Bouheraoua, J. Wang, and K. Atallah, “Slip recovery and prevention in Pseudo Direct Drive permanent magnet machines,” in 2013 IEEE Energy Conversion Congress and Exposition, ECCE 2013, 2013, pp. 2162–2169.

[52] M. Bouheraoua, J. Wang, and K. Atallah, “Design and implementation of an observer-based state feedback controller for a pseudo direct drive,” Iet Electr. Power Appl., vol. 7, no. November 2012, pp. 643–653, 2013.

[53] M. Bouheraoua, J. Wang, and K. Atallah, “Speed control for a Pseudo Direct Drive permanent magnet machine with one position sensor on low-speed rotor,” Proc. 2013 IEEE Int. Electr. Mach. Drives Conf. IEMDC 2013, pp. 986–992, 2013.

[54] M. Bouheraoua, J. Wang, and K. Atallah, “Speed control for a pseudo direct drive permanent-magnet machine with one position sensor on low-speed rotor,” in IEEE Transactions on Industry Applications, 2014.

[55] M. Bouheraoua, “Rotor Position Estimation of a Pseudo Direct Drive PM machine using Extended Kalman Filter,” in Energy Conversion Congress and Exposition (ECCE), 2015 IEEE, 2015, pp. 292–299.

[56] M. Bouheraoua, J. Wang, and K. Atallah, “Slip recovery and prevention in Pseudo Direct Drive permanent magnet machines,” IEEE Trans. Ind. Appl., vol. 51, no. 3, pp. 2291 – 2299, 2015.

[57] A. Penzkofer and K. Atallah, “Analytical Modeling and Optimization of Pseudo-Direct Drive Permanent Magnet Machines for Large Wind Turbines,” IEEE Trans. Magn., vol. 51, no. 12, 2015.

[58] A. Penzkofer and K. Atallah, “Scaling of Pseudo Direct-Drives for Wind Turbine

Application," IEEE Trans. Magn., vol. PP, no. 99, pp. 1–1, 2016.

[59] D. G. Dorrell, A. M. Knight, L. Evans, and M. Popescu, "Analysis and design techniques applied to hybrid vehicle drive machines-assessment of alternative IPM and induction motor topologies," IEEE Trans. Ind. Electron., vol. 59, no. 10, pp. 3690–3699, 2012.

[60] S. Mezani, T. Hamiti, L. Belguerras, T. Lubin, M. Rashed, C. Gerada, "Magnetically Geared Induction Machines," in Magnetics Conference (INTERMAG), 2015 IEEE , vol., no., pp.1-1, 11-15 May 2015.

[61] B. Bidouche, T. Lubin and S. Mezani, "Design and Analysis of a Magnetically Geared Induction Machine," *2018 XIII International Conference on Electrical Machines (ICEM)*, Alexandroupoli, 2018, pp. 629-634.

[62] B. Anvari, A. Kabir, R. Mikail, C. Tschida and C. Lin, "Magnticalley Geared Direct Online Machine," *2019 IEEE International Electric Machines & Drives Conference (IEMDC)*, San Diego, CA, USA, 2019, pp. 1559-1563.

[63] B. Bidouche, T. Lubin and S. Mezani, "Dynamic behaviour of a Magnetically Geared Induction Machine," 2019 19th International Symposium on Electromagnetic Fields in Mechatronics, Electrical and Electronic Engineering (ISEF), Nancy, France, 2019, pp. 1-2.

[64] A. el-Rafaie, M. Shah, "Comparison of Induction Machine Performance with Distributed and Fractional-Slot Concentrated Windings," Proc IEEE IAS Annual Meeting, Oct 2008.

[65] K. K. Uppalapati, W. B. Bomela, J. Z. Bird, M. D. Calvin and J. D. Wright, "Experimental Evaluation of Low-Speed Flux-Focusing Magnetic Gearboxes," in *IEEE Transactions on Industry Applications*, vol. 50, no. 6, pp. 3637-3643, Nov.-Dec. 2014.

[66] N. Frank and H. Toliyat, “Gearing ratios of a magnetic gear for wind turbines,” in Electric Machines and Drives Conference, 2009. IEMDC ’09. IEEE International, pp. 1224 –1230, may 2009.

[67] K. Atallah, S. Calverley, and D. Howe, “Design, analysis and realisation of a high-performance magnetic gear,” IEE Proc. Electr. Power Appl., vol. 151, no. 2, pp. 135-143, Mar. 2004.

[68] L. Jian, K. T. Chau, W. Li and J. Li, "A Novel Coaxial Magnetic Gear Using Bulk HTS for Industrial Applications," in IEEE Transactions on Applied Superconductivity, vol. 20, no. 3, pp. 981-984, June 2010.

[69] P. Padmanathan and J. Z. Bird, "A continuously variable magnetic gear," 2013 International Electric Machines & Drives Conference, Chicago, IL, 2013, pp. 367-373.

[70] J. Z. Bird, "Magnetically Geared Rotary Generators for Marine Hydrokinetic Power Take-Off – A Status Update," OCEANS 2019 - Marseille, Marseille, France, 2019, pp. 1-7.

[71] K. Uppalapati, J. Kadel, J. Wright, K. Li, W. Williams and J. Z. Bird, "A low assembly cost coaxial magnetic gearbox," *2016 IEEE 2nd Annual Southern Power Electronics Conference (SPEC)*, Auckland, 2016, pp. 1-6.

[72] D. Som *et al*., "Analysis and Testing of a Coaxial Magnetic Gearbox With Flux Concentration Halbach Rotors," in *IEEE Transactions on Magnetics*, vol. 53, no. 11, pp. 1-6, Nov. 2017, Art no. 8112206.

[73] Y. Li and M. Tomizuka, "Robust motion control of mechanical systems with compliance," in Decision and Control, 1996. Proceedings of the 35th IEEE, 1996,pp. 2462-2467 vol.3.

[74] R. L. Norton, Design of Machinery, (3rd ed.), McGraw-Hill Professional, 2004.

[75] R. G. Montague, C. Bingham, and K. Atallah, “Servo control of magnetic gears,” *Mechatronics*, IEEE/ASME *Transactions* on, vol. 17, pp. 269-278, April 2012.

[76] R. G. Montague, C. Bingham, and K. Atallah, "Magnetic gear dynamics for servo control," *MELECON* - 2010 15th IEEE *Mediterranean Electrotechnical Conference*,2010, pp. 1192-1197;

[77] R. G. Montague, C. Bingham, and K. Atallah, "Characterisation and modelling of magnetic couplings and gears for servo control systems," *Power Electronics, Machines and Drives (PEMD 2010), 5th IET International Conference on,* 2010, pp. 1-6.

[78] W. Bomela, J. Z. Bird and V. M. Acharya, "The Performance of a Transverse Flux Magnetic Gear," in *IEEE Transactions on Magnetics*, vol. 50, no. 1, pp. 1-4, Jan. 2014, Art no. 4000104.

[79] K. Li and J. Z. Bird, "A Review of the Volumetric Torque Density of Rotary Magnetic Gear Designs," *2018 XIII International Conference on Electrical Machines (ICEM)*, Alexandroupoli, 2018, pp. 2016-2022.

[80] S. Gerber and R. Wang, "Design and Evaluation of a Magnetically Geared PM Machine," in *IEEE Transactions on Magnetics*, vol. 51, no. 8, pp. 1-10, Aug. 2015, Art no. 8107010.

[81] Proto Lam, LLC. [Online]. Available: http://www.protolam.com/

[82] Bata's Electric. [Online]. Available: http://www.bataselectric.ca/

[83] National Cheng Kung University in Taiwan. [Online]. Available: https://web.ncku.edu.tw/index.php

[84] Engineering Services. [Online]. Available: http://www.denki.com.au/services.html

[85] Texas Instruments TMS320F2833x, TMS320F2823x Digital Signal Controllers (DSCs): Device Overview. [Online]. Available: http://www.ti.com/lit/ds/symlink/tms320f28332.pdf, pp. 1-2.